Advanced methods for orbital uncertainty characterization applied to Space Surveillance and Tracking

by

Alejandro Cano Sánchez

A dissertation submitted in partial fulfillment of the requirements for the degree of Doctor of Philosophy in

PhD Program in Aerospace Engineering

Universidad Carlos III de Madrid

Advisors:

Diego Escobar Antón
Joaquín Míguez Arenas

October 2024

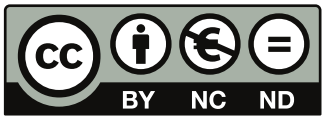

The most important step a man can take is not the first one.
It is always the next one.
Journey before destination.

Brandon Sanderson

Acknowledgments

Many people have contributed, in one way or another, to the development of this thesis and the maintenance of my mental health and happiness during these intense 4 years of work and research. I will try to be brief, though it is not my specialty.

I would like to start with my most sincere gratitude to Dr. Diego Escobar, my thesis advisor at GMV, and main culprit for my boarding on this PhD journey. Despite the tons of projects, the dozens of people to manage, and even a recently born daughter, he always found the time to guide this thesis. Without his vision, ideas, and dedication, this dissertation would not have been possible.

Right after Diego, I would like to heartily thank the other main culprit for this thesis, Dr. Alejandro Pastor (though he did warn me). It is difficult to enumerate the many details where he has helped me throughout these years at GMV. From debugging with me in the archaic versions of my code to helping me with bureaucracy, introducing me to the conferences community, and countless more. At times, I have to admit it is difficult to look up to someone so brilliant, hard-working, and generous, setting the bar so high. But I think that having him as a role model has made me a better researcher, engineer, and person.

Next, I would like to thank both my academic advisor Joaquin Miguez, and my academic consultant (or second tutor), Manuel Sanjurjo. Their academic experience has always provided key perspectives to dig deeper into details that are often overlooked in the industry. Moreover, and perhaps even as important, their help with academic bureaucracy has made my journey significantly easier.

I would also like to express my gratitude to the Community of Madrid, from which this project has received funding through its Industrial PhD program. I personally believe that the availability of programs like these is not just beneficial, but even necessary to close the expanding gap that exists between the industrial and academic worlds, which should work in a common front for the sake of their future.

Now, I would like to thank GMV for their support of this PhD, especially for providing the remaining funding required to complete this project. However, it would not be fair to exclude well-deserved acknowledgments to the Space Surveillance and Tracking and Space Traffic Management (SSTM) department. First, I would like to thank the head of this business unit, Alberto Águeda, for building such a talented team with such an amazing work environment. Thanks to his hard work, and that of all our managers and engineers, the team has grown so much during these 4 years that it would take too long to give everyone the space they deserve on these pages. Therefore, I would like to thank all those space junkers for the genuine workplace that they create with their companionship in face of challenges and overwork, building a team that is capable of anything, as we are showing to the world every day. Thank you for helping me grow professionally and for easing my stress with the PhD, even if only by being you all equally strained. Thank you for those lines of code written together with bugs that, hopefully, nobody will ever find.

But most importantly, thank you all for those stress-relief coffees, beers, pitiful padel tournaments, glorious football victories, and in the end, all the fun.

I would also like to express my gratitude to CNES Space Surveillance Department in Toulouse, for their welcoming during my research stay, their operational world discussions, and even more importantly, my access to their marvelous canteen that made me forget how to cook in three months.

Even though I have been constantly talking about what I consider friends, I cannot help but acknowledge the impact in my life of those preceding my work and research environments. To those whose friendship was forged during times of unintelligible algebra and fluid dynamics master classes, too-dangerous lab sessions, and sleepless exam nights, thank you for all those trips, from mountains to oceans, with more videos than a national geographic documentary. To those whose friendship was born in those beautiful times before I knew what an integral was, or during those nights at Toledo's Peraleda, thank you for sharing the joy and pain, for those not-so-relaxing beach trips, those endless evenings of philosophical discussions and beautiful sunrises after intense nights.

But now, I would like to give my heartfelt gratitude to my family, the very foundation of who I am. Thank you, aunts, cousins, and grandmothers for your unconditional love and support. Thanks brother, my Howler 1, for all the games shared, for all the moments built together, and for caring so much for our parents. Thank you, Mum and Dad, for all the efforts you have gone throughout your life to give me a better life than yours, and in the end, for giving me this chance to fulfill my dreams. I can never thank you enough for all the worked evenings and weekends to support my journey. I would have never made it this far without your example of hard work, strength, resistance, and life goals.

And last on this list, but first in my heart, thank you, Marta. I once heard that the good sailor is not the one who fights against the winds, but the one who uses the elements to find the way back home. I think we have become like that sailor, almost effortlessly finding our path in life, always towards one another even through thick and thin. Thank you for being always there, for that smile that erases all my worries, and for your warmth on my darkest nights.

Thank you all for shaping the way I am, and for accompanying me in this journey.

To those who are, and will be.
To those who were, but will always be.
Alejandro

Abstract

The large growth of human-related space activity in the last years has led to the overpopulation of objects orbiting the Earth, most of them being space debris, which jeopardizes the exploitation and sustainability of the space environment. For this reason, space agencies and government institutions are fostering space situational awareness activities to ensure the safety of spacecraft operations, improving their capabilities to detect and predict hazards to active and future space missions. Those activities are based on space surveillance and tracking activities, aimed at detecting space objects using sensor networks, estimating and predicting their orbits, and creating a catalog of objects to store their information for purposes such as manoeuvre detection, conjunction analysis, re-entry predictions, or fragmentation detection.

The quality of those services relies not only on the accurate estimation of the objects state, but also on its associated uncertainty. However, most common orbit determination systems in space surveillance activities, based on batch least-squares estimation, disregard the uncertainty present in the dynamic and measurement models of the space system. This leads to a lack of realism in the uncertainty estimates of those processes, which deteriorates significantly the reliability of space situational awareness products.

This dissertation focuses on advanced methodologies for uncertainty characterization and quantification in space surveillance and tracking applications, with the ultimate goal of developing accurate yet efficient methodologies to improve uncertainty realism with direct applicability to operational environments. First, one of the main drawbacks of most uncertainty characterization models is that realistic values of such model parameters are not available. Therefore, a robust framework to quantify the uncertainty in dynamic and measurement models is developed in this dissertation, based on observing the system uncertainty with orbital differences between estimated and predicted orbits and applying simple yet flexible and physically-based uncertainty models suitable to tackle specific error sources. These models are tailored to the most relevant errors in Earth's orbits, namely the atmospheric drag and solar proxies prediction in LEO, solar radiation pressure, or observation biases, distinguishing between different orbital regimes. Along this dissertation, these uncertainty quantification methods are consolidated in more complex applications to catalogs of objects to quantify uncertainty models common to multiple spacecraft, and then the characterization of the atmospheric drag uncertainty is improved by means of stochastic models including time correlation. This dissertation in focused on the operational applicability of the developed methodologies and the assessment of its capabilities in terms of covariance realism, which is validated in complex simulation environments but also with real observations as final verification of their performance.

Keywords: uncertainty quantification, space situational awareness, space surveillance and tracking, uncertainty realism, covariance determination.

Resumen

El gran crecimiento de la actividad espacial relacionada con el ser humano en los últimos años ha provocado la sobrepoblación de objetos orbitales alrededor de la Tierra, la mayoría de ellos basura espacial, lo que pone en peligro la explotación y sostenibilidad del espacio. Por este motivo, las agencias espaciales y las instituciones gubernamentales están fomentando actividades de conocimiento de la situación espacial para garantizar la seguridad de las operaciones espaciales, mejorando sus capacidades para detectar y predecir peligros para las misiones espaciales activas y futuras. Estas actividades se basan en actividades de vigilancia y seguimiento espacial, cuyo objetivo es detectar los objetos mediante redes de sensores, estimar y predecir sus órbitas, y crear un catálogo de objetos para almacenar su información con fines como la detección de maniobras, el análisis de conjunciones, la predicción de reentradas o la detección de fragmentaciones.

La calidad de esos servicios depende no sólo de la estimación precisa del estado del objeto, sino también de su incertidumbre asociada. Sin embargo, la mayoría de los sistemas de determinación de órbita habituales en las actividades de vigilancia espacial, basados en la estimación de mínimos cuadrados, no tienen en cuenta la incertidumbre presente en los modelos dinámicos y de medidas. Esto conduce a una falta de realismo en las estimaciones de incertidumbre de dichos procesos, lo que deteriora significativamente la fiabilidad de los productos de conocimiento de la situación espacial.

Esta tesis se centra en metodologías avanzadas para la caracterización y cuantificación de la incertidumbre en aplicaciones de vigilancia y seguimiento espacial, con el objetivo último de desarrollar metodologías precisas pero eficientes para mejorar el realismo de la incertidumbre con aplicabilidad directa a entornos operativos. En primer lugar, uno de los principales inconvenientes de la mayoría de los modelos de caracterización de la incertidumbre es que no se dispone de valores realistas de dichos parámetros del modelo. Por lo tanto, en esta tesis se desarrolla un marco robusto para cuantificar la incertidumbre en modelos dinámicos y de medidas, basado en la observación de la incertidumbre del sistema con diferencias orbitales entre las órbitas estimadas y las predichas, y en la aplicación de modelos de incertidumbre sencillos pero flexibles y con base física, adecuados para abordar fuentes de error específicas. Estos modelos se adaptan a los errores más relevantes en las órbitas terrestres, como el rozamiento atmosférico, la predicción de proxies solares, la presión de la radiación solar o los sesgos de observación, distinguiendo entre los distintos regímenes orbitales. A lo largo de esta tesis, estos métodos de cuantificación de la incertidumbre se consolidan en aplicaciones más complejas a catálogos de objetos para cuantificar modelos de incertidumbre comunes, y posteriormente se mejora la caracterización de la incertidumbre del rozamiento atmosférico mediante modelos estocásticos con correlación temporal. Esta tesis se centra en la aplicabilidad operativa de las metodologías desarrolladas y en la evaluación de sus capacidades de mejora del realismo de covarianza, que se valida en entornos de simulación complejos pero también con observaciones reales como verificación final de su rendimiento.

Palabras clave: quantificación de incertidumbre, conocimiento de la situatión espacial, vigilancia y seguimiento espacial, realismo de la incertidumbre, estimación de covarianza.

Published and submitted content

This thesis corresponds to a compendium of publications. The following articles are included as the core of this dissertation:

- **Paper 1**
  A. Cano, A. Pastor, D. Escobar, J. Míguez, M. Sanjurjo-Rivo, 2022,
  Improving uncertainty realism in orbit determination and propagation,
  Advances in Space Research, 72 (7), 2759-2777, ISSN 0273-1177
  10.1016/j.asr.2022.08.001
  Journal Impact Factor: 2.8

- **Paper 2**
  A. Cano, A. Pastor, S. Fernández, J. Míguez, M. Sanjurjo-Rivo, D. Escobar, 2022,
  Improving orbital uncertainty realism through covariance determination in GEO,
  The Journal of the Astronautical Sciences, 69, 1394–1420
  10.1007/s40295-022-00343-x
  Journal Impact Factor: 1.3

- **Paper 3**
  A. Cano, A. Pastor, J. Míguez, M. Sajurjo-Rivo, D. Escobar, 2023,
  Catalog-based atmosphere uncertainty quantification,
  The Journal of the Astronautical Sciences, 70 (42)
  10.1007/s40295-023-00403-w
  Journal Impact Factor: 1.3

- **Paper 4**
  A. Cano, M. Sajurjo-Rivo, J. Míguez, A. Pastor, D. Escobar, 2024,
  Atmospheric drag uncertainty quantification for orbit determination and propagation via Stochastic Consider Parameters,
  Advances in Space Research (submitted for publication)
  Journal Impact Factor: 2.8

In these publications, the distribution of the work between the authors has been the following. The research planning was done by Alejandro Cano and Diego Escobar, with the consultancy of Manuel Sanjurjo-Rivo and Joaquín Míguez. The code development, results simulations, and analysis were performed by Alejandro Cano, with supervision and guidance from Alejandro Pastor and Diego Escobar. The first versions of the manuscripts were written by Alejandro Cano. The final version of the manuscripts included corrections from Alejandro Pastor, Diego Escobar, Manuel Sanjurjo-Rivo, and Joaquín Míguez. Please refer to Section A for further research merits.

Organisation of the dissertation

This dissertation corresponds to a compendium of papers, including the original publications that led to the conclusion of this work. However, other sections are included for context and completeness. First, Chapter 1 contains a general introduction including the motivation, objectives, and a homogeneous state-of-the-art review covering the main topics of the thesis. The chapters that follow include the dissertation papers, each of them being preceded with a brief introduction highlighting its scientific contribution and its context during the development of this project. Finally, Chapter 6 includes the conclusions and future work. Additional information about other research merits including conference papers, co-authored publications, and attendance to relevant workshops is included in Appendix A. Important results from other researches not incorporated in the main body of the thesis can be found in Appendix B.

Contents

1

Introduction

Humankind has always felt the urge to explore, the necessity to understand our surroundings being coded in our survival instinct. This has led humanity to expand beyond our own planet, to outer space. Since the launch of the first satellite, the Sputnik in 1957, the number of spacecraft launches and space missions has increased almost yearly. However, this growth in the population of space objects orbiting the Earth has intensified significantly in recent years. On the one side, globalization allowed the private sector to enter the space business, leading to more than 80 countries being involved in space activities. On the other side, the emergence of the "New Space" concept [1] has democratized the access to the space business due to the standardization and cost reductions caused by the appearance of commercial-of-the-self products. This has meant a remarkable expansion of the private space sector for commercial purposes, with a multiplication of orbiting space objects including micro-satellites, CubeSats, and mega-constellations.

In such context, the status of the space environment is summarized in Figure 1.1, showing the amount of tracked objects in Earth orbits along time [2]. The different colors represent the source of the object, where active satellites are represented in dark blue (PL), and the rest correspond to space debris, defined as any non-functional man-made object orbiting around the Earth, according to the definition provided by the Inter-Agency Space Debris Coordination Committee (IADC) [3]. This latter group includes different origins of the objects such as payload debris (PD), rocket bodies (RB), fragmentations from payloads or rockets (PF and RF), or even from unidentified sources (UI). Overall, around 35000 objects are currently tracked by pace surveillance networks, approximately 12000 of them being active satellites. The rest correspond to trackable space debris, being larger than 10 cm in size. However, it is estimated that over 1 million objects with sizes between 1 cm and 10 cm are in orbit, capable of catastrophic damage [2]. Attending to the population per orbital regime, the Low Earth Orbit (LEO) region is the most crowded one with about 22000 currently tracked objects [2]. This region faces additional challenges, since most of the newly launched objects correspond to mega-constellations or CubeSats, with limited or null manoeuvring capabilities. Geostationary Orbit (GEO) and Medium Earth Orbit (MEO) orbits, fundamental for communication and navigation activities, present a significantly lower amount of objects. However, their services require specific slots and orbits for their required activity, and spacecraft collision or fragmentation events could

1

become extremely problematic due to the huge orbital lifetime of space debris in such orbital regimes.

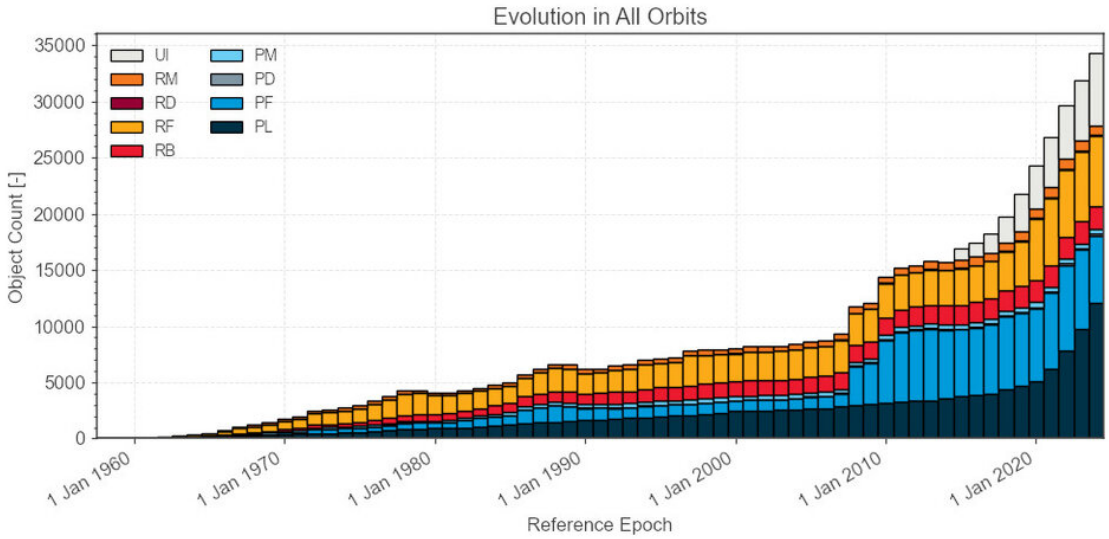

Figure 1.1: Number of tracked objects in Earth orbit over time, from [2].

The increasing trend that can be observed in Figure 1.1 is expected to exacerbate in the next years. The number of active satellites is expected to continue growing due to the already planned mega-constellations, other in-orbit or from-orbit services, and the overall reduction in launcher costs. Thus, the amount of space debris is expected to increase consequently. If unattended, this trend can lead to the well-known Kessler syndrome, which states that cascade effects in collisions and fragmentations would lead to an exponential growth of the space debris population, critically jeopardizing space activities [4]. This scenario, though deemed extremely pessimistic back in 1978, will become a reality with the current and predicted status of the space environment if no mitigation actions are taken. For instance, up to 600 catastrophic collisions are estimated during the next 200 years, given the current trend in launches [2], while fragmentation events are expected to become more common.

Therefore, to maintain the safety and sustainability of the space environment, two main activities must be carried out: mitigation and control. Regarding the former, the IADC was founded in 1993, aiming to coordinate the efforts between the main space agencies regarding debris mitigation activities. In 2002, the IADC proposed standards for End-Of-Life disposals and a reduction of on-orbit break-ups [5] following previous technical reports from the United Nations Committee on the Peaceful Uses of Outer Space (UNCOPUOS), which published in 1999 another report on the risk of man-made space debris [6]. However, their mitigation proposal guidelines are not legally binding, leading to very little acceptance. Events such as the Cosmos-Iridium on-orbit collision in 2009 or anti-satellite missile tests brought back attention to the space debris problem, leading to new revisions of the guidelines. Then, institutions such as the United Nations Office for Outer Space Affairs (UNOOSA) published space debris mitigation guidelines [7], again without any legal enforcement of their policies. Other agencies such as the European Space Agency (ESA) have recently updated their debris mitigation requirements, forcing

in their missions rules such as satellite passivation (to avoid fragmentations), collision avoidance capabilities, or a maximum of 5 years of orbit lifetime after the spacecraft end-of-life, among other proposals within the new Zero Debris Charter program [8].

However, regardless of these mitigation policies, it is necessary to maintain control and awareness of the space environment to ensure the safety of space activities, which led to the creation of Space Situational Awareness (SSA) services, and more recently, to Space Traffic Management (STM). The former is defined as the capability of detecting, predicting, and assessing any hazard towards to population of active satellites, whether coming from other spacecraft, space debris, natural Near-Earth Objects (NEOs), or the effect of the space weather. Europe started its ESA-SSA program back in 2009 to achieve independent SSA capabilities, which were mostly provided by the United States Department of Defense at the time. Regarding space debris, the most relevant services provided by SSA for space safety are the build-up and maintenance of a space objects catalog, manoeuvre detection and estimation, conjunction risk assessment, fragmentation analysis, and re-entry predictions.

Within those SSA services, Space Surveillance and Tracking (SST) activities are focused on the detection and tracking of both active satellites and space debris, which is required to provide the aforementioned services. Their main activities are twofold: the monitoring of the sky using space surveillance sensor networks to detect any object orbiting above the sensors, and the follow-up procedures to update the orbital information of the detected objects, like track correlation and posterior orbit determination. These activities lead to the generation of a space objects catalog, an automated database containing the most updated information of the known space objects which is the backbone of the rest of SSA services. Finally, STM concept appeared due to the increasingly congested space environment with the purpose of ensuring the safety of space operations, the orbits usability, and accessibility. It represents the efforts of the different policy-makers to reach a common set of standards and guidelines for the general use of the space, yet those still correspond to non-binding measures.

1.1 Motivation, scope and research gap

As discussed, SSA and STM services are the cornerstone for the safety and sustainability of space activities in the current and future space environment. These services are supported by the catalog of space objects, which requires routine updates of the orbit information upon the reception of new observations, which is generally referred to as custody maintenance. Robust custody maintenance is a complex task, requiring processes of data association (to determine to which object corresponds the observation), Orbit Determination (OD) and prediction, or manoeuvre detection and estimation. Then, the knowledge of the objects state and their predicted evolution is used for SSA services such as re-entry analysis, fragmentation detection, or conjunction analysis.

However, the quality and reliability of these services rely not only on the accurate knowledge of the object state, but also of its associated uncertainty. In catalog build-up and maintenance, track correlation methods are typically based on comparing the actual observation from the sensor with respect to synthetic observations generated via orbit propagation, using statistical distances based on the state uncertainty as association metrics [9, 10], such as the Covariance-Based Track Association (CBTA) algorithms [11,

1

12]. Similarly, most manoeuvre detection algorithms are based on finding statistically rare events between the predicted state of the object and the obtained observations, which could indicate the presence of a manoeuvre. Most manoeuvre detection metrics are based on normalization with the covariance matrix [13–16]. Furthermore, uncertainty plays a key role in most of the algorithms to compute the probability of collision during conjunction analysis, arguably the most relevant SSA service.

Therefore, a correct representation of the state uncertainty is necessary to improve the quality of SSA services. This is known as Uncertainty Realism (UR), being the main problem addressed throughout this thesis. More concretely, UR refers to obtaining the correct representation of the Probability Density Function (PDF) of the object state without any assumption on the distribution shape. However, UR can be reduced to covariance realism, retaining only up to the second order moment of the PDF, under the following assumptions: Gaussianity, unbiasedness, and consistency (orientation, shape, and size) [11]. Thus, covariance realism is necessary but not sufficient for uncertainty realism. However, the state covariance matrix is the most common uncertainty representation in SSA, derived from a trade-off between accuracy, complexity, and legacy of the operational SSA systems and algorithms. Even though there exist many studies that tackle non-linear representations of the state uncertainty and its propagation, linearity and Gaussian assumptions are typically maintained during the nominal SSA propagation arcs in LEO and GEO, with the major exception of very low altitude orbits, where non-linearities accumulate fast [17, 18]. This is further discussed in Section 1.3.

Coming back to the previous examples of SSA services, overly optimistic covariance matrices (i.e. too small) in catalog maintenance potentially lead to a lack of correlation (false negative associations) because the covariance does not contain the received observation [19]. On the contrary, excessively large covariance matrices cause ambiguity in the correlation for overly congested areas or close-formation flights, which is expected to become a common scenario in the future space environment. The lack of correlation, or the correlation to wrong objects (cross-tagging), is extremely detrimental to orbit determination and catalog maintenance. Similarly, in the case of manoeuvre detection, overly-optimistic covariances increase the number of false detections, since any slightly deviated track can appear statistically far from the state and its covariance. On the opposite side, oversized covariances have an impact on the sensitivity of the manoeuvre detection algorithm, leading to delayed manoeuvre detections, or the lack of them.

Regarding conjunction analysis, rectilinear motion and constant covariance are assumed during Probability of Collision (PoC) computation in short-duration encounters (around 95% of the total conjunctions [20]), due to the large relative velocity between both objects. This allows the reduction of the conjunction analysis to a 2-dimensional integral of the PDF over the conjunction region [21, 22], and thus, PoC methods are extremely sensitive to the covariance matrix of both encountering objects. Depending on the conjunction geometry, overly optimistic covariances tend to underestimate the PoC which can lead to missed conjunction events. Operators tend to apply safety factors or conservative computations of the covariance matrices. On the contrary, this causes the PoC to enter the so-called dilution region (i.e. a decrease of the PoC due to the dilution of the covariance in a too-large area). Therefore, the relevance of realistic covariances for the reliability of conjunction analysis is highlighted again.

Now, after discussing the relevance of covariance realism for the quality of SSA services, it is customary to understand the reasons for the lack of realism in operational SSA services. Many SST algorithms for orbit determination are based on weighted batch least-squares theory, which provides as nominal output the state and covariance matrix that best fits the available batch of observations within a given dynamical and measurement model. This is performed in an iterative process based on linearization against a reference state, which first corresponds to an initial guess, and then it is updated with the obtained solution in the current iteration [23]. The dynamical model used to define the orbital motion of the object is assumed as deterministic, and the state covariance considers only the measurements accuracy, receiving the name of noise-only covariance. Nonetheless, there are errors in the dynamical and measurement models that are not taken into account in these nominal batch estimation processes, which causes the noise-only covariance to be overly optimistic. This lack of covariance realism is also present in sequential filters, where the added process noise may not represent correctly the errors in the dynamic and measurement models.

In LEO orbits, the atmospheric drag is one of the leading forces acting on the spacecraft dynamics and depends on parameters such as the cross-sectional area, the object's mass and its interaction with the atmosphere (i.e. drag coefficient), and the atmospheric density. All these parameters correspond to sources of uncertainty for several reasons. In the case of non-collaborative objects such as space debris, the knowledge of cross-sectional area, mass, and drag coefficient (C_D) is limited or directly unknown. Thus, most orbit determination systems try to estimate the ballistic coefficient (B_c), that is, the combined contribution of the previous three parameters of the drag force. In batch least-squares estimation, a constant ballistic coefficient is estimated for the complete arc of observations. However, this ballistic coefficient suffers variations during the estimation arc coming from the unknown attitude of the object, orientation of the surfaces, materials, reflectivity, etc. On top of this, the atmospheric density presents a stochastic behavior due to its correlation with the space weather, including phenomena such as solar winds or geomagnetic effects, apart from depending on the altitude and location. Even though more details are provided in Section 1.3, the most accurate atmospheric density models present variations among them of more than 20% [24], showing the complexity and uncertainty present in the atmospheric density, which is not generally considered in SST applications.

Similarly to the drag force in LEO, the solar radiation pressure (SRP) force becomes one of the main perturbations in GEO orbits, caused by the momentum transfer from the Sun photons to the spacecraft. Apart from depending on the solar activity, this acceleration is affected by the surface area, object mass, reflectivity, and absorption of the object surfaces, which once more, are not known in SST applications. It is worth noting that the SRP force is also present in LEO orbits, though its relevance is significantly lower than the drag force there. Therefore, even though most systems also estimate the SRP as part of their orbit determination, the impact of its uncertainty in LEO orbits is negligible for SSA purposes.

Another relevant source of uncertainty in orbit determination algorithms comes from the measurements model. Observations (i.e. set of measurements taken at a certain timestamp) are the basis of estimation theory, and a conversion from the observation space to the state space is generally required. Such observations have a certain accuracy

and bias, derived from the sensor technology and type of measurement, which need to be considered in the orbit determination process. In SST, calibration campaigns are carried out periodically to determine the typical sensor biases and accuracy, using certain satellites as reference whose orbits are well-known such as Global Navigation Satellite System (GNSS) constellations. These calibration processes apply long arcs of observations to provide stable biases and sensor accuracy to be applicable until the next calibration (with bi-annual frequencies at best, in most cases). Thus, the biases are considered as constant, and the sensor accuracy is used to compute the already described noise-only covariance. However, the actual magnitude of the sensor biases is influenced by shorter period effects, such as the tropospheric and ionospheric corrections, the geometry of the observation, the size and location of the object, or even diurnal and seasonal changes in the sensor location. Thus, the errors made when applying a constant measurement bias are also disregarded in classical orbit estimation methods. This applies to any measurement kind, including range, range-rate, angles, or even time biases.

Therefore, space surveillance operations require efficient, reliable, and effective methodologies for uncertainty quantification and covariance realism improvement, especially given its relevance for SSA services, the aforementioned sources of uncertainty, and the expected evolution of the space environment. There exist classical methodologies to model the uncertainty in orbit determination systems such as *process noise* in filtering applications, or the *consider parameters* theory in batch estimation. However, their main drawback is that realistic quantities of the model uncertainty are not available, nor are methodologies to quantify them. Other techniques aim to improve the covariance realism without focusing on the sources of uncertainty, such as the application of scaling factors to artificially inflate the covariance, as applied in the Johnson Operations Center (JSC) [11]. However, the drawback of these artificial methods is that the physical meaning of the uncertainty quantification is lost, preventing the extrapolation of the quantified physical sources of uncertainty to other scenarios. A more detailed analysis of the state-of-the-art algorithms for uncertainty modeling is presented in Section 1.3.

To conclude, the motivation of this thesis is the relevance of realistic covariance estimates for SSA services. The research gap is that reliable and applicable methodologies to improve covariance realism in operational scenarios are unavailable. And, finally, the scope is to characterize and quantify the described sources of uncertainty that are present in classic orbit determination processes, with the ultimate goal of improving the safety and sustainability of the space environment.

1.2 Research objectives

Considering the previous motivation, the research objectives set at the beginning of this thesis are the following:

- **Objective 1:** Modeling uncertainty in dynamic and measurement models. This objective can be broken down into the following sub-objectives:
  - **Objective 1.1:** Development of uncertainty models for the effect of the atmosphere on objects in low Earth orbits, including errors in the calculation of atmospheric density as well as the drag coefficient, mass, and frontal area exposed by the object.
  - **Objective 1.2:** Development of uncertainty models for the effect of solar radiation pressure on objects in high Earth orbits, including errors in the calculation of solar pressure coefficient as well as the mass and frontal area exposed by the object.
  - **Objective 1.3:** Development of uncertainty models for the measurements used to calculate the orbit of objects, coming from both radars and telescopes.

  The reason for defining separate objectives for the effect of the atmosphere, solar radiation pressure, and sensor measurements, is that the necessary methods, while having many synergies, were expected to differ as they correspond to different processes. The first is dominated by the variation of the Earth's atmosphere, the second by the behavior of solar pressure, and the third by all the physics behind the operations of ground-based sensors.

- **Objective 2:** Quantification of uncertainty in dynamic models. This objective can be broken down into the following sub-objectives:
  - **Objective 2.1:** Quantification of uncertainty in models for low Earth orbit objects, including their validation with both simulated and real radar data.
  - **Objective 2.2:** Quantification of uncertainty in models for high Earth orbit objects, including their validation with both simulated and real telescope data.

  Unlike Objective 1, in this Objective 2 the secondary Objectives are not distinguished by type of dynamic model, but by type of object. This is because it is necessary to quantify the uncertainty of the models that affect each object simultaneously. However, it is possible to distinguish between low Earth orbits (LEO) and higher Earth orbits (MEO and GEO) since the perturbing forces that dominate the dynamics and the types of measurements are distinctly different.

1

1.3 State-of-the-art

This section is devoted to a brief literature review that homogenizes the concepts covered in the papers of this dissertation, intending to provide further insights into the uncertainty problem in space dynamics, its physical sources, and the existing methodologies to characterize and quantify it. This section also focuses on the definition of uncertainty and covariance realism, the techniques to improve or maintain such realism further in time, and the relevant metrics to measure realism in operational SST environments. The reader is advised that, since the core of this thesis corresponds to a paper compendium, many synergies and revisited contents will be found in the introductions of the papers included in this dissertation. Nonetheless, this section intends to provide a single view with further details about the main concepts of the thesis and the state-of-the-art to complement and expand the contents of the papers.

1.3.1 Uncertainty quantification in space dynamics

Uncertainty Quantification (UQ) is defined as the process of characterizing the sources of uncertainty, their estimation and prediction. More concretely, it involves:

1. The determination of the type and origin of the unmodeled errors.
2. Proposing models to characterize their behavior and map their effect into the variables of interest.
3. The estimation of the system uncertainty with the models proposed.
4. The propagation in time of the modeled and estimated uncertainty to predict the variables of interest.

As it could be expected, the first step is to understand the reasons for the presence of uncertainty in the system. Uncertainty can be classified into two categories: epistemic or aleatoric, though mixtures of both are also found [11]. Epistemic uncertainty refers to the limited knowledge or data in a system, which is expected to be reduced as the knowledge or data are expanded. Contrarily, aleatoric uncertainty refers to the physical variability found in natural systems or processes, being statistical in nature. Though irreducible, this kind of uncertainty is dealt with by properly describing the randomness of the system with a PDF. There exists a wide variety of uncertainty types that can be traced back to either epistemic or aleatoric natures, or a combination of both [25]. Thus, the impact of aleatoric uncertainty can be represented with an appropriate statistical model, whereas epistemic uncertainty is mitigated by improving the knowledge of the system. Throughout this thesis, the latter is dealt with by using high-accuracy models and the estimation of model biases, whereas the characterization and quantification of aleatoric uncertainty is the main focus. The specific sources of uncertainty considered in this thesis are further discussed in Section 1.3.2.

The next steps in UQ are, first, proposing a model to characterize the uncertainty in your system and, second, quantifying it for a given mathematical model of the system and a set of experimental data, estimating the discrepancy between the observations and underlying models and parameters used to represent the system. This is generally known

as the "inverse problem", where the unknown parameters of a system are estimated given a set of observations, as in the case of batch or filtering estimation. Thus, the overall concept of orbit determination can be defined as a UQ process.

Finally, the last fundamental problem of UQ is the Uncertainty Propagation (UP), which aims to characterize the time evolution of the state and its uncertainty along the dynamics of the problem. The majority of UP methods consist in the efficient and accurate propagation of an initially given PDF of a state, though there exist methods to include the impact of epistemic errors with PDF propagation [25]. Relevant guidelines and recommendations about UP methods tailored for SST can be found in [11], and a comprehensive review of UP methods can be found in [25–27]. As stated in Section 1.2, steps 1, 2, and 3 of UQ are the focus of this thesis, leaving advanced UP methods out of the scope.

Thus, the ultimate goal of UQ is to achieve a characterization of the state PDF that is representative of its true uncertainty. This is generally defined as UR, which requires all moments of the distribution to be properly characterized [11]. However, the majority of SSA and SST applications use the covariance matrix as uncertainty representation, retaining only up to the second-order moment of the state distribution. This is a legacy choice based on several trade-offs of computational efficiency, complexity, and accuracy. Firstly, the large amount of space objects expected in the catalogs in the current and future space environment imposes computational efficiency as one of the key factors in operational SSA and SST systems. These systems have been sequentially and progressively developed and tested throughout the years, accumulating experience and confidence in simple yet effective representations of the uncertainty such as the covariance matrix, as opposed to more complex ones. Finally, most SSA and SST algorithms used nowadays are based on linearization techniques or Gaussian assumptions, where the covariance matrix as uncertainty representation is a natural input or output, such as in collision risk assessment or orbit determination, respectively.

Therefore, it is customary to reduce the problem of UR to that of Covariance Realism in the SST context. Under Gaussian and linear assumptions, covariance realism requires the correct characterization of the two first moments of the PDF (mean and variance), as well as covariance consistency (correct orientation, shape, and size). In the general case, covariance realism is a necessary but not sufficient condition for uncertainty realism, but both are equivalent under Gaussian and linear assumptions.

1.3.2 Main physical sources of uncertainty in SST

The main sources of uncertainty in orbit estimation and propagation arise from the errors of the different models (measurement or dynamic) used to represent the true underlying physics of the system. The uncertainty in the measurement model refers to the errors between the real observation and the truth, also considering the mapping of the observation into the state space. Part of this uncertainty is the sensor accuracy, which in general, is known from the operator of the sensor or from calibration campaigns. The uncertainty in the dynamic models can be subdivided into two different sources: the structural and the parametric uncertainty. The former is due to a lack of representativeness of the true physics of the problem, of epistemic origin, whereas the parameter uncertainty is due to the lack of knowledge of the real value used for some of the model parameters,

which can be considered as both epistemic and aleatoric, despite being generally treated as the latter.

In LEO orbits, the most relevant source of uncertainty is the atmospheric drag [28], whose two main drivers are: the ballistic coefficient and the atmospheric density - see Equation (2.14). As previously mentioned, the uncertainty in the ballistic coefficient in the frame of SST arises from the lack of knowledge of the attitude of the Resident Space Object (RSO), its size, mass, or drag coefficient. The common approach in SST is to include it in the estimation process so that the ballistic coefficient that best fits the current observations is obtained. In the case of classic batch least-squares orbit determination, a constant ballistic coefficient is estimated for the complete observations arc. However, the uncertainty derived from this choice is typically disregarded, even though it can cause variations of an order of magnitude in the drag force. This is particularly relevant in the case of the drag coefficient, which serves as a regulator between the inertial and pressure forces acting on the object, normalizing the impact of the velocity, density, or area, and absorbing the effects of body geometry and its interaction with the medium. This leads to a significant influence of the surface orientation and material in the drag coefficient, inducing significant errors with the constant parameter estimation that are generally unaccounted for.

Regarding the atmospheric density, it shows a clear dependence on the object altitude and space weather, including solar activity, magnetosphere, and the dynamics of the lower atmosphere. Modern models assume its correlation with observable parameters (proxies) of solar activity and space weather. The most common ones, for legacy reasons, are the solar flux index ($F_{10.7}$), and a_p or k_p for daily planetary geomagnetic indexes. The contribution of these parameters to the atmospheric temperature and density is the main objective of the different atmospheric models. Several approaches have been proposed since the early beginning of space missions trying to fit parameterized equations to observations, from models relying more upon mathematics or averaging (Jacchia70) at the beginning, to modeling the molecular composition of the atmosphere at different altitudes to recompose the density (NRLMSISE models). Further details about the latter can be found in [29], whereas other reviews about the different atmospheric density models can be found in [24, 30].

However, the high variability of the space weather proxies combined with the difficulty of modeling the natural phenomena of the upper atmosphere leads to atmospheric density differences up to 20% even among the most modern models [24]. The main contributors to the variability in density are the diurnal and seasonal fluctuations of the solar activity. According to [31], the second major variation in density corresponds to the thermosphere heating derived from the Sun radiation. Despite the stability of the visible spectrum, the Sun energy emissions can be highly unsteady in the ultraviolet and X-ray wavelengths, which are the ones mostly absorbed by the thermosphere. The geomagnetic activity derived from solar events such as solar flares and mass ejection is another source of atmospheric density variation, where a fraction of the emitted charged particles reaches the Earth's atmosphere after crossing the magnetosphere.

Due to all these factors, the accuracy of atmospheric models and their proxies is widely studied. There exist discrepancies between the different agencies that provide values for such parameters. The effect of these discrepancies on orbit propagation and

lifetime was analyzed with a sensitivity analysis in [32], concluding that International Earth Rotation Society (IERS) values are the most precise source for Earth Orientation Parameters (EOPs), and that Celestrak showed important gaps in their space weather information. In this same work, the most relevant contributors to the drag uncertainty were analyzed, being the following the most relevant ones:

- The usage of predicted values for atmospheric proxies ($F_{10.7}$, a_p, k_p).
- The conversion between a_p and k_p, or the usage of $E_{10.7}$ instead of $F_{10.7}$.
- The interpolation techniques for space weather parameters.
- The spatial and temporal accuracy limitations of atmospheric models.
- The inherent uncertainty between atmospheric models.
- The lack of attitude variations treatment in most OD processes.

Similarly, the structural uncertainty in the current atmospheric models is widely studied. A review of different atmospheric drag models, their algorithms, and results applied to orbit determination was carried out in [24], concluding that there is not a unique and correct implementation, or model to be used. Instead, the suitability of the different models depends on the application and research details, requiring deeper tailoring to correct specific model errors. In this same study, NRLMSISE models are found more accurate than others above 500 km of altitude. Other studies comparing some of the most used models such as the JB2008 or the NRLMSISE-00 [33] conclude that the latter contains more leading physical background and possesses a higher resolution. Additionally, density variations due to tropospheric tidal variability are not well accounted for in current density empirical models at altitudes below 400 km [34], suffering local-time and longitude-dependent density variations that require model corrections. These errors can become especially critical for re-entry predictions. In fact, the performance of empirically based atmospheric models is being re-evaluated, as well as their limitations, proposing that a general circulation model is required in the long term [35], trying to better represent the coupling between the ionosphere and the magnetosphere.

Therefore, it is found that regarding the atmospheric density and the atmospheric drag, there are several sources of uncertainty, both of epistemic (inaccuracies in the models) and aleatoric nature (variability and unpredictability of the space weather). In these cases, it is customary to deal with such sources as aleatoric, trying to characterize both the biases and the dispersion with statistical distributions such as Gaussian or stochastic models [25, 34, 36, 37]. Examples of these models for atmospheric density are described in Section 1.3.3.

At higher altitude orbits where the presence of the Earth atmosphere is negligible, the solar radiation pressure becomes one of the main perturbing forces. It is caused by the momentum transfer of the Sun photons to the space object, including their impact, reflection, absorption, and re-emission. This perturbation is driven mostly by the momentum flux of the solar particles, the area-to-mass ratio, and the solar radiation coefficient [23]. As with the drag force, the mass and cross-sectional area are assumed constant throughout the estimation arcs, which is a known source of error. The solar

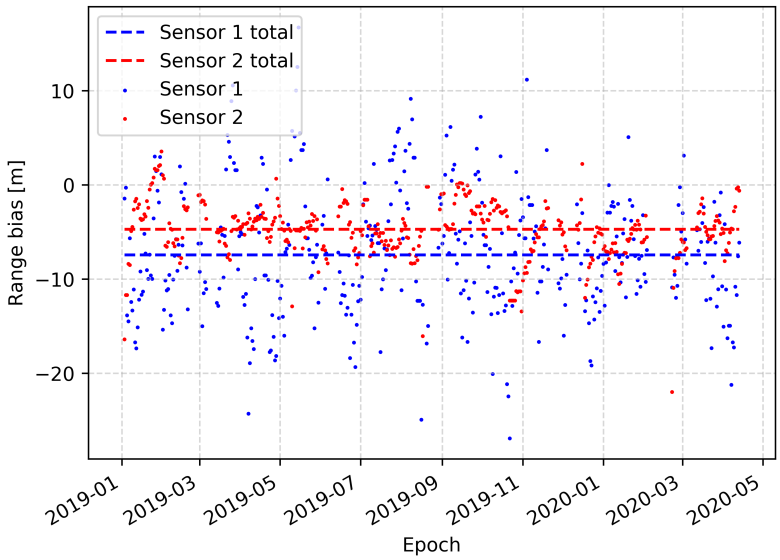

Figure 1.2: Range bias evolution with time for 2 different sensors. The calibrated biases of the sensors are shown in dashed lines (from [39]).

flux suffers aleatoric variability dependent on the solar activity, with seasonal and yearly cycles. The interaction of the photons with the object is represented in the solar radiation pressure coefficient C_{SRP}, which is affected by the reflectivity and absorptivity coefficients of the surface materials and their orientation, both unknown in SST. Similarly to the C_D, the C_{SRP} is generally estimated as part of the orbit determination process in SST and assumed as constant throughout the determination arc in classic batch least-squares estimation. Uncertainties between 1 and 3% were found in studies of the C_{SRP} variation on research satellites such as Ajisai and LAGEOS, which are sphere-shaped satellites of known size and materials [38]. Hence, errors in the SRP modeling of generic space debris are expected to be larger.

Apart from those two large sources of uncertainty in dynamic models, there exist several errors in the observations used for orbit determination that are generally disregarded. In classic orbit determination processes, the observation uncertainty is modeled by a sensor bias and associated accuracy, both being assumed constant and updated infrequently by calibration campaigns based on regulated conditions with reference satellites (typically with GNSS capabilities to have precise ephemeris as reference). Despite being mostly related to the technology of the observatory and their data processing algorithms, the sensor biases and accuracy absorb other environmental errors such as inaccuracies in the tropospheric or ionospheric corrections, or the annual and diurnal aberration. However, these errors are expected to vary depending on the geometry, environment, and time of the actual orbit determination as opposed to the calibration period, inducing errors with respect to the true observation bias. This is exemplified in Figure 1.2, where the time evolution of the range bias of two different sensors is shown. Each bias is computed comparing the real sensor observations with precise ephemeris of the analyzed object in arc-length windows of typical estimation arcs (7 days in this LEO example). The overall bias considering the complete set of measurements is depicted in dashed lines, observing a significant variability with

respect to the individual biases. Similar behavior is observed in range-rate or angular measurements [40], though it is worth mentioning that the impact of such bias errors in the orbit estimation depends on the relevance of the measurement type. In LEO orbits, range and range-rate measurements provide more accurate information for orbit determination, and thus its proper uncertainty characterization is more relevant than, for instance, radar angular measurements.

Moreover, observation errors are not only found in the measurements themselves but also in the clock time associated with the observation, which is especially relevant in MEO and GEO orbits. Errors in time biases can range from a few milliseconds in precise telescopes up to 70 milliseconds in CCD cameras [41] or even larger depending on the data processing systems [42]. Theferore, for all these reasons, uncertainty in the measurement models should be accounted for in orbit determination, which is one of the goals of this thesis. Further information about measurement errors in SST sensors can be found in chapter 5 of [11].

1.3.3 Uncertainty modeling

Although classic orbit determination methodologies such as batch least-squares or sequential filters are uncertainty quantification methods themselves, their classic formulations based on linearization are known to lack uncertainty and covariance realism unless further uncertainty characterization models are applied [28]. However, these techniques are still the core of most operational SSA and SST software due to their legacy, maturity, and favorable trade-off between achievable accuracy and computational burden. Thus, this section reviews the state-of-the-art methodologies devoted to improving the modeling and realism of the system uncertainty, some of them built on top of classical estimation methods, whereas others are transversal to orbit determination and propagation methods. More concretely, this thesis focuses on batch least-squares estimation processes, which are one of the most common algorithms used nowadays in SST. Please refer to [23, 28, 43] for further information about OD theory. Additionally, it is worth mentioning that despite being outside the scope of this thesis, there are several lines of research to improve the accuracy and reliability of classic orbit determination methods used in SST [44–47], where uncertainty realism is a key concern. A review of the state-of-the-art in OD can be found in [48].

Parameter uncertainty

Parameter uncertainty refers to the lack of knowledge of the true values of the different parameters involved in the physical models used to describe the behavior of a system. Provided that the model is able to completely represent the dynamics, the results will only be correct if the proper parameter values are used, being one of the major uncertainty sources in orbital dynamics. As summarized in [11], the treatment for the parameter uncertainty depends on observability. If the uncertain parameter can be directly estimated as part of the OD process, the effect of its uncertainty can be included in the differential equations of the dynamic system. However, the case in which the uncertain parameter cannot be included in the OD process is more complex, requiring a probabilistic treatment of the parameter, and resorting to Gaussian or stochastic models in these cases.

Process noise methods are common in filtering applications to model parameter

uncertainty in the dynamics model. It is a flexible methodology that consists in adding noise terms to the dynamics to characterize unmodeled errors, where different noise models are proposed in the literature depending on the specific problem or error source. Though still subject to debate, process noise techniques are preferred to stochastic accelerations because they are better tailored for parameter uncertainty if designed based on the physics of the problem [11]. However, process noise formulations can lose the physical traceability of their uncertainty representation since they are tailored to global process uncertainty and are based on noise fitting to observed biases [49]. Further information about process noise techniques applied to SSA can be found in [50].

Another alternative for parameter uncertainty modeling in the dynamic equations is the *consider parameter* theory [28, 51]. This methodology could be classified as a process noise technique and consists in extending the state space by including uncertain parameters in the mathematical models of the system, such as in the atmospheric force, solar radiation pressure force, or measurement models. These parameters are devised to follow a certain probability density function, which is classically chosen as a Gaussian distribution with a null mean (to maintain an unbiased estimation) and a certain variance. Then, the contribution of the parameter uncertainty to the state uncertainty is mapped through the derivatives of the *consider parameters* in the dynamics and measurement models. The *consider parameters* theory is generally associated with batch estimation, even though filtering algorithms such as in the Schmidt-Kalman filter include them [52, 53].

In general, parameter uncertainty methods have the advantage of being able to track the effect of specific physically-based uncertainties while maintaining a tractable level of complexity and computational cost, especially when simplified to Gaussian models such as in the *consider parameters* theory, which makes them suitable for operational systems. However, they present two major drawbacks. On the one side, realistic values for the uncertain parameters are unknown in SST. This indicates the necessity of developing cost-effective uncertainty estimation methodologies to improve realism in operational environments, which as mentioned in Section 1.2, is one of the main objectives of the thesis. On the other side, Gaussian and constant-error models as applied in the *consider parameters* theory or other process noise models do not characterize adequately the behavior of stochastic variables such as the aforementioned atmospheric density.

Stochastic uncertainty models

For the inverse problem, a widely studied option to characterize the structural uncertainty in the dynamics is to revisit the deterministic assumption of the underlying mathematical models. To this end, process noise or Stochastic Differential Equations (SDE) are proposed in the literature in order to account for the unmodeled uncertainty sources, where different approaches are presented depending on the target source. However, the most recurrent uncertainty source in SST where stochastic models have been widely proposed is the aforementioned aleatoric behavior of atmospheric drag.

White noise is a customary first approach to represent the drag uncertainty during OD and prediction. A time-dependent atmospheric density error model based on white and Brownian noise for the representation of the solar flux proxies is derived in [54], where historical data is used to adjust the noise parameters. Following up on their work, in [55] a state vector error covariance matrix in Geocentric Celestial Reference Frame (GCRF) frame

[56] is developed analytically to model the atmospheric drag uncertainty by including a white noise model for the most relevant proxy for atmospheric density, the solar flux $F_{10.7}$. While white noise is applied during the estimation, Brownian motion is applied to propagation, extending the classical batch weighted least-squares and sequential batch weighted least-squares formulation. Further impact on density fluctuations on orbit prediction was analyzed in [34, 36, 37].

Trying to represent more closely the complexity of the stochastic behavior of the atmospheric density and drag force, Ornstein-Uhlenbeck models can be proposed. These families of noise processes are also based on white noise but include several parameters that are able to control the tendency to a mean value. This interesting property can be exploited to model stochastic atmospheric density, which is known to follow mean variations due to day-night or yearly cycles. Time-dependent parameters defining this stochastic model are proposed in [57], so that the noise is able to follow the expected large-scale fluctuations of the thermospheric density. In their work, the properly tuned Ornstein-Uhlenbeck noise is shown to represent the stochastic behavior observed when applying different state-of-the-art atmospheric density models.

Other authors suggest that the atmospheric model uncertainty should present correlation, both in time and space. The objective is to model the physical phenomena in space dynamics for which perturbations occurring at consecutive time steps or close spatial positions are subjected to similar sources (i.e. similar altitudes or location and space weather activity), and thus their unmodeled error should present certain correlation. A widely studied family of stochastic noise that allows the inclusion of different correlation time-scales for uncertainty modeling are the Gauss-Markov processes (having 1st and 2nd order schemes) [58]. In [51], nominal batch estimation was compared against Kalman filter estimation, the latter implementing a Gauss-Markov model as process noise. It was found the covariance matrix of the Kalman estimation yielded better covariance realism for longer propagation. Moreover, the noise correlation scales (whether temporal or spatial) can be estimated as part of the estimation process by state augmentation [59] or other estimation techniques (chapter 4 of [53]), though applications to SST are not generally found due to the large complexity of introducing these techniques in operational contexts.

Other methodologies

This subsection gathers other relevant methodologies devoted to improving uncertainty realism without focusing on specific models of the uncertainty sources.

Empirical covariance

Empirical covariance methods arise as an alternative to compute the complete uncertainty in the estimation process, not requiring historical data and without the assumption of noise invariance [60]. The concept behind the empirical state error covariance matrix is to include all the uncertainty reflected in the measurements residuals, not only the expected accuracy of each measurement [61]. This can be achieved by keeping the outer product of the measurements, maintaining the statistical form of the least-squares solution but achieving a statistical expression for the covariance of the state. The expectation of this state error covariance matrix coincides with the nominal noise-only covariance. This formulation allows to include all the uncertainty present in the measurements, being able to account for punctual variations in the noise. The

1

two main drawbacks of this methodology are that the different sources of uncertainty cannot be distinguished, losing the physical interpretation, and that a high amount of measurements are required, which is not always the case in data-starved contexts such as SST.

Particle filters

Particle filters can be defined as Monte Carlo sequential methods where arbitrary non-Gaussian distributions are represented by a set of samples, where the selection, combination, and regeneration of these samples define the different varieties of particle filter methods [62, 63]. Thus, they allow the generalization of linear filtering techniques to handle nonlinear and non-Gaussian dynamical and measurement models. They have been applied mostly to object tracking [64, 65].

Inflation techniques

As previously described, the nominal covariance matrices obtained with classic batch least-square methods or sequential filters are known to lack realism when they only account for the observation uncertainty, in this case leading to overly-optimistic covariance (i.e. smaller than the true uncertainty). For this reason, inflation techniques are proposed to artificially increase the covariance size, trying to improve its realism. In [66], a covariance inflation is proposed based on increasing the initial position uncertainty to match the observed velocity error, trying to overcome non-linearities in the propagation after Initial Orbit Determination (IOD). Even though the scaling of the initial covariance tends to overestimate the true uncertainty in position, the evolution of the covariance along time is expected to contain better the true uncertainty upon propagation, until large-scale non-linearities build-up. Others authors explore the usage of the Mahalanobis distance of the orbital differences to find a scale factor for the covariance [67], either a specific one for each principal component of the covariance or a single correction factor. This has the advantage of yielding a significant improvement of the covariance realism since the scaling factors are found after fitting observation data. However, the artificial scale factors are not representative of particular uncertainty sources, complicating the physical traceability of the solution and preventing the extrapolation of the results to other similar uncertainty processes or objects of the catalogs, being only representative of the current model observations. Nonetheless, the versatility of these sort of methods lead to their use nowadays in operation centers such as the JSC [11], previously mentioned.

Alternative state representation

The state representation, that is, the set of variables used to represent the state, has a significant influence on covariance realism and its maintenance during orbit propagation. The effect of non-linearities in uncertainty propagation considering three different representations of the state vector (position and velocity in Cartesian space, osculating polar variables or mean Keplerian orbital element) was analyzed in [68], concluding that the mean Keplerian orbital elements representation provided the best fit to Monte Carlo simulations and provided a longer uncertainty realism maintenance. A similar analysis was conducted in [69], this time comparing between osculating position and velocity, osculating equinoctial elements, and mean equinoctial elements [70], finding that the latter option resulted in a better covariance representation. Therefore, it can be inferred that severe discrepancies arise from using Cartesian reference frames instead of element-based systems such as orbital elements, as well as from the linearization of errors

in non-linear equations of motion. However, despite the multiple realism advantages of using equinoctial or other osculating elements, their use is mainly extended in trajectory analysis and optimization, and they are not extensively used in SST due to their complexity and difficult compatibility with operational systems.

For this reason, other non-linear reference frames are proposed in the literature. In [12], a curvilinear set of coordinates is proposed to overcome the limitations of polar coordinates for elliptical orbits. This proposal is based on the local orbital frame TNW, but in this case employing a normal axis (cN) that is always normal to the closest point of the nominal orbit, instead of being normal to the velocity. Similarly, a precise transformation between Cartesian and curvilinear coordinates following the orbit motion is presented in [71], in this case taking advantage of Clohessy and Wiltshire relative motion coordinates [72]. In [73], the QtW reference frame is introduced, which allows to capture the curvature of the orbit motion by including the effect on time in the frame definition, reducing the non-linearity and delaying the degradation of the uncertainty realism. Starting from the well-known QSW local orbital frame [74], this frame performs a time-dependent transformation in the along-track direction (S), transforming it into a relative time with respect to a reference or mean orbit position.

Additionally, other authors suggest using specifically derived PDFs that are able to describe more accurately the uncertainty characteristics of the orbital motion. Typical Gaussian uncertainty ellipsoids fail to represent the so-called "banana-like" shape of the uncertainty after some propagation time. The representation of the state uncertainty in a cylindrical manifold obtained by a combination of Gaussian and Von-Mises distributions is proposed in [75]. They represent the first five components of the state in equinoctial elements with a multivariate Gaussian distribution, and the last angular components with Von-Mises one. This representation of the uncertainty is able to adapt to the curvature of the dynamics, allowing to retain the uncertainty realism.

1.3.4 Covariance realism assessment

In order to achieve uncertainty or covariance realism, it is customary to define first how to measure the level of realism. In the SST community (and astrodynamics in general), this is generally done by resorting to different statistical metrics to evaluate the underlying hypothesis, which in the case of covariance realism, corresponds to unbiasedness, consistency, and the correct representation of the mean and covariance of the distribution. It is worth mentioning that, among the wide variety of statistical analysis metrics available [76], metrics suitable for covariance realism in SST are sought to be generic (non system-dependent), agnostic to the coordinate systems, non-intrusive (to facilitate its applicability), computationally efficient and robust. The most relevant metrics applied in the context of this thesis are described next, though further options and descriptions can be found in [11, 77].

A well-known metric used for statistical analysis of Gaussian distributions is the Mahalanobis distance, which represents how far a sample state is from a reference state, while projecting it into the covariance space - see Equation (2.17) [78]. In other words, this metric describes how far the sample state is from the reference in terms of covariance size. Though originally devised for Gaussian distributions, the Mahalanobis distance can be generalized for non-Guassian distributions as described in Chapter 8 of [11], where

other alternatives such as the averaged uncertainty realism metrics are also proposed.

Under Gaussian and linear assumptions, the Mahalanobis distance has the property of behaving as a $\chi^2(N)$ distribution, where N corresponds to the number of Degrees of Freedom (DoF), in this case, the number of state variables. The χ^2 distribution is defined as the sum of the square of N mutually independent standard normal distributions [76]. It is relevant to highlight the requirement of independent normal distributions for the corresponding DoF of the χ^2 distribution. In the case of the Mahalanobis distance, it implies that no correlation exists between the sample state and the reference, which is an assumption found in several studies [11, 79]. However, this may not be the case in applications with real data, where the reference orbit used for the Mahalanobis distance is also subject to model errors and obtained via orbit determination and propagation with common sensors or dynamic models. Additionally, orbit states obtained from subsequent orbit determination arcs may share a large fraction of the observations, leading to highly correlated estimates. Though further detailed in the papers included in this dissertation, the impact of this correlation is minimized as follows:

- The uncertainty is quantified in the covariance of both states in the Mahalanobis distance (sample and reference).
- The reference state does not share any observation with the sample state on its orbit determination arc.
- The sample state does not share more than 30% of the observations with the next sample state (as a trade-off due to the limited availability of real data).

Thus, if the state covariance is such that the Mahalanobis distance distribution is found to be unbiased (null-mean), consistent with the number of samples, and follows the theoretical χ^2 behavior, then the covariance is defined as realistic. Therefore, a distribution matching between the test and target distributions can be applied to assess the achieved level of realism. A wide family of statistical comparison techniques is the Empirical Distribution Function (EDF) statistics, which measure the discrepancy between the Cumulative Distribution Functions (CDFs) of the test and reference distributions. In general, they are based on the empirical approximations of the CDF of the target distribution, and its comparison against the observed CDF of the test distribution. Throughout this thesis, the Kolmogorov-Smirnov (KS) and Cramer-von-Mises (CvM) test statistics have been explored, two of the most relevant EDF metrics in SST. The former corresponds to a supremum statistic, consisting in measuring the maximum absolute difference in the CDFs of the distributions. It has been widely used in the literature due to its flexibility and suitability for realism bounds analysis, which facilitates its interpretation for normality tests [77], or other applications such as conjunction analysis [80]. However, this EDF test has insufficient statistical power, that is, it tends to favor the null hypothesis, as only 1-point of the distribution is being tested rather than analyzing the mean, scale, or shape of the distribution, as discussed in [77]. Regarding the Cramer-von-Mises test, it corresponds to a quadratic statistic in a least-square sense. This metric is considered more statistically meaningful than the previous one since it accounts for the differences of all the points of the distribution, rather than the maximum difference. Moreover, it is more

robust to the number of statistical samples, being able to correct for tail sensitivity better than other methods [11]. Other relevant EDF metrics are the Pearson's Chi-squared test, the Anderson-Darling statistic, or the Watson statistic (focused on circular probability). Further details about these EDF metrics or other alternatives can be found in [76], though a detailed description of the applied Cramer-von-Mises and Kolmogorov-Smirnov tests can be found in the methodology of the papers included in this dissertation.

Another relevant metric to assess covariance realism is the covariance containment [43, 66]. It consists in evaluating the amount of samples of the test distribution that are contained inside different $k\sigma$ ellipsoids of the covariance, with $k \in [1, 2, 3, 4]$. At each σ-level, the fraction of samples laying inside is compared against the theoretical fraction expected from a multi-variate Gaussian distribution of the same dimension [66]. This metric benefits from a more visual representation of the covariance realism level, being simpler and more tractable to the physical properties of the covariance, making it suitable for operational SST applications.

Finally, it is worth discussing the validity of the core assumptions of covariance realism, that is, Gaussianity and linearity. Even though space dynamics are highly non-linear, linear assumptions are the core of many orbit determination and propagation algorithms such as batch estimation or Kalman filters, where the covariance is also linearly propagated. These assumptions are expected to deteriorate for sufficiently long arcs, both in orbit determination and in propagation, due to the accumulation of non-linearities. SST algorithms try to minimize this problem by selecting suitable dynamic model arc lengths of validity depending on the orbital regime and the acting perturbing forces [81]. Operational trade-offs in SST range from short arcs between 1 to 3 days at low altitude orbits (subject to high drag non-linearities), 7 to 10 days in higher LEO orbits, and up to more than 20 days in MEO and GEO, considering the typical estimation uncertainty. In this thesis, linear covariance propagation was chosen due to compatibility with operational systems and computational efficiency, while expecting to maintain its accuracy for the appropriate estimation and propagation arcs. More complex uncertainty propagation methods more suitable when Gaussian assumptions are not maintained, are left out of the scope of this thesis. Nonetheless, it is necessary to check the validity of such assumptions prior to applying uncertainty modeling techniques tailored for covariance realism improvement. Throughout this thesis, Michael's normality tests were carried out [82, 83] both with simulated and real data. It allows a straightforward visual representation of the acceptable Gaussianity region in a normal probability plot, being shown more robust than the Kolmogorov-Smirnov normality test due to its powerful tail outlier rejection.

2

Covariance determination for improving uncertainty realism in orbit determination and propagation

2.0 Scientific contribution and context

This paper proposes the *Covariance Determination* methodology, a novel algorithm to improve covariance realism in operational scenarios. Firstly, the *consider parameters* theory is proposed to model the uncertainty during batch least-squares orbit determination. Then, realistic values for the *consider parameter* variances are obtained based on the Mahalanbis distance from orbital differences between estimated and propagated orbits, which is fitted to the theoretical χ^2 distribution by minimizing an EDF metric. On realistic simulation environments, this paper focuses on the most relevant sources of uncertainty in LEO: drag model, atmospheric proxies, and range bias.

Therefore, the main contribution of the paper is the novel methodology to quantify uncertainty with simple yet effective models of the uncertainty (*consider parameters*), showing a remarkable covariance realism improvement with significant operational suitability. As part of the methodology, a relevant contribution is the use of estimated orbits, yet uncorrelated, as reference orbits for the computation of the Mahalanobis distance, as opposed to having an assumed "true" orbit, or precise ephemeris, which is not generally available for non-collaborative objects such as space debris. This avoids the use of external data to quantify the uncertainty. Another relevant contribution of this paper is the validation of multiple consider parameters optimization, showing that it is possible to correctly decouple the impact of the different sources of uncertainty even if only quantifying it by comparing predicted and estimated ephemeris.

In the context of the thesis, this was the first paper to establish and validate the *Covariance Determination* methodology, which was to become a solid base from which to continue improving the uncertainty models and their operational applicability. The reader is advised most of the contents of the introduction of this manuscript share content with Section 1.3, as the introduction of this paper was planned to give a wide overview of the uncertainty modeling and sources, especially in LEO orbits.

A. Cano[1,2], **A. Pastor**[1], **D. Escobar**[1], **J. Míguez**[2], **M. Sanjurjo-Rivo**[2],
[1]GMV, 11 Isaac Newton, 28670 Tres Cantos, Madrid, Spain,
[2]Universidad Carlos III de Madrid, 30 Avenida Universidad, 28911 Leganés, Madrid, Spain,
Advances in Space Research (2022) 69: 1394–1420
10.1016/j.asr.2022.08.001

2

The reliability of the uncertainty characterization, also known as uncertainty realism, is of the uttermost importance for Space Situational Awareness (SSA) services. Among the many sources of uncertainty in the space environment, the most relevant one is the inherent uncertainty of the dynamic models, which is generally not considered in the batch least-squares Orbit Determination (OD) processes in operational scenarios. A classical approach to account for these sources of uncertainty is the theory of consider parameters. In this approach, a set of uncertain parameters are included in the underlying dynamical model, in such a way that the model uncertainty is represented by the variances of these parameters. However, realistic variances of these consider parameters are not known a-priori. This work introduces a methodology to infer the variance of consider parameters based on the observed distribution of the Mahalanobis distance of the orbital differences between predicted and estimated orbits, which theoretically should follow a chi-square distribution under Gaussian assumptions. Empirical Distribution Function statistics such as the Cramer-von-Mises and the Kolmogorov-Smirnov distances are used to determine optimum consider parameter variances. The methodology is presented in this paper and validated in a series of simulated scenarios emulating the complexity of operational applications.

Keywords: uncertainty realism, covariance realism, space situational awareness, covariance determination, Mahalanobis distance, Cramer-von-Mises, Kolmogorov-Smirnov

2.1 Introduction

The provision of most of the services in Space Traffic Management (STM) and SSA relies on the proper characterization of the orbital uncertainty. This is known as uncertainty realism, and focuses on the correct representation of the Probability Density Function (PDF) of the orbital state. Uncertainty realism can be reduced to covariance realism under Gaussian assumptions, requiring not only an unbiased estimation but also covariance consistency (correct covariance orientation, shape, and scale). When these requirements are met, the PDF representing the uncertainty of the system can be fully characterized by its two first moments, gathered in a state and its associated covariance matrix. These are strong assumptions, though widely applied in operational SSA environments, where Resident Space Objects (RSOs) uncertainty is represented by the state and its associated covariance. Thus, covariance realism can be understood as a necessary but not sufficient condition for uncertainty realism. The misrepresentation of the uncertainty of a RSO impacts STM and SSA products, being crucial for various tasks: RSO cataloging, collision risk assessment, fragmentation analysis, re-entry prediction, track association, manoeuvre detection or sensor tasking and scheduling, among others. Many existing Orbit Determination processes are based on weighted batch least-squares theory and provide the estimation (state and covariance) as the nominal output, given

that measurements are sufficient and available. Along this process, the dynamical model defining the motion of the orbiting object is assumed to be deterministic, and the estimation accuracy is determined considering only the uncertainty of the observations [23]. The resulting covariance matrix in this estimation process is known as the noise-only covariance [28]. However, one of the main sources of uncertainty during OD and subsequent propagation arises from the errors in the underlying dynamical models, which are typically disregarded [28, 84]. For instance, when the ballistic coefficient is estimated in an OD process, the uncertainty of the atmospheric model is not considered, and thus the induced uncertainty on the rest of the state is not accounted for during the orbit determination and propagation. This results in overly-optimistic noise-only covariance matrices, which causes the covariance realism to degrade since the atmospheric density uncertainty will have an impact on the uncertainty of the estimated state, especially in the along-track position direction [56].

Therefore it is customary, for SSA and particularly for Space Surveillance and Tracking (SST) purposes, to characterize and determine the inherent uncertainty in the dynamic or measurement models and their effects, which is commonly known as uncertainty quantification (UQ). Two fundamental problems can be distinguished for uncertainty quantification. On the one hand, the quantification of the uncertainty present in the system models, parameters, or data, also known as the inverse problem or inverse UQ [11]. On the other hand, the propagation of uncertainty (UP). The latter concentrates on how to characterize the evolution of the system uncertainty, accurately and efficiently. Most UP methods focus on the propagation of an initially given Probability Density Function (PDF) of a state, though there exist methods for the propagation of epistemic uncertainty that do not rely on PDF propagation [25]. However, this is not the focus of the present work, where linearized propagation techniques are used. The inverse problem, on the contrary, consists in assessing the differences between the observed behavior of a system and the underlying models and parameters used to represent it. This is the target of the work at hand.

Regarding the uncertainty in the modeling, a possible (not exclusive) approach is to revisit the deterministic assumption in the equations of motion. Specifically, one may account for the model uncertainty by introducing stochastic dynamics or process noise, exploring different stochastic modeling such as Brownian motion, Ornstein-Uhlenbeck or Gauss-Markov processes [11]. The inverse problem also tackles the parameter uncertainty, this is, the modeling of uncertain parameter present in the dynamics or measurements equations. If the uncertain parameter (whether static or time-dependent) can be observed or estimated, it is possible to include its impact in the evolution of the differential equations of motion. In the end, the goal of parameter uncertainty modeling is not only the a-posteriori quantification of the errors, but also to represent the relationship between the uncertain parameter and the state variance.

There exists a wide variety of techniques that target directly the complete inverse problem. Process noise methods, which consist in including additional noise terms in the dynamics to account for un-modeled error sources, are generally accepted over stochastic acceleration methods since they can account for both dynamic model and parameter uncertainty, especially if they are physically-based [11]. However, many

process noise solutions, based on noise fitting to observed orbital uncertainty, lack the physical meaning of the different sources of the uncertainty since they are focused on global process uncertainty rather than each individual source. For instance, process noise estimation via calibration process is proposed in [49, 50]. Even though these techniques are typically used for filtering applications rather than in batch processing, some works describe the computation of a process noise matrix that accounts for the drag uncertainty and include it in the batch least-squares estimation process [55]. Other approaches suggest the use of empirical covariance matrices to include all residuals of the estimation process in the covariance computation, regardless of whether the uncertainty has been modeled or not [60, 61, 85]. This proposal claims to account more accurately for noise time-variations rather than process noise or *consider parameter* analysis, at the expense of missing the physical interpretation of the uncertainty. Finally, particle filters are also a state-of-the-art technique that allows to retain higher moments of the target PDF by the selection of specific sigma points in pseudo Monte Carlo analysis [65]. The key of these methods is the trade-off between accuracy and computational cost.

Therefore, uncertainty (and covariance) realism improvement is a direct consequence of reaching the UQ goals, this is, the characterization of the system uncertainty. However, apart from the aforementioned UQ methods, there are other techniques conceived to improve covariance realism without focusing on the sources of uncertainty and their modeling. For instance, state distribution in mean elements may be better represented by a multivariate normal distribution [68, 86]. Other typical representations of the state and covariance in non-linear reference frames that are able to slow down the realism degradation upon propagation are being widely studied, such as in [73]. In an operational environment, operators require simple techniques in order to improve covariance realism since, as previously discussed, the nominal batch least-squares OD processes provide optimistic covariance estimations when only accounting for the measurements uncertainty. The most common options are: (1) the previously mentioned process noise and (2) scaling techniques, which inflate the covariance by means of scaling factors. Some authors propose the computation of such scaling based on increasing the initial position uncertainty to match the velocity error [66]. Others explore the use of the Mahalanobis distance of the orbital differences to find the scale factor [67]. However, a common drawback of artificially increasing the covariance is that the physical meaning of the correction is lost, not being able to understand the contributions of each source of uncertainty. These sort of methods based on artificially scaling the covariance matrix are used nowadays in operation centers such as the Space Operations Center (CSpOC) [11].

It is seen that simple and reliable UQ method that provide realistic characterization of the uncertainty are required by operators nowadays. One of the classical approaches for parameter UQ in the dynamic equations is the *consider parameters* theory, which can be classified within the process noise techniques [28]. It consists in extending the state space by including parameters in the dynamic models, such as atmospheric force, solar radiation pressure force or measurement models. These parameters are devised to follow a certain model with its corresponding uncertainty, e.g. a Gaussian distribution with a null mean (to maintain an unbiased estimation) and a certain variance. This allows the representation of unaccounted error sources of the dynamical or measurement models by including the parameter uncertainty. This formulation can be combined with batch estimation or

filtering algorithms such as in the Schmidt-Kalman filter [52, 53]. This approach provides the advantage of tracking the effect of the specific uncertain physically-based parameters that are included, as opposed to artificial scaling factors. However, one of the main drawbacks of the *consider parameter* theory is that realistic variances of such parameters are not normally known, a common problem in process noise methods. Overly optimistic, or oversized, variances may fail to model the uncertainty of parameters in the estimation and subsequent propagation of the covariance, not achieving covariance realism.

The aim of this work is to present a novel methodology to determine the variance of the considered parameters to improve the realism of the state covariance matrices obtained from operational OD processes. The method is based on the orbital differences between estimated and predicted orbits. Under Gaussian assumptions, the differences between both orbits projected into the covariance space, i.e. Mahalanobis distance, should follow a χ^2 distribution to achieve covariance realism. Thus, the variance of the *consider parameters* can be determined by means of a statistical comparison process between the observed Mahalanobis distance distribution and the expected one, i.e. a χ^2 distribution. We refer to estimated orbits as those ones obtained after an Orbit Determination process, backed up with observations. Predicted orbits refer to the propagation of those estimates with the same dynamical model to the future. The work carried out focuses on Low Earth Orbits (LEO) regimes, tackling some of the most relevant uncertainty sources such as the atmospheric density in the drag force acceleration, the range bias in the radar measurements or the solar proxies prediction [24].

A precursor analysis based on the *consider parameter* theory to improve the covariance realism is performed in [87]. There, it is proposed to correct the noise-only covariance with a least squares fitting to a so-called observed covariance, the latter being obtained as an empirical covariance based on orbital differences from a statistically representative population of different orbit determinations. This approach has a main drawback. To compute such empirical covariance, orbital differences corresponding to multiple orbital positions and observation scenarios (observations geometry, number of measurements, etc) are mixed. In the work presented here, this issue is mitigated by the normalization obtained with the Mahalanobis distance, which is the cornerstone of the work in this paper. The estimated covariance in a batch least-squared process is affected as well by the orbit position of the estimation epoch and the observation scenario. Thus, orbital differences normalized by their associated covariance (i.e. Mahalanobis distance) could be treated as samples from the same distribution, concretely as a χ^2 distribution under Gaussian assumptions if the covariance is realistic, since as discussed later, the Mahalanobis distance of each sample shall be constant in time under certain assumptions. Preliminary studies that analysed the applicability of this methodology to LEO or GEO regimes can be found in [88, 89], respectively.

The remainder of the paper is organized as follows: in Section 2.2 the *consider parameter* theory is reviewed and the methodology is presented. In Section 2.3, the simulation process and environment are described. Next, the results of the proposed covariance determination methodology are shown in Section 2.4. The focus is placed on the physical interpretation of the *consider parameter* variances obtained and the level of covariance realism enhancement achieved. Finally, Section 2.5 summarizes the conclusions of this

work and the future work to be performed.

2.2 Methodology

This section revisits in first place the *consider parameters* theory and its direct effect on the covariance computation. Then, the specific formulation derived to include the *consider parameter* theory in the Mahalanobis distance computation is described. Finally, the *consider parameter* models devised in this work are defined.

2.2.1 Consider parameters theory in batch least-squares algorithm for orbit determination

The complete description of the *consider parameter* theory (or consider covariance analysis, as termed by some authors) can be found in many references such as [23, 28]. For brevity, only the final derivation in the nominal batch least-squares process is described next. Let us define the estimated state vector as

$$\mathbf{y}_{\mathbf{est}} = \begin{pmatrix} \mathbf{r}(t) \\ \mathbf{v}(t) \\ \mathbf{p}(t) \end{pmatrix} \in \mathbb{R}^{n_y}, \tag{2.1}$$

being $\mathbf{r}(t)$, $\mathbf{v}(t)$ and n_y the position, velocity and estimated state dimension, respectively. $\mathbf{p}(t)$ represents the estimated parameters, either applied to the force or the measurement models. Typical examples of these parameters are the Drag Coefficient (C_d) in LEO orbits or the Solar Radiation Pressure Coefficient (C_r) in GEO. The *consider parameters* to be modeled in our system can be gathered in a *consider parameter* vector

$$\mathbf{y}_c = \begin{pmatrix} c_1 \\ \vdots \\ c_n \end{pmatrix} \in \mathbb{R}^{n_c}, \tag{2.2}$$

where n_c is the number of *consider parameters*. They are defined to follow a Normal distribution of the form

$$c_i \sim \mathrm{N}\left(0, \sigma_i^2\right), i = 1, \cdots, n. \tag{2.3}$$

The null mean definition allows the expected value of the orbit estimation to remain unbiased [28]. On the contrary, the covariance of the estimation is affected. Recalling the nominal batch least-squares estimation, the noise-only covariance is

$$\mathbf{P}_n = \left(\mathbf{H}_y^T \mathbf{W} \mathbf{H}_y\right)^{-1} \in \mathbb{R}^{n_y \times n_y}, \tag{2.4}$$

where $\mathbf{H_y}$ corresponds to the Jacobian of the observations with respect to the estimated state, and $\mathbf{W}$ is the weighting matrix containing the confidence of each measurement and the possible correlation among the measurements. Then, the consider covariance results in:

$$\mathbf{P}_c = \mathbf{P}_n + \left(\mathbf{P}_n \mathbf{H}_y^T \mathbf{W}\right)\left(\mathbf{H}_c \mathbf{C} \mathbf{H}_c^T\right)\left(\mathbf{P}_n \mathbf{H}_y^T \mathbf{W}\right)^T, \tag{2.5}$$

where $\mathbf{H}_c$ is the Jacobian of the observations with respect to the *consider parameters* and

$$\mathbf{C} = \begin{pmatrix} \sigma_1^2 & \cdots & 0 \\ \vdots & \ddots & \vdots \\ 0 & \cdots & \sigma_n^2 \end{pmatrix}, \tag{2.6}$$

contains the variances of the *consider parameters*, where no correlation between them is assumed. Equation (2.5) can be simplified to obtain

$$\mathbf{P}_c = \mathbf{P}_n + \mathbf{K}\mathbf{C}\mathbf{K}^T \in \mathbb{R}^{n_y \times n_y}, \tag{2.7}$$

with

$$\mathbf{K} = \mathbf{P}_n \left(\mathbf{H}_y^T \mathbf{W} \mathbf{H}_c\right) \in \mathbb{R}^{n_y \times n_c}, \tag{2.8}$$

where n_c is the number of *consider parameters*. Therefore, the consider covariance is obtained as the noise-only covariance plus a covariance correction, which depends linearly on the *consider parameter* variances.

2.2.2 Consider parameters effect in orbit propagation

The consider covariance is obtained at estimation epoch and models the effect of the uncertainty of the *consider parameters* that affect the estimation, regardless whether their uncertainty affects the force or the measurement model. However, our interest in enhancing the covariance realism extends also to the covariance propagation for SST purposes. In this paper, we assume linear propagation of the covariance matrix, as it is generally applied in most operational scenarios in SST. More complex and accurate uncertainty propagation methods are out of the scope of this work since Gaussianity is a cornerstone assumption in the proposed methodology. In this respect, Michael's normality tests can be applied to assess data linearity [82, 83]. A complete derivation of linear propagation theory can be found in many well-known references, such as [28]. First, let us define the extended state vector as

$$\mathbf{y_{ext}} = \begin{pmatrix} \mathbf{r}(t) \\ \mathbf{v}(t) \\ \mathbf{p}(t) \\ c_1 \\ \vdots \\ c_n \end{pmatrix} \in \mathbb{R}^{n_y + n_c}, \tag{2.9}$$

which is composed of the estimated parameters plus the *consider parameters* of our analysis. In the end, to account for the effect of the main dynamic parameters in the propagation of the state, it is required to integrate the variational equations. Its solution is the Extended State Transition Matrix (ESTM)

2

$$\boldsymbol{\Psi}(t,t_0) = \begin{pmatrix} \boldsymbol{\Phi}(t,t_0) & \mathbf{S}(t,t_0) \\ \mathbf{0} & \mathbf{I} \end{pmatrix} \tag{2.10}$$
$$\boldsymbol{\Psi} \in \mathbb{R}^{(n_y+n_c)\times(n_y+n_c)};\ \boldsymbol{\Phi} \in \mathbb{R}^{6\times 6};\ \mathbf{S} \in \mathbb{R}^{6\times n_p};\ \mathbf{I} \in \mathbb{R}^{n_p\times n_p}$$

where:

- n_p is the number of dynamical parameters to consider during propagation, which in this case corresponds to the estimated dynamical parameters plus the *consider parameters*, excluding position and velocity, hence, $n_p = (n_y - 6) + n_c$
- $\boldsymbol{\Phi}(t,t_0)$ corresponds to the state transition matrix, which relates the position and velocity at any time t with respect to the initial state at time t_0.
- $\mathbf{S}(t,t_0)$ is the so-called sensitivity matrix, which contains the partial derivatives of the state vector with respect to the model dynamical parameters, both estimated and considered. These parameters are defined as constant in the dynamic model as is customary in many propagation methods [23], though in this case having a certain variance that the proposed methodology intends to estimate.

The ESTM can be computed by solving numerically its associated partial differential equations as shown in [28]. The typical linear covariance propagation applying the state transition matrix would be

$$\mathbf{P}_n(t) = \boldsymbol{\Phi}(t,t_0)\mathbf{P}_n(t_0)\boldsymbol{\Phi}(t,t_0)^T. \tag{2.11}$$

However, to account for the effect of the uncertainty of the *consider parameters* in our covariance propagation, we define the extended consider covariance

$$\mathbf{P}_{c_{ext}}(t_0) = \begin{pmatrix} \mathbf{P}_c & \mathbf{0} \\ \mathbf{0} & \mathbf{C} \end{pmatrix} = \begin{pmatrix} \mathbf{P}_n + \mathbf{KCK}^T & \mathbf{0} \\ \mathbf{0} & \mathbf{C} \end{pmatrix} \in \mathbb{R}^{(n_y+n_c)\times(n_y+n_c)}, \tag{2.12}$$

where in addition to the classical consider covariance, the uncertainty of the *consider parameters* is also explicitly included. Thus, the extended covariance at any time, using the ESTM, is

$$\mathbf{P}_{c_{ext}}(t) = \boldsymbol{\Psi}(t,t_0)\mathbf{P}_{c_{ext}}(t_0)\boldsymbol{\Psi}(t,t_0)^T. \tag{2.13}$$

By using the ESTM, the effect of the uncertainty of the model parameters is mapped into the position and velocity covariance not only at estimation, but also along the propagation. Of course, depending on the choice of *consider parameters*, they may affect only the estimation process, the propagation process, or both. This is a relevant factor to take into account in the analysis, and is further discussed for each *consider parameter*. The goal of the work at hand is to determine the values of $\mathbf{C}$ so that the consider covariance realism is improved.

2.2.3 Specific consider parameters

In this section, the main *consider parameters* that have been modeled in our work are presented. All of them follow the definition of Equation (2.3). The general methodology presented in Sections 2.2.1 and 2.2.2 allows to include any desired *consider parameter* in the dynamic or measurement model. A relevant benefit of this methodology is that each parameter can be defined to model a specific uncertainty source, tailored to any orbital regime, which in principle allows to maintain the trace of the error sources. However, this traceability can be compromised by the correlation between the different *consider parameter* models, which may lead to the contribution of each uncertainty source to be hard to decouple. Therefore, another target of the work presented here is to assess the ability of the proposed methodology to maintain such traceability.

Aerodynamic model consider parameter

The classical drag force equation including the aerodynamic model consider parameter is defined as:

$$\mathbf{a}_{\text{drag}} = -\frac{1}{2}\rho\frac{C_d A}{m}\|\mathbf{v}_{\text{rel}}\|^2\frac{\mathbf{v}_{\text{rel}}}{\|\mathbf{v}_{\text{rel}}\|}(1+c_{AE}), \tag{2.14}$$

where ρ is the atmospheric density, C_d the drag coefficient, A the cross-sectional area, m the object mass and $\mathbf{v}_{rel}$ is the relative speed vector of the object with respect to the atmosphere. Finally c_{AE} is the *consider parameter*, whose objective is to model the error in the atmospheric density and ballistic coefficient, containing C_d as well as mass and cross-sectional area uncertainty. The uncertainty of this parameter affects both the estimation and propagation arc.

Range bias

This parameter is included to represent possible errors in the measurement model and calibration process. In this case, the measurement model becomes

$$z^* = z + c_z, \tag{2.15}$$

where z represents the range measurement and c_z is the range bias error *consider parameter*. Note that Equation (2.15) could represent any other measurement retrieved from a sensor, which in the case of a typical radar for SST purposes includes azimuth and elevation angles, range and range rate. The purpose of this *consider parameter* is to model the variance of the range bias of the sensor network, modeled as constant for each OD arc. Even though a sensor network mean bias can be applied after sensor calibration using previous data, an error is committed in subsequent OD arcs. The uncertainty of such error is what the proposed range bias *consider parameter* aims to model.

Atmospheric proxies prediction consider parameter

The aim of this parameter is to represent another relevant source of uncertainty in LEO, related to the uncertainty associated to the prediction of the atmospheric $F_{10.7}$ or A_p proxies that are used to compute the atmospheric density at future times. Not only the proxies observations may vary depending on the source, but also the predicted values

error represent a relevant uncertainty source [32]. The *consider parameter* c_{PE} model is introduced in the drag force, namely,

$$\mathbf{a}_{\text{drag}} = -\frac{1}{2}\rho\frac{C_d A}{m}\|\mathbf{v}_{\text{rel}}\|^2\frac{\mathbf{v}_{\text{rel}}}{\|\mathbf{v}_{\text{rel}}\|}\left(1+c_{PE}\cdot t_{\text{pred}}\right), \tag{2.16}$$

where t_{pred} is the prediction time (days), thus, c_{PE} has units of frequency $[days^{-1}]$. The source of uncertainty to be modeled here is considered to be only present during the orbit propagation and proportional to the prediction time, which is defined to start the day the first forecasted proxy is used in the atmospheric model. Although such a model will not have an impact during the orbit estimation, its associated covariance will affect the propagation of the state via the ESTM. This leads to a dominance of this model error after long propagation intervals, allowing to decouple its contribution from other modeled uncertainty sources.

Observed space weather data from NOAA is applied during OD, assumed as true, whereas predicted proxies are used during propagation as is detailed in Section 2.3.4. It can be noted that, as concluded in other studies such as in [32], the observed space weather data has its own uncertainty, arising from different observations and data processing of the different space weather sources. In the work presented here, this uncertainty during orbit estimation is modeled as Gaussian, and thus, it is contained inside the aerodynamic model *consider parameter* previously defined.

2.2.4 Covariance determination method

Mahalanobis distance with consider covariance

The Mahalanobis distance (d_M) is a well-known statistical metric that describes how far a state $y(t)$ is from a certain reference $y_{ref}(t)$, projected into the covariance space [78]. The squared Mahalanobis distance is:

$$d_M^2 = \left(\mathbf{y}-\mathbf{y}_{ref}\right)^T\left(\mathbf{P}+\mathbf{P}_{ref}\right)^{-1}\left(\mathbf{y}-\mathbf{y}_{ref}\right), \tag{2.17}$$

where $\mathbf{P}$ and $\mathbf{P}_{ref}$ are the covariance matrices of the state and the reference, respectively. Both matrices are computed from Equation 2.13, each one using their corresponding estimated covariances and ESTM matrices. Note that the orbit used as reference can also suffer from model errors, and thus the *consider parameter* correction impact on its noise-only covariance must also be considered as in Equation 2.13. Equation 2.17 assumes that no correlation exists between both variables $\mathbf{y}$ and $\mathbf{y_{ref}}$, though this is not guaranteed, for instance, when the sensor network is common to both state estimations. The assumption of no correlation between the state and the reference is found in other studies such as [11] or [79]. In the work presented here, we also assume no correlation between the state and the reference, mitigating any possible correlation by ensuring that the computed reference orbit, $\mathbf{y_{ref}}$, does not share any observation with the orbit state under analysis, $\mathbf{y}$. Nonetheless, the validity of this assumption is assessed during the simulation results provided in this work. In addition to this, the covariance of the reference can be neglected when it is several orders of magnitude smaller. This occurs when the used reference orbit is assumed perfect (without uncertainty) [66, 69] or when

their sources are known to be highly accurate such as Precise Orbit Determination outputs.

For simplicity, the reference covariance is omitted in the following equations, although it is considered in the computations when applicable. In order to introduce the *consider parameter* effect, we recall the definition of the extended state vector of Equation (2.9) and combine Equations (2.12-2.11) with Equation (2.17), which yields

$$d_M^2(t) = \Delta\mathbf{y}(t)^T \left(\mathbf{\Psi}(t,t_0) \begin{pmatrix} \mathbf{P}_n + \mathbf{K}\mathbf{C}\mathbf{K}^T & \mathbf{0} \\ \mathbf{0} & \mathbf{C} \end{pmatrix} \mathbf{\Psi}(t,t_0)^T \right)^{-1} \Delta\mathbf{y}(t), \tag{2.18}$$

where $\Delta\mathbf{y}(t) = \mathbf{y_{ext}}(t) - \mathbf{y_{ref}}(t)$. Equation (2.18) allows to compute the Mahalanobis distance at any epoch along the propagation arc as a function of the *consider parameter* variances contained in matrix $\mathbf{C}$, assuming that a batch least-squares parameter estimation process has been performed, followed by a propagation step.

Consider parameters variance determination

Under linear and Gaussian assumptions, this is, when the differences between the state and the reference are normally distributed and the covariance is representative of such distribution (i.e. realistic), the squared Mahalanobis distance should follow a χ^2 distribution, whose detailed characteristics may be found in [76]. Equation (2.18) allows us to evaluate the Mahalanobis distance at any propagation epoch by computing the orbital differences between a predicted orbit and a reference. Thus, if a population of estimated (and later propagated) orbits are available, together with reference orbits, it is possible to look for the *consider parameter* variances in matrix $\mathbf{C}$ so that the squared Mahalanobis distance population resembles the expected theoretical χ^2 distribution. Hence, computing the *consider parameter* variances is reduced to a statistical comparison process, where the free variables are the variances of the *consider parameters*. The covariance determination process can be divided in three main steps:

1. For a population of orbits, perform an OD process to obtain the noise-only covariance and the components of matrix $\mathbf{K}$. Then propagate the estimated states to obtain the predicted orbits and the ESTM.
2. For each predicted orbit, compute the orbital differences at any desired propagation epoch comparing against a reference orbit.
3. With all the data from the orbits population to construct Equation (2.18), obtain the *consider parameters* variance that minimizes a certain metric of statistical comparison between the observed squared Mahalanobis distance distribution and the χ^2 distribution. The different metrics and minimization solver are described in Section 2.2.4.

Therefore, the objective is to retrieve the *consider parameter* distribution that has affected the population of orbits. This can be done provided that a sufficient amount of samples is available, where 'sufficient' means that a prescribed accuracy target can be attained as a trade-off between accuracy and amount of data available. This is further discussed in Section 2.4.3. The methodology looks for orbits affected by errors that are modeled to

follow the *consider parameter* definitions of Section 2.2.3, this is, each orbit is affected by a constant error, drawn from the proposed *consider parameter* distribution whose variance we aim to estimate. The diversity of errors observed in the population allows to determine the variance of the proposed *consider parameters* applying the proposed covariance determination methodology. If the variance of the parameters is properly captured and the proposed models are representative of the system uncertainty, we can correct the estimated covariance and improve the covariance realism, as is seen in Section 2.4. In that regard, if the methodology is demonstrated to provide satisfactory and accurate results, being able to decouple the *consider parameters* impact and any other orbit correlation, we can maintain the trace of the error sources and their tailored correction in the covariance matrix.

One of the final objectives of this methodology is its operational applicability. To obtain a population of orbits of a single object in a SSA scenario, where the data is scarce, we have to resort to orbits estimated at different epochs, with different space weather proxies or even observation geometry. This is the reason why we propose the Mahalanobis distance metric to unify the orbits population under the same distribution (i.e. χ^2). On the one side, we are comparing against a reference orbit, and on the other side we are normalizing such differences with a covariance matrix generated from an OD process that will be coherently affected by the same diversity of estimation epochs and OD conditions. In fact, the Mahalanobis distance for each orbit is expected to remain approximately constant under Gaussian assumptions and sufficiently linear dynamics [69].

Reference orbit for Mahalanobis distance

An orbit to be used as reference is required to compute the Mahalanobis distance. In many studies, the reference orbit used for the Mahalanobis distance computations is an assumed true, errorless orbit [66, 69]. In the context of this work, this orbit is defined as the "true reference" and its covariance can be neglected. In real operations, these kind of references may be available as Precise Orbit Determination products, with orbit precision of the order of 1 cm. However, these solutions require the collaboration of the satellites for such precise computations.

Thus, these solutions are not generally available in most operational situations in SST, where non-collaborative RSO are the main targets. For this purpose, this work proposes to use estimated orbits as reference orbits to compare against the propagated ones. In other words, if measurements are available for a certain period of time, we can use measurements in the propagation arc of another orbit to determine a reference orbit, whose absolute estimation error is several orders of magnitude lower that the propagated orbit under analysis. This has been defined as the Operational reference orbit (see Figure 2.1). As was discussed in Section 2.2.4, this operational reference has a non-negligible covariance since it is estimated after an orbit determination process. Therefore, its covariance must be included when computing the Mahalanobis distance. The process to generate the Operational reference orbit in the presented simulations is detailed later in Section 2.3.1.

Both types of reference orbits (the "true" and the "operational") are tested in this work. Achieving similar performances of the methodology when using any of these references

is of paramount importance for the operational applicability of the proposed covariance determination method, as it would not require external and precise ephemeris to use as reference.

Statistical comparison metrics and solver

The statistical comparison process consists in comparing the Cumulative Distribution Function (CDF) of the observed squared Mahalanobis distances with the χ^2 distribution CDF of as many degrees of freedom (DoF) as the ones included in the Mahalanobis distance computation. This can be reduced to the minimization of an Empirical Distribution Function statistic (EDF). These kind of tests are based on measuring the discrepancy between the EDF (step function that approximates the CDF of a population) and a given function such as the χ^2. Among the multiple options available in the state-of-the-art [11, 76], two relevant metrics are presented and compared along this work:

1. **Cramer-von-Mises (CvM)**: it is a quadratic statistic, based on the squared differences between both distributions, in this case with constant weights. A directly applicable formulation for the Cramer-von-Mises statistic to test if a given population $X_1, \cdots, X_n$ comes from a χ^2 distribution is

$$J = \frac{1}{12n} + \sum_{i=1}^{n} \left(\chi^2_{CDF}(X_i) - \frac{2i-1}{2n} \right)^2, \tag{2.19}$$

   where n is the total amount of samples, being sorted in increasing order. The null hypothesis of this test is that the candidate distribution belongs to the χ^2 distribution. Such hypothesis can be can be rejected with a 99.9% confidence level if the metric reaches values above 1.16 approximately. For a more robust applicability of such metric, upper tail correction factors as described in [76] can be applied.

2. **Kolmogorov-Smirnov (KS)**: it is a supremum statistic that consists in the maximum vertical difference between the empirical and theoretical CDFs, i.e.,

$$D = \max \left(|\chi^2_{CDF}(X_i) - \frac{i}{n}| \right). \tag{2.20}$$

   As before, n is the total amount of samples, sharing the same null hypothesis as the Cramer-von-Mises statistic. In this case, the null hypothesis can be rejected for metrics higher than 1.95 at same 99.9% confidence level. Again, tail correction factors can be applied.

To minimize those metrics, the Differential Evolution algorithm [90] is applied, which consists in a heuristic approach for global multivariate function optimization, suitable also for nonlinear or non-differentiable functions. Instead of requiring an initial guess, this algorithm allows to define boundary regions for the optimized variables, in this case, the *consider parameter* variances. The boundaries applied for the *consider parameter* variances in all the simulations carried out in this work are shown in Table 2.1. As expected, the smaller the search region is, the faster the algorithm converges to the global solution. These values have been selected as a compromise between operational applicability and computational efficiency, representing a wide enough region to ensure that the unknown solution is contained, but maintaining physically logical upper boundaries.

Table 2.1: Minimization boundaries

	σ_{AE} [%]	σ_{PE} [%/day]	σ_{RB} [m]
Upper bound	60	60	200
Lower Bound	0	0	0

2.3 Validation environment

2.3.1 Simulation scheme

To test the covariance realism improvement achieved with the proposed methodology, a validation campaign in a simulated environment has been carried out. The simulation process to generate a realistic environment is described next. Figure 2.1 is included for further details of the process. It depicts a timeline of a Monte Carlo sample, consisting in an orbit determination and propagation process and differentiating between the reference orbit and the estimated/predicted orbit obtained during each process iteration.

- **True reference orbit:** it is obtained propagating a reference state associated to an existing RSO (see Table 2.2) from a certain reference epoch. The dynamic model of this propagation is deterministic and is not perturbed with randomly generated samples of the *consider parameters* (see Table 2.3 for further details). The length of this propagation arc is sufficient to cover all required arcs of posterior orbits.

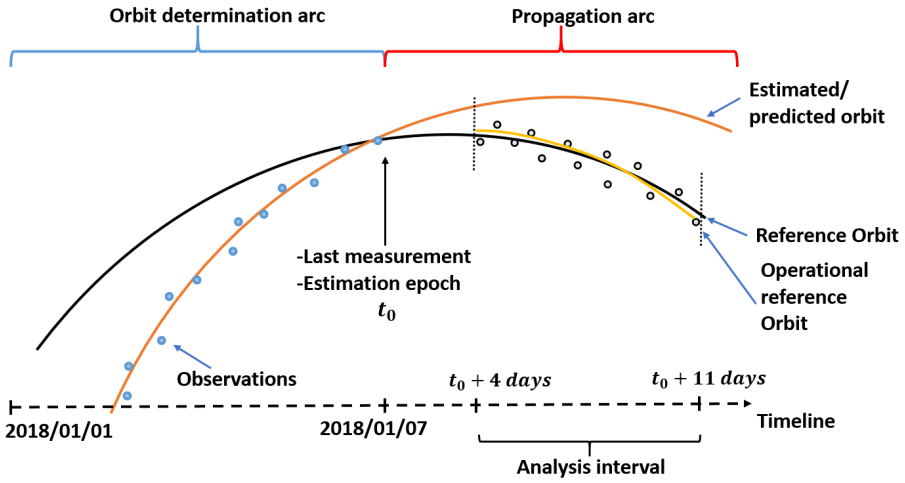

Figure 2.1: Orbit estimation and propagation scheme for 1 Monte Carlo sample.

- **Monte Carlo iterations**:
  - **Simulated orbit:** from the reference state, a propagation is performed over 7 days backwards from the estimation epoch (t_0), which are the nominal OD arcs of interest in LEO applications. Along this step, the aerodynamic model perturbation is included, obtaining a simulated orbit. Though for each sample the aerodynamic model perturbation (c_{AE}) is constant, each value is drawn from a Gaussian distribution with null mean and a simulated variance, following the *consider parameter* expectations of the perturbations. Recovering the input

variance through our covariance determination methodology would serve as validation. The space weather information used along this step corresponds to observed proxies as provided by the Space Weather Prediction Center (NOAA), assumed to be the true proxies.

- **Tracks generation:** From such perturbed orbit, tracks are simulated from a ground-based sensor, in this case, corresponding to a LEO radar with similar visibility capabilities and accuracy as a real operational case (see Table 2.4 for the measurements noise and Table 2.5 for the radar characteristics). The range bias perturbation (c_{RB}) is introduced in this step analogously to the previous perturbation. An example of the resulting observations can be seen in Figure 2.1. Approximately, between 8 to 10 tracks are generated, of around 2 minutes of duration each, providing between 750 and 1000 measurements (range, range-rate, azimuth an elevation). These numbers vary from one iteration to the next one due to the visibility intervals (orbit revisit period and orbit geometry).
- **Orbit determination and propagation:** an OD is performed with the simulated measurements, again with a 7 days determination arc. The estimated state is then propagated forward 11 days from the estimation epoch (t_0), corresponding to the last measurement, obtaining the predicted orbit and the extended state transition matrix. To realistically introduce the effect of the uncertainty in the solar proxies prediction (c_{PE}), true proxies are used only up to the estimation epoch, and as in daily satellite operations, algorithms for the prediction of space weather proxies are used complete the required set. Further details about this prediction are given in Section 2.3.4.
- **Operational reference orbit:** as previously defined, the purpose of this orbit is to check whether the methodology works when using a reference orbit that has been obtained in an orbit determination process. To this end, tracks are simulated as if the True reference orbit was observed, again with the same sensor network. Another OD process is performed using this new set of measurements and the true space weather proxies. For consistency, the length of the determination arc of this orbit is set to coincide with the determination arc of the orbit under analysis, equal to 7 days. The tracks generation and OD arc in this case is set to range from t_0+4 up to t_0+11, which corresponds to the interval of interest for our orbit comparisons and covariance matrix correction. Recall that t_0 is defined from the previously estimated/propagated orbit. Figure 2.1 depicts this process. It is important to notice that this Operational reference orbit has a certain non-negligible covariance matrix as part of the OD process that needs to be included in the Mahalanobis distance computation.

In order to generate more samples following an operational-like scenario, a new sample is created shifting the reference epoch by one day and repeating the previous list of steps again, applying different samples of the perturbations at each iteration. Once the complete population of estimated and predicted orbits is obtained, together with their covariance time-evolution, the covariance determination methodology previously explained can be applied to estimate the variance of the different *consider parameters*. The expected values of such variances correspond to those used in the simulation process,

for the drag force, for the range bias, and for the space weather prediction, which are described in Section 2.3.4.

2.3.2 State vector components in the Mahalanobis distance

As previously discussed, one of the keys of the proposed methodology is the assumption that the Mahalanobis distance metric allows to include all orbital differences in the same theoretical χ^2 distribution. Under Gaussian and linear assumptions, the Mahalanobis distance for each orbit should remain approximately constant if the system errors are properly modeled.

Nonetheless, numerical instabilities were observed in the computation of the Mahalanobis distance when considering the complete state vector dimensions. These instabilities were tracked down to non-linearities that appeared in the position-velocity cross terms of the covariance matrix after 4 days of propagation, which caused ill-conditioning of the matrix and an exponential growth of the Mahalanobis distance in 1 principal component of the velocity. This same phenomenon was also seen in [69], where they attribute it to the inability of the Cartesian coordinates to maintain the Gaussianity. The connection between those non-linearities after propagation and OD characteristics such as observability, track length, orbit geometry or sensor network is a future line of research. Moreover, testing the proposed methodology in coordinates that maintain better the linearity such as equinoctial elements or curvilinear coordinates is a clear line of improvement.

However, other authors propose similar Mahalanobis distances and χ^2 distributions analysis where only position covariance is considered, arguing that position covariance realism is of higher relevance for high velocity collision risk assessments, which is one of the most common types of RSO encounters [67]. Additionally, the position-only Mahalanobis distance remains sufficiently stable for the circular orbits under analysis. Therefore, in the Mahalanobis distance computation of the work presented here, we consider components related to the position differences projected to TNW local frame. Carrying out the analysis in local frames aligned with the satellite motion provide further insight on the effect of the considered perturbations. The impact of this choice in the proposed methodology is assessed with the simulated scenario results shown in Section 2.4.

2.3.3 Reference state, dynamic and sensor model

This section will briefly state the simulated scenario settings used to conduct the work presented here. The initial reference state is described in Table 2.2, representing a LEO object at around 800 km altitude. The reference epoch is the starting epoch of the simulation scheme described above. The dynamic model characteristics are described in Table 2.3, and the simulated noise of the radar measurements during the track generation can be seen in Table 2.4.

Table 2.2: Simulated reference RSO state.

Semi-major axis	7186.878 km
Eccentricity	0.001113
Inclination	98.72 º
RAAN	77.03 º
Arg of pericenter	111.436 º
True anomaly	71.98 º
Epoch (UTC)	2018-01-07 00:00:00.000
Mass	500 kg
SRP area	10 m^2
Drag area	10 m^2
Drag coefficient	2.0

Table 2.3: Dynamical model characteristics.

Reference frame	J2000 ECI
Gravity field	16x16
Third body perturbations	Sun & Moon
Earth geodetic surface	ERS-1
Polar motion and UT1	IERS C04 08
Earth pole model	IERS 2010 conventions
Earth precession/ nutation	IERS 2010 conventions
Atmospheric model	NLRMSISE-90
Solar radiation pressure	Constant area
Drag force	Constant area

Table 2.4: Measurement noise considered

Measurement type	σ	**Units**
Two-way range (ground-satellite)	10	m
Two-way range rate (ground-satellite)	300	mm/s
Satellite azimuth and elevation	1	º

Table 2.5: Characteristics of simulated radar

Field of view		Pyramidal asymmetric
Line of sight	**Azimuth**	180 º
	Elevation	75 º
Aperture	**Azimuth**	±43 º
	Elevation	+15º/-10º
Geodetic coordinates	**Longitude**	-5.5911 º
	Latitude	37.16643 º
	Height	0.1423 km
Observation spacing		5 seconds

2.3.4 Covariance determination configuration

Common tests characteristics

This subsection describes the common characteristics of the test cases conducted in this analysis. Special characteristics of the selected test cases for analysis are presented later in Table 2.6.

- **Analysis interval:** arc where the Mahalanobis distances are computed. In this case, from $t_0 + 4$ to $t_0 + 11$ days in a 1 day time-step, obtaining a total of 8 different analysis epochs for each orbit. Analyzing multiple epochs in the propagation arc not only provides additional elements to the Mahalanobis distance population, but it also allows to provide a *consider parameter* variance representative of a wider arc. Though it may appear that different arbitrary points of the orbits are mixed in the same analysis, this is mitigated by the Mahalanobis distance concept, which normalizes the orbital differences with their covariance. The beginning of analysis interval is chosen at $t_0 + 4$ to let the atmosphere errors to dominate the covariance. Despite typical propagation arcs of LEO applications range up to $t_0 + 7$, it is relevant to include further propagation to properly characterize the proxies prediction error. Both the aerodynamic and the atmospheric proxies *consider parameter* models impact the aerodynamic drag force. Thus, a wider analysis window is crucial to discern the linear impact of the proxies *consider parameter* model (Equation 2.16).
- **Time frame:** time step between each Monte Carlo sample. Set to 1 day forward shift, analogously to an operational scenario.
- **RMS rejection:** as customary in most statistical applications, a 3 RMS rejection criteria has been set on the Mahalanobis distance distribution, which on average has led to a 4% of rejection.

Simulated uncertainty

This subsection describes the simulated variances chosen for the different test cases, which are introduced into the simulations as explained in Section 2.3.1. All test cases in Section 2.4 contain the same perturbation levels for the aerodynamic and range bias *consider parameter* models, for benchmarking purposes, corresponding to:

- Aerodynamic model (σ_{AE}): 20%. This values is chosen as representative based on state-of-the-art studies, which state that around a 10-20% of uncertainty can be expected for the atmospheric density models [24, 91].
- Range bias (σ_{RB}): 20 m. This value has been chosen from operational scenarios expectations of previous analysis such as [88].

Regarding the simulation of the uncertainty of the atmospheric proxies prediction, a preliminary analysis is conducted to assess the level of uncertainty expected in an operational scenario. We select an harmonic pulsation prediction model for the typical 11 years solar cycle. Starting at the beginning of the simulation scheme (2018-01-01), in time steps of 1 day, in a 1 year period, we obtain 11-days predictions of the solar proxies for each step. Then, we compare the prediction of $F_{10.7}$ and A_p proxies against the observed

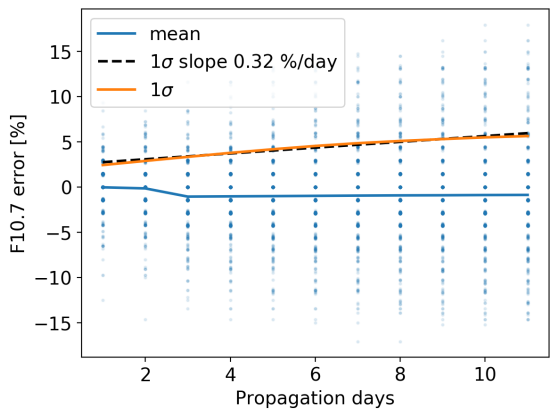

Figure 2.2: F10.7 relative prediction error as a function of prediction time.

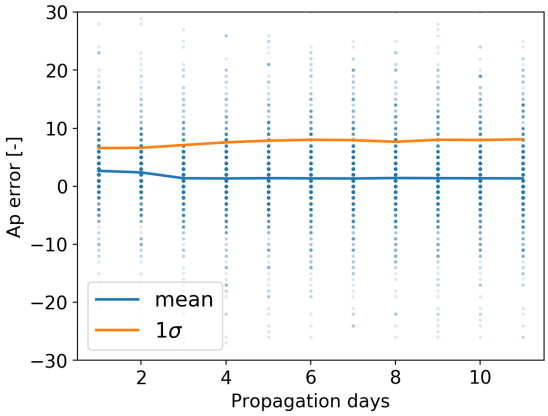

Figure 2.3: Ap absolute prediction error as a function of prediction time.

values (NOAA). The results are shown in Figures 2.2 and 2.3 for the $F_{10.7}$ and A_p proxies, respectively. In the former one, despite an almost null mean, a linear growth of the 1σ value is appreciated, with a slope of 0.32%/day. This behavior has led us to propose the linear growth model for the Proxies prediction model error of Section 2.2.3. In Figure 2.3, on the contrary, a constant 1σ absolute error of 8 units is observed for A_p.

However, the proposed linear model for the atmospheric proxies prediction error is applied in the aerodynamic force. To determine the impact that the observed proxies uncertainty supposes on the aerodynamic force, we introduce a perturbation equivalent to the observed 1σ values of $F_{10.7}$ and A_p for a single orbit propagation. These results are presented in Figures 2.4 and 2.5. These figures represent the relative difference of drag acceleration between 2 orbits: an unperturbed orbit with the real proxies, and the second one including the 1σ level perturbations. In Figure 2.4, only the $F_{10.7}$ proxy has been perturbed, observing also a linear acceleration difference evolution, of an order of magnitude similar to the slope of the $F_{10.7}$ proxy itself. However, when the A_p perturbation is also included as shown in Figure 2.5, not only the slope is increased, but also a significant bias is obtained.

This analysis is useful to anticipate uncertainty levels expected in the presented simulation environment derived for the proxies prediction error, where the 1σ proxies uncertainty are translated in slopes of $1.35\%/day$ errors in the aerodynamic force. In light of these results, the following 2 cases have been considered to introduce the atmospheric proxies error in the simulations:

- Operational forecast: corresponding to the exact same forecast applied for the preliminary analysis, to be representative of operational prediction errors.
- Controlled proxies error: a simulated standard deviation of 3%/day is introduced with the proposed model of Section 2.2.3. The value is chosen to be of the order of magnitude of the expected variance of the real forecast as discussed above. This allows to test if the method is able to properly characterize the uncertainty in a scenario in which we have full control on the input perturbations, introducing

them as in the proposed model similarly to the aerodynamic model and range bias perturbation.

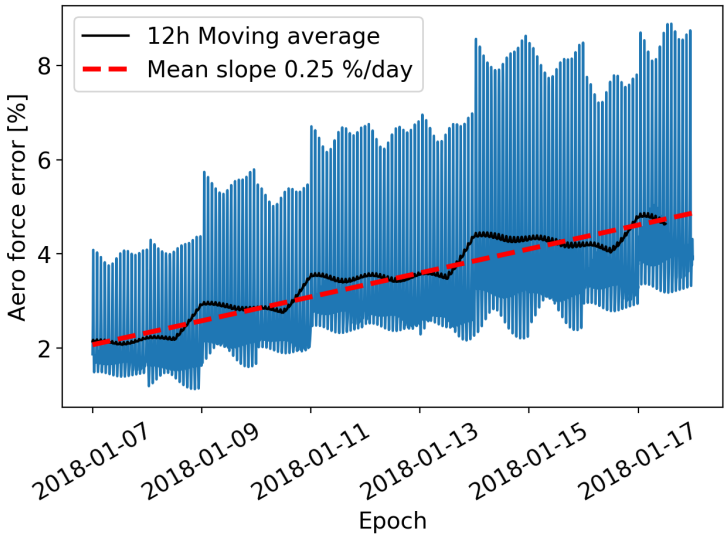

Figure 2.4: Aerodynamic acceleration relative error with predicted $F_{10.7}$ 1σ perturbation.

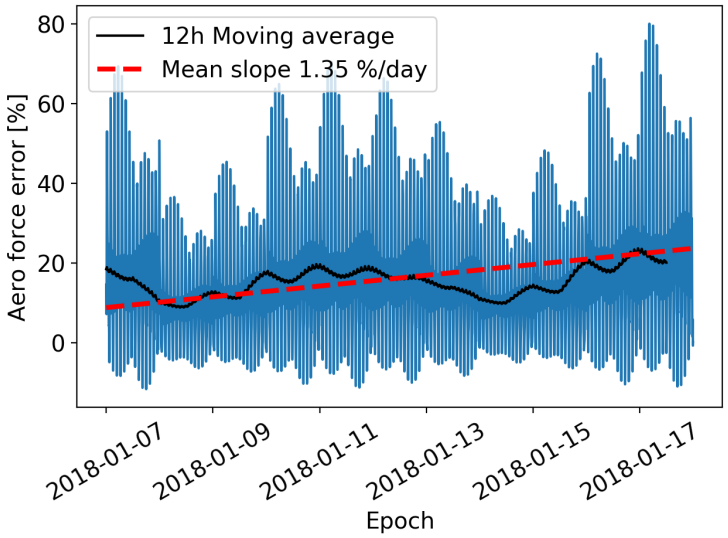

Figure 2.5: Aerodynamic acceleration relative error with predicted $F_{10.7}$ 1σ and A_p 1σ perturbation.

2.4 Results

In this section, the results of selected tests cases are presented and analyzed in relation to the effectiveness of the proposed covariance determination methodology to characterize the uncertainty of the system. The section is divided in 4 subsections. The first two discuss the results of the different test cases, the first one using the True reference orbit (Section 2.4.1) and the second one applying the Operational reference orbit (Section 2.4.2).

The third subsection presents a brief analysis on the accuracy of the methodology (Section 2.4.3). The last subsection discusses the performance of the covariance determination methodology in terms of covariance realism (Section 2.4.4).

Table 2.6 shows these results for 7 test cases, where the columns for each case correspond respectively to: 1) the identification number of each test case 2) the determined *consider parameters* standard deviation after applying the presented covariance determination process 3) the accuracy of the determined *consider parameters* standard deviation results as compared with the uncertainty introduced in the simulations 4) the final statistical comparison metric obtained 5) the relevant features of each case, such as the used reference, the chosen metric and the amount of Monte Carlos samples (i.e. orbits estimated and propagated). Let us explain the Relevant features column of Table 2.6. For each test, we are differentiating when the true reference orbit is used for the Mahalanobis distance computations or whether the previously defined Operational reference one is considered. Also, the chosen statistical metric is mentioned, either Cramer-von-Mises ("CvM") or Kolmogorov-Smirnov ("KS"). The amount of samples used during the computations is also shown. Finally, for each test case, the chosen option to introduce the atmospheric proxies prediction error is included, either the variance according to the proposed model ("Controlled PE") or the operational forecast ("Op. forecast"). Additionally, note that in the case of the proxies prediction *consider parameter*, accuracy is only provided for the controlled perturbations case, as only in such scenario we have a properly known target uncertainty.

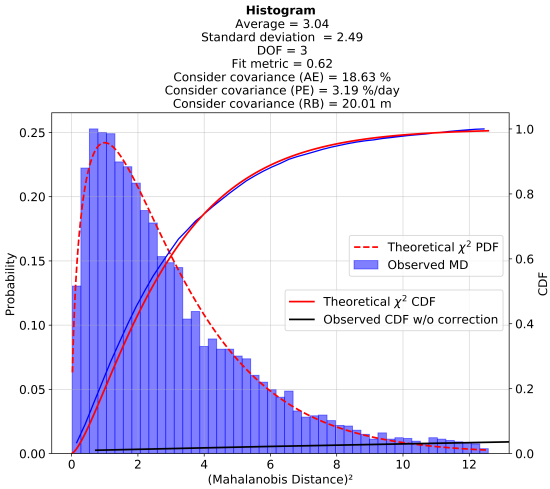

Figure 2.6: Test 2. Squared Mahalanobis distance distribution with optimum consider covariance results.

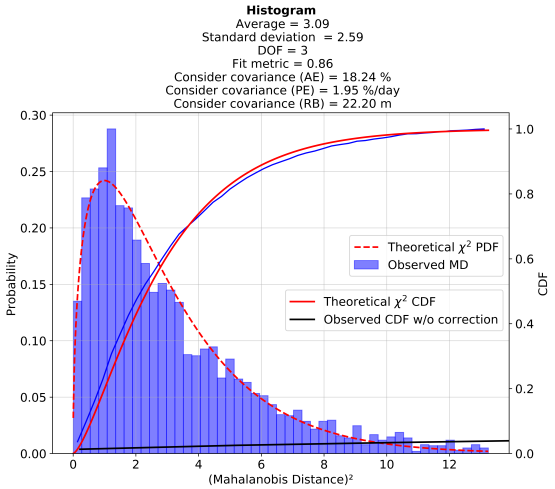

Figure 2.7: Test 3. Squared Mahalanobis distance distribution with optimum consider covariance results.

2.4.1 True reference orbit

Test Case 1 uses the unperturbed true orbit as reference for the Mahalanobis distance computations, with 500 samples. As is seen in Section 2.4.3, this number has been selected as a compromise between having sufficient statistical samples for enough accuracy, but maintaining a realistic time-span (1.5 years approximately), which is relevant in

Table 2.6: Selected test cases characteristics and results

Id	Consider parameter results	Accuracy ‖%‖	Metric	Relevant features
1	σ_{AE} = 18.18% σ_{RB} = 21.8m σ_{PE} = 3.64 %/day	9.1 9 21	0.4	True reference CvM metric 500 samples Controlled PE
2	σ_{AE} = 18.63% σ_{RB} = 20.01m σ_{PE} = 3.19 %/day	6.9 0.05 6.3	0.62	True reference CvM metric 1000 samples Controlled PE
3	σ_{AE} = 18.24% σ_{RB} = 22.2m σ_{PE} = 1.95 %/day	8.8 11 -	0.86	True reference CvM metric 500 samples Op. forecast
4	σ_{AE} = 19.69% σ_{RB} = 22.97m σ_{PE} = 1.27 %/day	1.6 14.9 -	1.5	True reference KS metric 500 samples Op. forecast
5	σ_{AE} = 21.02% σ_{RB} = 24.73m σ_{PE} = 0.00 %/day	5.1 23.7 -	1.67	True reference CvM metric 500 samples Op. forecast without PE
6	σ_{AE} = 19.49% σ_{RB} = 22.08m σ_{PE} = 1.93 %/day	2.6 10.4 -	0.82	Op. Ref. CvM metric 500 samples Op. forecast
7	σ_{AE} = 19.52% σ_{RB} = 21.49m σ_{PE} = 1.81 %/day	2.4 7.5 -	1.68	Op. Ref. CvM metric 1000 samples Op. forecast

operational scenarios. In this test, the atmospheric proxies prediction error uncertainty has been introduced in the system with the fully controlled model. As observed in Table 2.6, an accuracy better than a 10% is obtained for the aerodynamic model error and range bias error, whereas a lower accuracy is found for the prediction error. As is further discussed later, the Cramer-von-Mises test statistic shows the lowest value of all test cases, pointing out a proper model matching between the actual uncertainty and the proposed models. Being able to characterize properly the different sources of uncertainty introduced in the system is an indicator of the ability of the covariance determination method to maintain the trace of the error sources, decoupling their impact on the orbits despite the methodology assumptions that neglected the correlation between the *consider parameters* and the analyzed orbits.

Test Case 2 shares the same configuration as Test Case 1, with the controlled perturbation of the atmospheric proxies, but in this case increasing the samples up to 1000. This test case

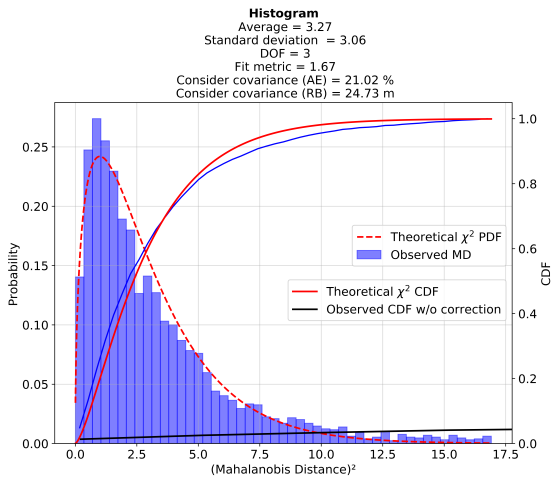

Figure 2.8: Test 5. Squared Mahalanobis distance distribution with optimum consider covariance results.

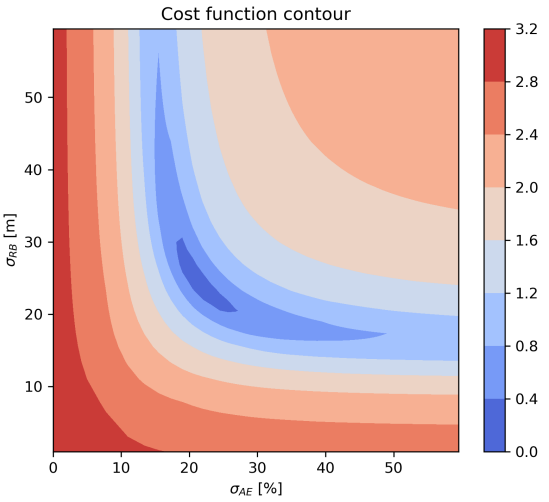

Figure 2.9: Test 5. Cramer-von-Mises metric logarithmic contour as a function of aerodynamic model and range bias *consider parameter* standard deviations.

allows to demonstrate that the accuracy of the proposed methodology increases with the amount of samples, as would be expected, though further discussion about the accuracy of the method is provided in Section 2.4.3. Additionally, the Cramer-von-Mises metric still rejects the null hypothesis, maintaining a good fit between the system uncertainty and the proposed models as can be seen in Figure 2.6. This figure shows the histogram of the final squared Mahalanobis distance distribution after applying the determined *consider parameter* variances, together with its empirical CDF as blue line. It also depicts the theoretical PDF and CDF of the χ^2 distribution of the corresponding DoF as red lines, as well as the empirical CDF of the distribution when no *consider parameter* correction is applied as a black line. This test case shows that the methodology is able to provide accurate results with a proper statistical matching when the system uncertainty is correctly modeled, as in this controlled case.

Test Case 3 shares again the same configuration as Test Case 1, but now applying the operational atmospheric forecast procedures. It can be noted that the *consider parameter* variances obtained with the proposed covariance determination methodology are representative of the introduced perturbation in the presented simulations. In both the aerodynamic model and range bias, the obtained results differ by less than a 11% to the target values (20% for σ_{AE}, 20m for σ_{RB}). In terms of the Proxies prediction error, the method has determined a 1.95%/day, whose order of magnitude is similar to the expected uncertainty as discussed in Section 2.3.4 and observed in Figure 2.5. Regarding the Cramer-von-Mises statistical comparison metric, a score of 0.86 is obtained, thus not rejecting the null hypothesis. The obtained squared Mahalanobis distance distribution is shown in Figure 2.7. Overall, the distribution matches the expected χ^2 behavior, despite being slightly overpopulated on the first quarter of the CDF, which is ultimately appreciated in the test metric, being larger than in Test Case 1. Recovering the χ^2 behavior is a direct indicator of covariance realism improvement, which is the

main objective of the method. This indicates that the determined covariance is able to characterize the uncertainty of the system better than when no correction is applied. Although this is further analyzed later via covariance containment tests, the CDF of the initial non-corrected squared Mahalanobis distance distribution is included in Figure 2.7, for comparison. It can be clearly seen how the initial distribution is far from resembling a χ^2 behavior, obtaining less than 5% of the population in the range showed in the figure. These remarkably large squared Mahalanobis distances in the non-corrected distribution are due to an overly optimistic size of the noise-only convariance.

Test Case 4 is analogous to Test Case 3 except for the optimization metric used, in this case, Kolmogorov-Smirnov. The results of Table 2.6 point out that similar consider variances are obtained, indicating that both metrics arrive to similar results. A small trade-off between aerodynamic model uncertainty and proxies prediction uncertainty is observed in this case. Again, the obtained Kolmogorov-Smirnov metric does not allow to reject the null hypothesis.

Test Case 5 allows to show the benefits of upgrading the uncertainty model of the system. In this test case that shares the same characteristics as Test Case 3, no *consider parameter* correction for the Proxies Prediction error has been included. The obtained squared Mahalanobis distance distribution for this case can be seen in Figure 2.8. The Cramer-von-Mises metric is above the threshold of 1.16, which rejects the null hypothesis that the population belongs to a χ^2 distribution. For further insight when only 2 *consider parameters* are present, a contour plot of the CvM metric as a function of both *consider parameters* is shown in Figure 2.9. Here, the existence of a global minimum can be observed, corresponding to the optimum *consider parameters* found by the proposed methodology. However, the existence of such minimum does not ensure a correct statistical comparison, as is the case when the used models are not sufficient. This confirms that a better uncertainty characterization is obtained when the solar prediction uncertainty is included as a *consider parameter* when predicted atmospheric weather forecasts are used. As expected, the better the uncertainty of the system is modeled, the better the proposed covariance determination method is able to improve the covariance realism. This highlights the relevance of properly modeling all sources of uncertainty in the space environment.

2.4.2 Operational reference orbit

Test Case 6 uses the Operational Reference orbit for orbital differences computations. The similarity of these results with the ones obtained in Test Case 3 indicates that the covariance determination is able to achieve satisfactory results without requiring an assumed perfect orbit. In an operational environment, this allows to use orbit determinations with observations during the propagation arc, not depending on external sources of precise ephemeris and showing the operational applicability of the proposed method in SSA operational environments. As was described previously, the uncertainty of such OD must be taken into consideration for a correct Mahalanobis distance computation. Even though in the chosen simulation scenario the operational references orbits did not contain any model error (only measurements error), the proposed methodology is able to cope with modeling errors in the operational reference orbit since, as explained in

Equation 2.18, the covariance of the reference orbit is also corrected by the *consider parameter* variances.

Finally, Test Case 7 has been included to show a benchmark with an increased number of orbits in the case of using both the Operational Reference orbit and the operational atmospheric proxies forecast. On the one hand, the accuracy of the optimum *consider parameter* variances is improved for the aerodynamic model and the range bias. Increasing the statistical population allows the method to better characterize the uncertainty, as was also seen in Test Case 2. On the other hand, the Cramer-von-Mises statistic obtained leads to the rejection of the null hypothesis. As can be seen in Figure 2.10, the obtained distribution does not significantly deviates from the theoretical χ^2 behavior. Nonetheless, the increased population allows the Cramer-von-Mises test to have sufficient statistical evidence that the distribution does not match the χ^2 behavior. This is attributed to a mismatch between the used model for the prediction of proxies and the one used in the covariance determination methodology. The fact that the statistical comparison in Test Case 2 is significantly better (see Figure 2.6) points out that the proposed model for the atmospheric proxies prediction is not sufficient when the operational forecast procedure is applied. Recalling the analysis of Section 2.3, the introduced uncertainty had two differentiated sources, the $F_{10.7}$ Solar Flux and the A_p Geomagnetic Index. Though the retrieved consider covariance (σ_{PE}) is in line with the expectations derived from the $F_{10.7}$ uncertainty, the A_p uncertainty has not been characterized. Not tackling this non-negligible uncertainty source leads to the model mismatching showed on the metric.

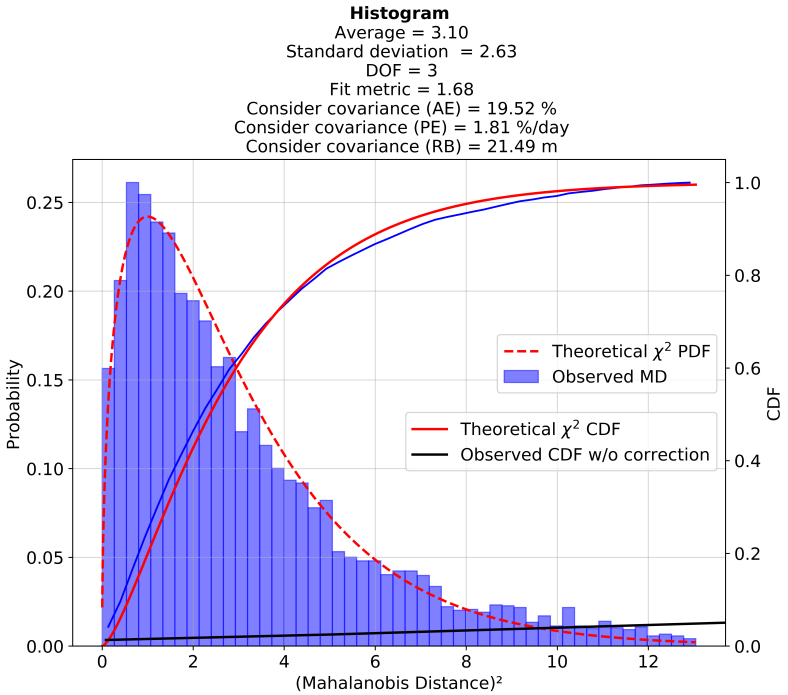

Figure 2.10: Test 7. Squared Mahalanobis distance distribution with optimum consider covariance results.

2.4.3 Accuracy analysis

It has been seen in the previously discussed results that, as expected, the accuracy of the method improves when increasing the amount of samples included in the analysis. In this subsection, the accuracy of the covariance determination method is assessed in two different ways. Firstly, we assess the number of orbits (or samples) that are required by the statistical minimization process. Figure 2.11 shows the RMS of the accuracy achieved by the covariance determination method as a function of the number of orbits, in the simulation scenario of Test cases 1 and 2. Figure 2.11 shows that the choice of the number of orbits to include in the analysis corresponds to a trade-off between accuracy and the amount of data available. When using approximately more than 700 orbits, an accuracy of the order of 5% is achieved. An accuracy of around 15% is expected in the range between 100-600 orbits, whereas it decreases significantly for less than 100 orbits, since not enough samples are available to characterize the uncertainty of the system.

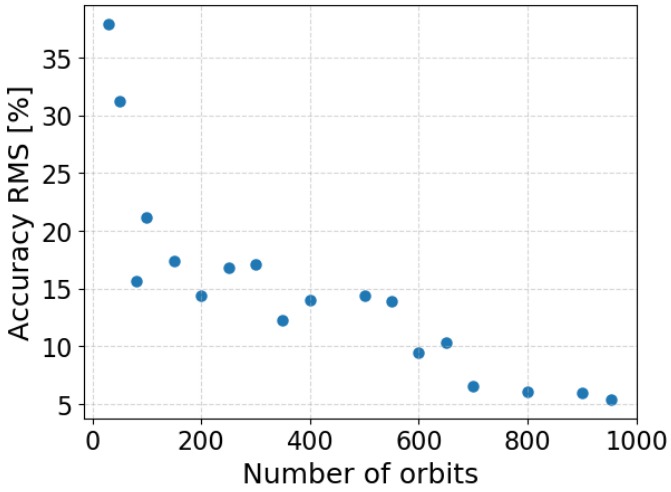

Figure 2.11: Covariance determination method accuracy as a function of the number of orbits.

Secondly, the provided accuracy results presented in Table 2.6 correspond to a single execution of the simulation for each Test case scenario. However, this result would correspond to a "sample" of the method accuracy, since slightly different results may appear when repeating the simulations, applying different realizations of the perturbations and measurement noise. Table 2.7 shows the *consider parameter* variances results for test case 1 with 10 different seeds for the noise and perturbation generation.

Even though only 10 repetitions of the simulations have been carried out, these results provide insight on the expected standard deviation of the methodology accuracy. Extending this analysis to more repetitions and to the other test cases scenarios is proposed for future work. The mean values of the *consider parameter* variances are close to the target values, with the target value being included inside the standard deviation. The worst accuracy is found for the proxies prediction error, which is attributed to its coupling with the aerodynamic model error, which reduces its traceability. The mean of the accuracy RMS remains at 10% even for 500 orbits, with a standard deviation of a 4%, which is considered satisfactory.

Table 2.7: Test cases 1 accuracy standard deviation

N=500	Computed σ			Accuracy RMS [%]
Seed	AE [%]	PE [%/day]	RB [m]	
1	18.18	3.64	21.80	14.36
2	18.76	3.35	21.37	8.59
3	21.35	2.97	20.95	4.80
4	20.77	3.83	19.42	16.21
5	19.53	3.60	19.41	11.75
6	21.83	3.06	19.98	5.41
7	20.19	3.24	20.23	4.70
8	19.01	3.52	21.21	10.98
9	19.99	3.57	19.17	11.23
10	18.92	3.62	19.37	12.47
Mean	19.85	3.44	20.29	10.05
std	1.22	0.28	0.85	4.16

2.4.4 Covariance containment

Under Gaussian assumptions, if the observed squared Mahalanobis distance follows a χ^2 distribution, an improvement in the covariance realism would be directly achieved. In this respect, covariance containment tests such as the one proposed by [43] provide further physical insight and visual representation of the proposed methodology effectiveness. To evaluate if the covariance is representative of the orbital differences, the Mahalanobis distance can be used as a metric to see the amount of points that lay inside a $k\sigma$ ellipsoid ($k = 1, 2, 3, 4$) and compare it against the theoretical expected fraction for a multivariate Gaussian distribution of the same number of DoF. In the presented cases, it corresponds to 3 DoF (TNW position differences).

Test Case 6 results are chosen for this analysis due to a greater resemblance to an operational scenario, as it maintains a realistic amount of data, it uses the Operational reference for comparison and achieves sufficient accuracy. Figures 2.12 and 2.13 depict the orbital differences in TNW for such test case for a 3σ ellipsoid using the noise-only covariance and the determined consider covariance, respectively. Those points laying outside the ellipsoid are marked as red dots, as green otherwise. Firstly, the covariance containment result in Figure 2.13 is close to the expected theoretical containment of a 3 DoF Gaussian distribution (see Table 2.9), showing a remarkable enhancement of the covariance realism as opposed to the outstandingly low containment of the noise-only covariance of Figure 2.12. Bear in mind that such test case contained orbital differences for a wide propagation interval.

This correction of the covariance realism, derived from the computed *consider parameters* variances, is clearly dominant in the Along-track uncertainty component, where the order of magnitude of orbital differences is several times greater than the other 2 components, the Normal and Cross-track directions. This is the expected behavior for LEO objects for the analyzed error sources. The atmospheric drag force affects satellites on the direction of the velocity and thus both aerodynamic and proxies prediction errors are accumulated in the Along-track direction. Similarly, range-bias errors induce orbital differences in the

direction of motion coinciding again with the Along-track direction in the nearly-circular orbit considered. We can distinguish three contributions to the covariance correction, recalling that the *consider parameter* correction is applied at estimation epoch:

- The aerodynamic model *consider parameter* variance affects mostly the drag coefficient covariance at estimation epoch, and such correction at estimation epoch is mapped into position covariance via the ESTM during the orbit propagation.
- The range bias variance affects the Along-track position and velocity covariance at estimation epoch, not affecting directly the propagation since it corresponds to a measurement model error. Of course, such initial inflation on position and velocity components will indeed impact the covariance propagation.
- The variance of the proxies prediction *consider parameter* does not provide any correction at estimation epoch, since there is no uncertainty on the proxies during the determination arc. However, the impact of this *consider parameter* is mapped to the position covariance due to the effect of the complete ESTM propagation.

Despite the observed increment of the covariance realism, it is relevant to analyse the improvement achieved at each analyzed propagation epoch. The individual containment results for such epochs can be seen in Table 2.9 and its counterpart using the noise-only covariance in Table 2.8. All shown results share the common consider covariance correction using the optimum results of Test Case 6. A color scale has been added to facilitate the comparisons. Overall, as previously mentioned, the covariance realism provided by the uncorrected noise-only covariance is significantly lower than the determined consider covariance, for the noise levels introduced in the presented simulations. It can be noted that the 3σ average containment of Table 2.9 differs slightly from the one showed in Figure 2.13. The reason is the outliers rejection process. On the results showed in the figure, all data is analyzed simultaneously, which causes the RMS rejection process to reject more data from conflicting epochs such as $t_0 + 11$ days, as is further explained below. These rejected outliers are not accounted for in the covariance containment, increasing slightly the containment percentage. On the contrary, the daily results of Table 2.9 have their own individual outlier rejection, leading to the slight differences observed between both results.

The individual containment results are, on average, around the expected theoretical results though presenting oscillations. This is expected since a singular *consider parameters* correction is aiming to correct the covariance at different propagation epochs simultaneously, whereas the uncertainty present in each of them is expected to vary. However, including all epochs in the same optimisation not only allows to provide the most representative solution for the interval, but also provides an additional amount of statistical population, facilitating the analysis. Two different regions of Table 2.9 are highlighted as reddish colors. First, the containment results at the 4^{th} propagation day are lower than expected for 1σ and 2σ ellipsoids. For short propagation periods, the estimation uncertainty is still relevant as compared to the covariance inflation introduced by the *consider parameter* correction, reducing the covariance realism enhancement of the methodology. Second, reduced covariance realism performance is observed at $t_0 + 11$ days. This is undoubtedly related to the inaccuracies of the solar proxies prediction model as

was seen in Test Case 7. After long propagations, not only the linearity assumptions are stressed, but also the effect of the proxies prediction errors gain relevance as compared to the other sources. Therefore, not modeling such uncertainty perfectly is causing the containment at such regions to decay. However, it is important to highlight that long propagation arcs need to be included in the proposed covariance determination methodology so that the effect of the solar proxies prediction can be distinguished from the effect of the aerodynamic model error.

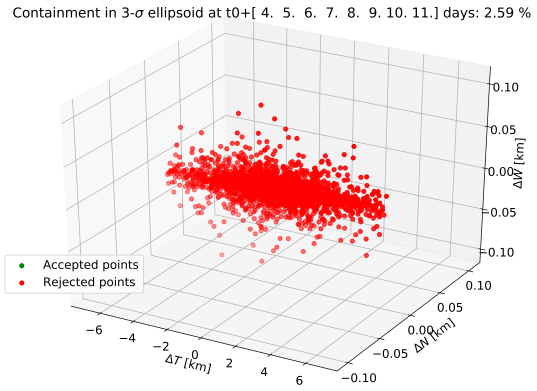

Figure 2.12: Test 4. Noise-only covariance 3σ containment.

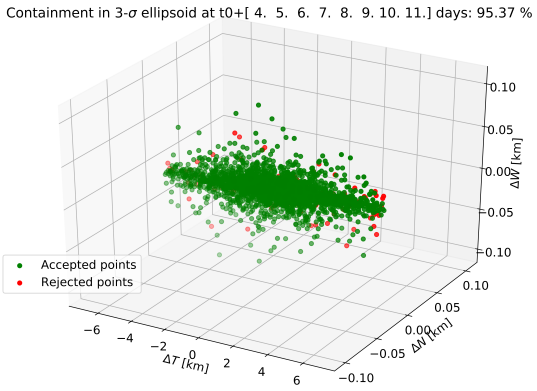

Figure 2.13: Test 4. Consider covariance 3σ containment with determined *consider parameter* variances.

Table 2.8: Test 4. Noise-only covariance containment

Epoch [days]	Without consider parameter correction [%]			
	1σ	2σ	3σ	4σ
t0+4	0	1.34	2.01	3.57
t0+5	0.45	1.12	2.01	3.58
t0+6	0	0.45	3.17	3.85
t0+7	0.68	1.81	2.71	4.52
t0+8	0	0.9	2.71	3.85
t0+9	0.44	1.98	2.86	4.4
t0+10	0.45	0.91	2.49	3.63
t0+11	0	1.35	2.7	4.5
Average	**0.25**	**1.23**	**2.58**	**3.99**
Theoretical (3DoF)	**19.9**	**73.9**	**97.1**	**99.87**

Table 2.9: Test 4. Consider covariance containment

Epoch [days]	Applying consider parameter correction [%]			
	1σ	2σ	3σ	4σ
t0+4	16.2	67.8	94.03	100
t0+5	22.41	73.57	98.52	100
t0+6	20.13	73.38	96.32	100
t0+7	23.33	75.38	98.27	100
t0+8	19.96	69.75	96.14	100
t0+9	24.78	74.35	94.78	100
t0+10	20.22	69.11	93.11	99.56
t0+11	24.1	70.5	88.51	97.75
Average	**21.39**	**71.73**	**94.96**	**99.66**
Theoretical (3DoF)	**19.9**	**73.9**	**97.1**	**99.87**

2.5 Conclusions

This work has introduced a novel methodology to characterize the uncertainty in the space environment and improve the covariance realism. To this end, the *consider parameter* theory of batch least-squares methods has been applied in combination with Extended State Transition Matrix propagation to improve the covariance realism by means of the modeled *consider parameters*. This work focused on the aerodynamic model error, the

range bias error and the error of the prediction of space weather proxies. The theoretical base to map the effect of the additional parameters in the covariance affecting both the estimation or the propagation arc has been developed. To compute the unknown variances of such parameters, a minimization process has been proposed based on the comparison between the observed Mahalanobis distance distribution and its theoretical χ^2 behaviour under Gaussian assumptions, using predicted and estimated orbits to compute the orbital differences.

The results, obtained in a simulated scenario, showed that the proposed methodology is able to characterize the system uncertainty accurately for the aerodynamic model error, the range bias error and the atmospheric proxies prediction when the uncertainty present in the system follows the proposed models. A straightforward advantage of the proposed covariance determination method is that a physics-based traceability of the uncertainty sources is maintained. EDF statistics such as Cramer-von-Mises or Kolmogorov-Smirnov were successfully applied along the statistical comparison process, not only improving the method robustness as compared to previous studies [88, 89], but also providing direct information about the quality of the proposed uncertainty models. When applying the operational proxies forecast method, despite the clear improvement in the statistical comparison as opposed to not including it, the tests metrics showed that the observed squared Mahalanobis distance distribution diverged from the χ^2 distribution when sufficient statistical samples were included in the analysis. This is a clear line of improvement, mostly related to the characterization of the A_p proxy uncertainty, highlighting the relevance of the uncertainty model for the proposed covariance determination methodology.

Furthermore, the method has provided accurate results when selecting the Operational reference orbit, this is, when using estimated orbits as reference to obtain the Mahalanobis distance instead of an unperturbed, "true" orbit. This is relevant for the operational scenarios aimed at, since generally, external data such as precise orbit products are not available for most satellites or space debris objects.

Finally, covariance containment tests have provided a clear visualization of the covariance realism improvement achieved with the proposed covariance determination method as compared to the expected containment of a multivariate Gaussian distribution. The covariance is elongated mostly on the Along-track direction to accommodate the uncertainty present in the aerodynamic force. Overall, the obtained containment shows satisfactory accuracy to the theoretical containment results except on the beginning and end of the analysis arc. This is again a line of improvement, also related with the quality of the proposed uncertainty models.

Nonetheless, there is still a long road ahead. Apart from the proxies prediction model refinement to better characterize the effect of A_p proxy uncertainty, it is customary to move onto real data to completely assess the performance of the proposed method and *consider parameters*. Further analysis of the methodology accuracy standard deviation in different scenarios is also required for future research. Additionally, the Gaussian assumptions that represent the basis of this method should be revisited, widening the method for other distributions such as log-normal or Gauss-von-Mises, as well as more

complex uncertainty models such as stochastic Brownian motion, Ornstein-Uhlenbeck, Gauss-Markov processes or even time-space correlations in atmospheric uncertainty.

Acknowledgments

This project has received funding from the “Comunidad de Madrid" under “Ayudas destinadas a la realización de doctorados industriales" program (project IND2020/TIC-17539).

3

Improving orbital uncertainty realism through Covariance Determination in GEO

3.0 Scientific contribution and context

The main contribution of this paper is the validation of the *Covariance Determination* methodology in GEO environments, focusing on solar radiation pressure and time bias uncertainty. This paper showed that the *Covariance Determination* methodology is agnostic to the uncertainty source used, being adaptable to other orbital regimes. Moreover, it helped to understand the different contributions to the covariance growth that is achieved with either dynamic or measurement models *consider parameters*, the former being most relevant upon propagation, the latter being critical at the estimation epoch.

This paper, though published later than the previous one of Chapter 2, was actually developed earlier for the AMOS 2022 conference [89]. Thus, even though sharing most of the basis of the *Covariance Determination*, it has slight changes such as the EDF metrics used in the optimization. However, the goal of the paper was to show the capability to model and quantify uncertainty sources in GEO environments, which is one of the objectives of the thesis as seen in Section 1.2. The introduction of this paper shares several concepts with the one from Section 2, as it can be considered as an extension of Section 2 to GEO.

A. Cano[1,2], **A. Pastor**[1], **S. Fernández**[1], **J. Míguez**[2], **M. Sanjurjo-Rivo**[2], **D. Escobar**[1],
[1]GMV, 11 Isaac Newton, 28670 Tres Cantos, Madrid, Spain,
[2]Universidad Carlos III de Madrid, 30 Avenida Universidad, 28911 Leganés, Madrid, Spain,
The Journal of the Astronautical Sciences (2022) 69: 1394–1420
10.1007/s40295-022-00343-x

The reliability of the uncertainty characterization, also known as uncertainty realism, is of the uttermost importance for Space Situational Awareness (SSA) services. Among the different sources of uncertainty related to the orbits of Resident Space Objects (RSOs), the uncertainty of dynamic models is one of the most relevant ones, although it is not always included in orbit determination processes. A classical approach to account for these sources of uncertainty is the consider parameters theory, which consists in including parameters in the underlying dynamical models whose variance aims to represent the uncertainty of the system. However, realistic variances of these consider parameters are not known a-priori. This work presents a method to infer the variance of the consider parameters, based on the distribution of the Mahalanobis distance of the orbital differences between predicted and estimated orbits, which theoretically shall follow a χ^2 distribution under Gaussian assumption. This paper presents results in a simulated scenario focusing on Geostationary (GEO) regimes. The effectiveness and traceability of the uncertainty sources is assessed via covariance realism metrics.

Keywords: uncertainty realism, covariance realism, space situational awareness, covariance determination, Mahalanobis distance, chi-square distribution

3.1 Introduction

Orbital uncertainty plays a key role for the provision of Space Situational Awareness (SSA) services, including catalog maintenance, risk assessment or maneuver detection, among others. Therefore its adequate characterization, also defined as uncertainty realism, is of paramount importance. Uncertainty realism focuses on correctly representing the Probability Density Function (PDF) of the orbital state. Under Gaussian assumption, uncertainty realism can be reduced to covariance realism, requiring only the two first moments of the PDF for the proper characterization of the system uncertainty, gathered in a state and its associated covariance matrix.

Many Orbit Determination (OD) processes in Space Surveillance and Tracking (SST) are based on weighted batch least-squares algorithms, which rely on available and sufficient measurements to produce an estimate (orbital state and covariance matrix). During this process, the dynamics governing the system is usually assumed deterministic, with measurement noise as the only source of uncertainty. Thus, the obtained covariance matrix is able to account only for the measurements noise, being known as the noise-only covariance [28]. However, one of the main sources of uncertainty during OD and subsequent propagation arises from the lack of knowledge in the underlying dynamical models, which is typically disregarded. The impact of this uncertainty is crucial not only for the state estimation but also for the time evolution of its associated uncertainty due to its inherent correlation with the state variables. This leads to an overly-optimistic noise-only covariance matrix time evolution and, eventually, the loss of covariance realism.

Therefore, it is customary for SSA and particularly for SST purposes to characterize and determine such uncertainty and its effects, which is commonly known as Uncertainty Quantification (UQ). Two fundamental problems can be distinguished for UQ: the propagation of uncertainty and the inverse problem (model and parameter uncertainty) [11]. The former is focused on how to propagate forward an initially given PDF of a state, accurately and efficiently. The inverse problem, on the contrary, consists in assessing the differences between the observed behavior of a system and the underlying models and parameters used to represent it. Regarding the uncertainty in the modeling, a common approach is to drop the deterministic assumption of the equations of motion, recurring to stochastic noise models such as Brownian motion, Ornstein-Uhlenbeck or Gauss-Markov processes [11, 54, 57]. The other target of the inverse problem is the parameter uncertainty, whose objective is to represent the uncertainty in specific terms of the dynamic or measurement equations. This is the core of the work at hand, specifically focusing on uncertain parameters that can be estimated during the OD process as dynamic parameters, not only for the quantification of its uncertainty but also to represent the relationship between the uncertain parameters and the state variance.

There are other techniques conceived to improve covariance realism without focusing on the sources of uncertainty and their modeling. For instance, Gaussian and linear assumptions are held longer in time when the state is represented in mean orbital elements, allowing the covariance matrix to represent more realistically the uncertainty of Monte Carlo simulations [68, 86]. Other typical representations of the state and covariance in non-linear reference frames that are able to slow down the realism degradation upon propagation are being widely studied, such as the QtW frame in [73]. However, despite the advantage of representing the state of the object in orbital elements for covariance realism, we concern ourselves to Cartesian state representation. Even though the proposed methodology is agnostic to the state representation, the operational goal of this work leads us to remain using Cartesian coordinates as is customary in most SST operational scenarios. Other approaches suggest the use of empirical covariance matrices to include all residuals of the estimation process in the covariance computation, regardless of whether the uncertainty has been specifically modeled or not [60, 61, 85]. This proposal claims to account more accurately for noise time-variations rather than process noise or *consider parameter* analysis, at the expense of the physical interpretation of the uncertainty.

In an operational environment, simple and robust techniques are required to improve covariance realism since, as previously discussed, the nominal covariance determination methods tend to provide optimistic results. The most applied solutions are:

- Kalman filters with process noise matrix to introduce the model uncertainty into the system. These UQ methods are gaining acceptance over stochastic acceleration methods in the current state of the art since they can account for both dynamic model and parameter uncertainty. However, a physically-based derivation of a process noise is rather challenging [55]. Other authors suggest calibration methods to estimate such process noise [49], but typical solutions lack the physical meaning of the applied correction and are not suitable for batch processing, the common framework of SST.
- Scaling techniques which inflate the covariance by certain factors. Some authors propose the computation of such scaling based on increasing the initial position uncertainty to match the velocity error [66] whereas other options explore the

usage of the Mahalanobis distance of the orbital differences to find the scale factor [67]. However, a common drawback of artificially increasing the covariance is that the physical meaning of the correction is lost, not being able to understand the contributions of each source of uncertainty. These sort of methods are used nowadays in operation centers such as Space Operations Center (CSpOC) [11].

An additional option to be discussed is the consider analysis theory, which is a classical approach for parameter uncertainty analysis in the equations of motion for OD processes [28]. It consists in extending the state space by including parameters in the dynamic models, such as atmospheric force, solar radiation pressure force or measurement models. These parameters are assumed to follow a Gaussian distribution with a null mean and a certain variance. A null mean allows to maintain an unbiased estimation, whereas the uncertainty of the parameter is accounted for in the state covariance matrix. The *consider parameter* theory is thus designed to tackle the parameter uncertainty of the previously described UQ inverse problem, inflating the estimated covariance to account for such parameter uncertainty. This theory is compatible with both batch and filter applications such as in the Schmidt-Kalman filter [52, 53] and provides the clear advantage of assessing the effect of specific uncertain parameters in the process, maintaining the physical meaning of the covariance correction as opposed to scaling factors techniques. However, one of the main drawbacks of the *consider parameter* theory is that realistic variances of such parameters are not normally known. This can lead either to overly-sized or underestimated state covariance matrices, failing to model the uncertainty of the system and thus, not achieving covariance realism.

This work presents a novel methodology to determine the variance of the *consider parameters* included in the dynamical model of an RSO. It is based on the orbital differences (position, velocity, or both) between estimated and predicted orbits projected into the covariance space (i.e. Mahalanobis distance), which under Gaussian assumptions shall follow a χ^2 distribution to achieve covariance realism. In other words, if the orbital differences are normally distributed and correctly represented by a covariance matrix, the Mahalanobis distance distribution is equivalent to the squared sum of a normal distributions from each component of the orbital differences (i.e. a χ^2 distribution), provided that no correlation exists between them. Therefore, a minimization process can be designed to obtain the *consider parameter* variances that provide the best match between the observed Mahalanobis distance distribution and the expected χ^2 one.

A similar analysis based on the *consider parameter* theory to improve the covariance realism is performed in [87], a precursor work for this study. There, it is proposed to correct the noise-only covariance with a least squares fitting to a so-called observed covariance, this latter being obtained from Monte Carlo orbital differences aggregation. This approach has a main drawback, which is that to compute such observed covariance, orbital differences at distinct orbital positions are mixed from orbit estimates based on different observation scenarios. This issue is mitigated by the normalization obtained with the Mahalanobis distance concept, which is the cornerstone of the methodology presented in this paper.

In the work at hand, the covariance determination methodology is applied to GEO RSOs, continuing the efforts of previous studies that applied the proposed methodology to Low Earth Orbit (LEO) RSOs for drag and range bias uncertainty [88]. The realism of

the determined covariance matrices remains as the cornerstone of this study, and thus specific covariance realism metrics such as the covariance containment are analyzed. For a geostationary orbit, two of the main sources of uncertainty that come into play are related to the Solar Radiation Pressure (SRP) and the time bias of the sensors, which are analyzed in the presented work.

The paper is structured as follows: in Section 3.2, the *consider parameter* theory in the context of batch least-squares estimation is revisited, as well as the linear covariance propagation. In Section 3.3, the proposed models for the *consider parameters* and the covariance determination methodology is described, together with the validation approach. In Section 3.4, the results of the simulation campaigns carried out for validation are presented and discussed. Finally Section 3.5 contains the conclusions and future steps of this study.

3.2 Background

This section briefly describes the *consider parameter* theory in the context of the common batch least-squares processes in SST, as well as the linear propagation of the covariance.

3.2.1 Consider parameter theory in batch least-squares algorithm for orbit determination

The complete description of the *consider parameter* theory (or consider covariance analysis, as termed by some authors) can be found in [23, 28]. For brevity, only the final derivation in the nominal batch least-squares process is described next. Let us define the estimated state vector as

$$\mathbf{y}_{est} = \begin{pmatrix} \mathbf{r}(t) \\ \mathbf{v}(t) \\ \mathbf{p}(t) \end{pmatrix} \in \mathbb{R}^{n_y}, \tag{3.1}$$

where $\mathbf{r}(t)$, $\mathbf{v}(t)$ and n_y are the position, velocity and estimated state dimension, respectively. The estimated parameters, $\mathbf{p}(t)$, are applied either to the force or the measurement models. Typical examples of these parameters are the drag coefficient (C_d) in LEO or the solar radiation pressure coefficient (C_r) in GEO. Following the nominal OD process [28], the noise-only covariance is

$$\mathbf{P}_n = \left(\mathbf{H}_y^T \mathbf{W} \mathbf{H}_y\right)^{-1} \in \mathbb{R}^{n_y \times n_y}, \tag{3.2}$$

where $\mathbf{H_y}$ corresponds to the Jacobian of the observations with respect to the estimated state, and $\mathbf{W}$ is the weighting matrix containing the confidence of each measurement and the possible correlation among the measurements.

The *consider parameters* to be modeled in our system can be gathered in the *consider parameter* vector

$$\mathbf{y}_c = \begin{pmatrix} c_1 \\ \vdots \\ c_{n_c} \end{pmatrix} \in \mathbb{R}^{n_c}, \tag{3.3}$$

where n_c is the number of *consider parameters*. They are defined to follow a normal distribution, i.e,

$$c_i \sim \mathrm{N}\left(0, \sigma_i^2\right);\ i = 1, \cdots, n_c. \tag{3.4}$$

This definition allows the expected value of the orbit estimation to remain unbiased provided that the *consider parameters* have null mean and their variances are uncorrelated with the measurement noise. On the contrary, the covariance of the estimation is affected. The consider covariance, which is defined as the covariance of a state vector accounting for the uncertainty of both the measurements and the dynamical parameters, is

$$\mathbf{P}_c = \mathbf{P}_n + \left(\mathbf{P}_n \mathbf{H}_y^T \mathbf{W}\right)\left(\mathbf{H}_c \mathbf{C} \mathbf{H}_c^T\right)\left(\mathbf{P}_n \mathbf{H}_y^T \mathbf{W}\right)^T, \tag{3.5}$$

where $\mathbf{H}_c$ is the Jacobian of the observations with respect to the *consider parameters* and

$$\mathbf{C} = \begin{pmatrix} \sigma_1^2 & \cdots & 0 \\ \vdots & \ddots & \vdots \\ 0 & \cdots & \sigma_{n_c}^2 \end{pmatrix} \tag{3.6}$$

contains the variances of the *consider parameters*, where no correlation between them is assumed. Eq. (3.5) can be simplified to obtain

$$\mathbf{P}_c = \mathbf{P}_n + \mathbf{K}\mathbf{C}\mathbf{K}^T \in \mathbb{R}^{n_y \times n_y} \quad \text{and} \tag{3.7}$$

$$\mathbf{K} = \mathbf{P}_n \left(\mathbf{H}_y^T \mathbf{W} \mathbf{H}_c\right) \in \mathbb{R}^{n_y \times n_c}, \tag{3.8}$$

where n_c and n_y are the number of *consider parameters* and the state vector dimension, respectively. Therefore, the consider covariance is obtained as the noise-only covariance plus a covariance correction, which depends linearly on the *consider parameter* variances.

3.2.2 Linear covariance propagation

The consider covariance is obtained at estimation epoch and models the effect of the uncertainty of the *consider parameters* that affect the estimation, regardless whether their uncertainty affects the force or the measurement models. However, our interest in enhancing the covariance realism extends also to the covariance propagation for SST purposes. In this paper, we assume linear propagation of the covariance matrix, as it is generally applied in most operational scenarios in SST. More complex and accurate uncertainty propagation methods are out of the scope of this work since Gaussianity is a cornerstone assumption in the proposed methodology. In this respect, Michael's normality tests can be applied to assess data linearity [82, 83]. A complete derivation of linear propagation theory can be found in many well-known references, such as [28]. In the end, to account for the effect of the main dynamic parameters in the propagation of the state, it is required to integrate the variational equations, whose solution is the Extended State Transition Matrix (ESTM)

$$\mathbf{\Psi}(t, t_0) = \begin{pmatrix} \mathbf{\Phi}(t, t_0) & \mathrm{S}(t, t_0) \\ \mathbf{0} & \mathbf{I} \end{pmatrix}, \tag{3.9}$$

where $\mathbf{\Psi} \in \mathbb{R}^{n_y \times n_y}, \mathbf{\Phi} \in \mathbb{R}^{6\times 6}, \mathbf{S} \in \mathbb{R}^{6\times n_p}, \mathbf{I} \in \mathbb{R}^{n_p \times n_p}$ and:

- n_p is the number of dynamical parameters to consider during propagation, which in this case corresponds to the estimated dynamical parameters, excluding position and velocity, hence, $n_p = n_y - 6$.
- $\mathbf{\Phi}(t, t_0)$ corresponds to the state transition matrix, which relates the position and velocity at any time t with respect to the initial state at time t_0.
- $\mathrm{S}(t, t_0)$ is the so-called sensitivity matrix, which contains the partial derivatives of the state vector with respect to the model dynamical parameters, which are assumed to be constant.

The ESTM can be computed by solving numerically its associated partial differential equations as shown in [28]. Linear covariance propagation is then carried out as

$$\mathbf{P}_c(t) = \mathbf{\Psi}(t, t_0)\mathbf{P}_c(t_0)\mathbf{\Psi}(t, t_0)^T. \tag{3.10}$$

By using the ESTM, the effect of the uncertainty of the dynamical model parameters is mapped into the position and velocity covariance not only at estimation, but also along the propagation.

3.3 Methodology

In this section, we define first the *consider parameters* proposed to model the uncertainty in GEO. Then, we describe the concept of the Mahalanobis distance and its connection to the χ^2 probability distribution and develop the proposed procedure to effectively calculate the *consider parameter* variances that define the uncertainty levels of the dynamic model and compute the consider covariance. Finally, the validation procedure is described.

3.3.1 Consider parameter models

As we mentioned previously, two *consider parameters* of interest are included in our analysis: in the SRP force and the time bias of the sensor. This subsection describes their proposed models.

Solar radiation pressure

Following the classical definition [28], the SRP acceleration equation with the first *consider parameter* reads

$$\mathbf{a}_{SRP} = -P_{SRP} C_R \frac{A}{m} \frac{r}{r^3} AU^2 (1 + c_{SRP}), \tag{3.11}$$

where P_{SRP} is the solar radiation pressure, C_R is the solar radiation coefficient, A is the cross-sectional area, m is the mass of the object, r is the distance to the sun, AU expresses the magnitude of an astronomical unit and c_{SRP} is the *consider parameter* associated to the SRP, which is devised to follow a Gaussian distribution as defined in Equation (3.4) with standard deviation σ_{SRP}. The aim of this parameter is to model the uncertainty that can be associated to most of the components of Equation (3.11). The mass may vary for maneuverable satellites, the cross-section area is assumed constant along the estimation and propagation, which is not true in general; the solar radiation pressure

and the solar radiation coefficient are affected by the Sun's behavior (solar cycles) and satellite surface variability (light reflection and absorption), which are not modeled for most SST applications.

Sensor clock time bias

The second *consider parameter* aims to represent the variability in the time bias present in the sensors when time-stamping the measurements. It is characterized as

$$t^* = t + c_{TB}, \tag{3.12}$$

where t denotes time and c_{TB} is the *consider parameter* associated to the time bias, also following the definition of Equation (3.4) with standard deviation σ_{TB}. This *consider parameter* is affecting the measurement model and is associated to each observation.

3.3.2 Covariance determination method

This subsection describes the combination of the *consider parameter* theory with the concept of Mahalanobis distance and defines the proposed methodology to determine the consider covariance.

Mahalanobis distance and consider covariance determination

The Mahalanobis distance is a well-known statistical metric that describes how far a state $\mathbf{y}(t)$ is from a certain reference $\mathbf{y}_{ref}(t)$, projected into the covariance space [78]. This is:

$$d_M^2(t) = \left(\mathbf{y} - \mathbf{y}_{ref}\right)^T \left(\mathbf{P} + \mathbf{P}_{ref}\right)^{-1} \left(\mathbf{y} - \mathbf{y}_{ref}\right), \tag{3.13}$$

where $\mathbf{P}$ and $\mathbf{P}_{ref}$ are the covariance of both the state and the reference, respectively. However, the covariance of the reference is generally several orders of magnitude smaller, which enables us to neglect it many applications. For the sake of clarity, the reference covariance is omitted in the following equations, although it is considered in the computations when applicable. In order to introduce the *consider parameter* effect, we recall the definition of the state vector of Equation (3.1) and combine Equation (3.10) with Equation (3.13), which yields

$$d_M^2 = \Delta\mathbf{y}(t)^T \left(\mathbf{\Psi}(t, t_0) \left(\mathbf{P}_n + \mathbf{K}\mathbf{C}\mathbf{K}^T\right) \mathbf{\Psi}(t, t_0)^T\right)^{-1} \Delta\mathbf{y}(t). \tag{3.14}$$

Thus, Equation (3.14) allows the computation of the squared Mahalanobis distance at any propagation epoch as a function of the *consider parameter* variances included inside matrix $\mathbf{C}$. It is worth mentioning that the projection of the orbital differences in the covariance space allows to combine samples derived from ODs at different epochs and conditions, which is of paramount importance for an operational scenario.

Consider parameter variance determination

It remains to describe the method to compute the variance of the proposed *consider parameters* that is applied in this work following the previous line of research of [88]. Under linear and Gaussian assumptions, this is, when the differences between the state and the reference are normally distributed and the covariance is representative of such

distribution (i.e. realistic), a population of squared Mahalanobis distances should follow a χ^2 distribution, whose detailed characteristics may be found in [76]. Additionally, the χ^2 distribution requires the aggregated normal distributions to be uncorrelated. Consequently, to reduce the correlation between the state variables, the Mahalanobis distance is computed in the In-track, normal , and cross-track (TNW) local frame [56]. The in-track axis is defined as tangential to the orbit and parallel to the velocity. The normal axis is placed in the orbit plane, perpendicular to the in-track axis, and the cross-track axis is perpendicular to the orbit plane. Using local frames aligned with the satellite motion allows to reduce the correlation of orbital differences and helps to trace the impact of the uncertainty sources modeled in the analysis.

Equation (3.14) allows us to compute such Mahalanobis distance at any desired epoch during the propagation arc by comparing an estimated and later propagated (predicted) orbit against a reference. Therefore, if a sufficient number of predicted orbits is available, it is possible to look for the variance of the *consider parameters* represented in matrix $\mathbf{C}$ so that the squared Mahalanobis distance population resembles the theoretical χ^2 distribution. In the work presented here, this optimization problem is based on minimizing the differences between two Cumulative Distribution Functions (CDFs), the observed one and the theoretical χ^2 one. In this case, the theoretical χ^2 distribution should have as many Degrees Of Freedom (DoF) as components of the orbital differences are included in the Mahalanobis distance. This minimization process can be adapted to any desired number of *consider parameters*, being able to combine the two proposed for our analysis (SRP and time bias). The cost function to minimize in order to determine the *consider parameter* variances is defined next for completion. It consists in grouping the observed squared Mahalanobis distances in N_b bins, comparing their joined probability against the theoretical χ^2 one as

$$J = \sqrt{\sum_{i=1}^{N_b} \left(CDF_E(bin_i) - CDF_{\chi^2}(bin_i) \right)^2}, \tag{3.15}$$

where CDF_E corresponds to the empirical CDF of the ith bin, and CDF_{χ^2} the CDF of the χ^2 distribution. Considering more statistically robust CDF comparison metrics was out of the scope of the present work. However, the application of other metrics such as Cramer-von-Mises or Kolmogorov-Smirnov [76] is an open line of research.

3.3.3 Validation chain

In this section, we describe a process to generate the required data to apply the proposed covariance determination method in a simulated scenario for validation purposes.

The presented methodology can be validated by checking if the obtained *consider parameter* variances are representative of the uncertainty present in the system. To confirm this, we run a Monte Carlo iterative scheme in which we simulate a population of orbits. Under simulation conditions, we are able to impose the uncertainty levels in the time bias and SRP. Thus, we condition the outputs of the optimization process to known, controlled values for validation purposes. The steps of the data generation are described below. For further clarification of this scheme, the different kinds of orbits in a relative propagation timeline is shown in Figure 3.1 exemplifying a single Monte Carlo iteration.

- From a GEO reference state associated to an existing RSO and a certain epoch (t_0; estimation epoch), we perform an orbit propagation process to obtain the *reference orbit*, which is used to obtain the orbital differences required for the Mahalanobis distance in Equation (3.14). The details of the RSO can be found in Table 3.1. The dynamic model of this propagation is deterministic, without including any additional perturbation in the SRP or time bias models. See Table 3.2 for model details on the dynamic model characteristics.
- In a Monte Carlo process, we generate a population of orbits sampling the Gaussian distribution of the *consider parameters* models, and introducing each sample as a constant perturbation for each orbit. We then perform the following steps per iteration, also depicted in Figure 3.1:
  1. We propagate the reference state backwards 28 days considering a SRP *consider parameter* perturbation sample in the dynamics. We refer to this propagated orbit as the simulated orbit.
  2. We generate tracks of the simulated orbits using a model of a ground-based telescope, whose details can be found in Table 3.3. We introduce the time bias uncertainty on each simulated observation, again selecting a perturbation sample from the *consider parameter* model defined in Section 3.3.1. Along the generation of these simulated observations, the measurement noise is also included.
  3. We perform an OD process based on the simulated tracks. We have inputs from a period spanning between t_0-28 days and t_0, where t_0 corresponds to the time of estimation. The estimation output (state and noise-only covariance) are obtained at such epoch, which is set at the epoch of the last available measurement in the OD arc of 28 days. The resulting orbit is known as the estimated orbit.
  4. The estimated state is propagated up to the desired propagation arc, in this case 21 days to have complete coverage of typical prediction periods in GEO, using now the same unperturbed dynamic model of Table 3.2. This orbit is known as the *predicted orbit*.
- From one iteration to the next, the simulation time frame is shifted one day forward, so that the generation of observations in the OD process is aligned in time as in an operational scenario. 400 samples, which correspond to more than 1 year of daily tracking data for an object, are expected to suffice for the statistical computations of the proposed methodology, as was found in the simulations performed in previous studies [88].
- **Operational reference orbit:** We propose an alternative orbit to use for the computation of the orbital differences of Equation (3.14) other than the aforementioned *reference orbit*. The *operational reference orbit* consists in the output of an OD whose determination arc includes the propagation epochs of interest for each Monte Carlo iteration. In other words, if we want to analyze the current orbit between t_0+7 days and t_0+21 days, we can use as reference the output of another OD whose arc ranges from t_0 days up to t_0+28 (see Figure 3.1). The reason behind this choice is that, for most SST operational environments, precise orbits whose ephemeris can be assumed perfect are not commonly accessible. For instance, external sources of precise GNSS orbit data is not available when the targets are

non-collaborative objects such as space debris. It is important to remark that, the estimation corresponding to this *operational reference orbit* has certain noise-only covariance due to the measurements uncertainty. Thus, it is necessary to include its noise-only covariance inside the Mahalanobis distance computation of Equation (3.14).

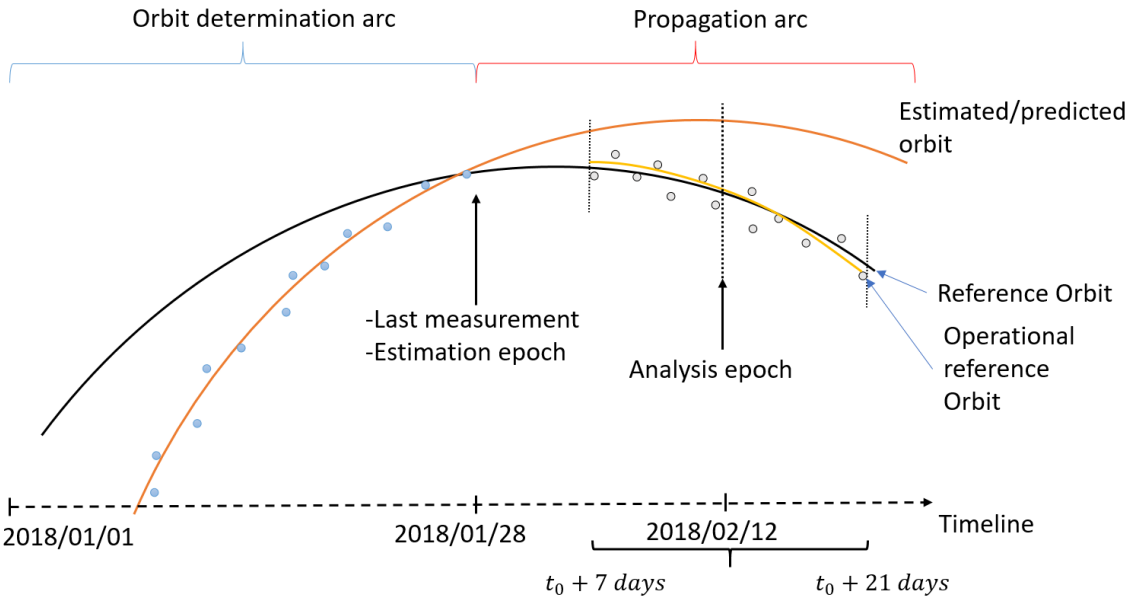

Figure 3.1: Monte Carlo scheme showing the process to generate the *predicted* and *reference* orbits, the typical propagation arc and analysis epochs, and the *operational reference orbit.*

The Mahalanobis distances can be calculated once all the necessary data for all the orbits is available at the desired analysis epochs. Then, the proposed covariance determination methodology can be applied. This process is summarized in Algorithm 1.

Algorithm 1 Covariance determination

1: Propagate reference state N days ⇒ Reference Orbit
2: **for** i = 1:N **do**
3: Set initial state at day i from Reference Orbit
4: Propagate backwards 28 days ⇐ c_{PE} perturbation
5: Generate tracks ⇐ c_{TB} perturbation and sensor noise
6: Orbit Determination of 28 days ⇒ **K**
7: Orbit Propagation of 21 days ⇒ **Ψ**
8: **end for**
9: Using matrices **K** and **Ψ** and the generated orbits ⇒ d_M^2 population of size N (Equation 3.14)
10: Find **C** that minimizes J (Equation 3.15) so that d_M^2 follows a χ^2 distribution

3.4 Results and discussion

This section is divided in three different subsections. The first one describes the characteristics of the simulated environment, providing details on the dynamical model used and the expected uncertainty levels. The second section describes the results of the validation chain of the proposed covariance determination methodology in several test scenarios. Finally, the effectiveness that the proposed methodology achieves in terms of covariance realism is further analyzed.

3.4.1 Simulation environment

For the sake of completeness, this section characterizes the conditions under which the validation test sequence has been performed. Table 3.1 contains the information corresponding to the reference RSO. Table 3.2 defines the applied dynamic model. Finally, Table 3.3 describes the parameters of the simulated telescope used for the generation of orbit tracks (set of measurements).

Table 3.1: Reference RSO parameters

Semi-major axis	42190.42 km
Eccentricity	6.826·10-5
Inclination	13.906°
RAAN	339.651°
Argument of pericenter	312.092°
True anomaly	229.845°
Mass	500 kg
Solar radiation area	40 m^2
SRP coefficient	1.3
Reference epoch	2018-01-28 00:00:00.000 UTC

Table 3.2: Dynamical model characteristics

Reference frame	J2000 ECI
Gravity field	16x16
Third body perturbations	Sun & Moon
Earth geodetic surface	ERS-1
Polar motion and UT1	IERS C04 08
Earth pole model	IERS 2010 conventions
Earth precession/ nutation	IERS 2010 conventions
Atmospheric model	NLRMSISE-90
Solar radiation pressure	Constant area

The tracking strategy, using the telescope described in Table 3.3, consists on series of three measuring intervals per night. Every night, the telescope takes measurements at intervals of 15 minutes located at the beginning, middle and end of the night, with a time-step of 20 seconds. The exact position of the intervals within the night may

Table 3.3: Telescope parameters

Latitude	55.444°
Longitude	-4.638°
Height	800 m
Measurement noise	0.5 mdeg

vary slightly due to shadow conditions. This approach is taken to resemble telescope availability in an operational scenario.

It remains to describe the chosen uncertainty variances for the validation campaign. To this end, it is customary to resort to the literature for expected uncertainty levels in operational environments for the target uncertainty sources that have been modeled as *consider parameters*. Regarding the SRP uncertainty, according to [28] an annual variation of 3.3% is estimated. Other studies performed for Ajisai and LAGEOS geodetic satellites [38] identified variations ranging between 1% and 3%. Thus, for the purposes of the work at hand, a 5% standard deviation in SRP has been considered a realistic uncertainty for validation. Nonetheless, higher uncertainty levels are also analyzed in Section 3.4 for validation purposes. The characterization of the time bias behavior is more complex, mostly due to its strong dependence on the type of instrument. From [41] and [42], typical uncertainty levels ranging from 1 to more than 100 ms can be extracted. Similarly to the SRP case, 100 ms of standard deviation has been selected as a realistic uncertainty for validation, despite reaching higher values in the presented results.

3.4.2 Simulation results

The main objective of the validation phase is to verify that the uncertainty introduced in the Monte Carlo simulation is correctly retrieved as *consider parameter* variances in the optimization process. To verify this, we propose a sequence of validation tests, summarized in Table 3.4. Only the most relevant test cases are included.

The tests become gradually more complex. The first three series (I to III) represent the core validation pipeline, in which we subject the dynamic model to perturbations significantly higher than the ones suggested by the literature (Section 3.4.1) to verify the robustness of the presented covariance determination method in highly-perturbed environments where data Gaussianity is stressed to the limits of the methodology assumptions. In the first series, we restrain our analysis to the estimation epoch t_0, starting from null perturbation. We then proceed to include perturbations as uncertainty in the system. In the second series, we extend the analysis to a future epoch, located at 15 days of propagation into the future. The third series is representative of the final complexity of the methodology, combining Mahalanobis distance calculations from epochs located all over an interval of 14 days, with a time-step of one day. Including different epochs of the propagation arc in the same optimization process has the objective of computing a single *consider parameter* variance that is able to improve the realism of the covariance in the complete interval of interest, which is a desired operational feature. The fourth series is conceptually equal to the third, but show a case with reduced perturbation levels in line with the discussion Section 3.4.1, looking for values of uncertainty closer to the ones expected in the literature.

Table 3.4: Simulation tests results summary

Case	Comparison orbit	Analysis epoch	Input	Results	Accuracy |%|
I-A	Ref.	t_0	-	-	-
I-B	Ref.	t_0	σ_{SRP}=30% σ_{CB}=1000ms	σ_{SRP}=27.93% σ_{CB}=1071.17ms	6.9 7.1
II-A	Ref.	t_0+15	σ_{SRP}=30% σ_{CB}=1000ms	σ_{SRP}=28.02% σ_{CB}=988.23ms	6.6 1.2
II-B	Op. ref.	t_0+15	σ_{SRP}=30% σ_{CB}=1000ms	σ_{SRP}=26.73% σ_{CB}=1001.23ms	10.9 0.1
III-A	Ref.	t_0+7-21 (interval)	σ_{SRP}=30% σ_{CB}=1000ms	σ_{SRP}=28.26% σ_{CB}=1083.46ms	5.8 8.4
III-B	Op. ref.	t_0+7-21 (interval)	σ_{SRP}=30% σ_{CB}=1000 ms	σ_{SRP}=29.40% σ_{CB}=982.75ms	2.0 1.7
IV-A	Op. ref.	t_0+7-21 (interval)	σ_{SRP}=5% σ_{CB}=100ms	σ_{SRP}=4.56% σ_{CB}=100.22ms	8.8 0.2

The analyses were performed discarding velocity components (in the minimization phase), due to the accumulation of small errors in the in-track velocity after propagation. Apart from the velocity components being several orders of magnitude smaller than the position ones, the expected precision of the in-track velocity was found to be the smallest covariance term among the velocity components. This lead to ill-conditioning of the covariance and an exponential increase in the Mahalanobis distance for high perturbations after more than 3 days of propagation. Therefore, only 4 DoF remain for the χ^2 distribution, namely the position differences (TNW frame) and the SRP coefficient. Nonetheless, since a series of different position ephemeris are considered, the dynamics of the system are fully regarded in the computations.

The overall results of the validation test sequence, paying special attention to the last ones due to their increased level of complexity, has shown to provide satisfactory results when computing the *consider parameter* variances. The deviations between the input perturbations and output *consider parameter* variances did not exceed 11% for any of the perturbations in any of the cases.

The starting point of the validation (Case I-A) explores the ideal situation in which no perturbation is present in the dynamic model. Then, if the measurement noise is properly characterized, the noise-only covariance is expected to be representative of the uncertainty of the system, and the squared Mahalanobis distance distribution should directly resemble a χ^2 one. Figure 3.2 shows the results of this case, where this fact can be appreciated. The retrieved distribution is very close to the χ^2 distribution without applying any *consider parameter* correction. This is a clear indication that in the sole presence of measurement noise, the noise-only covariance is able to represent the uncertainty of the system. Moreover, It can be noted that the number of DoF in this case is 7. As opposed to the rest of the tests, series I cases are analyzed at t_0, not suffering from in-track velocity error accumulation during propagation.

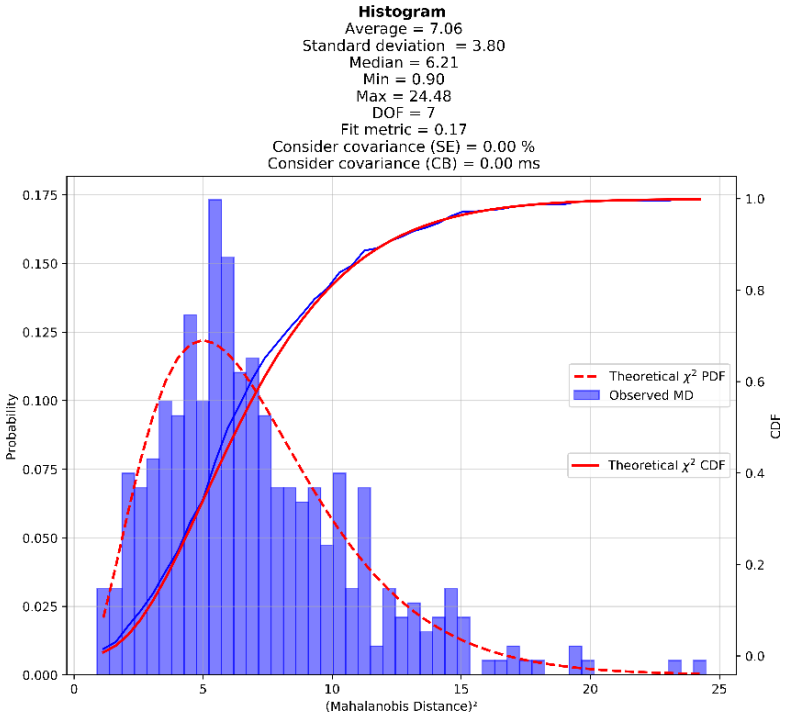

Figure 3.2: Case I-A.

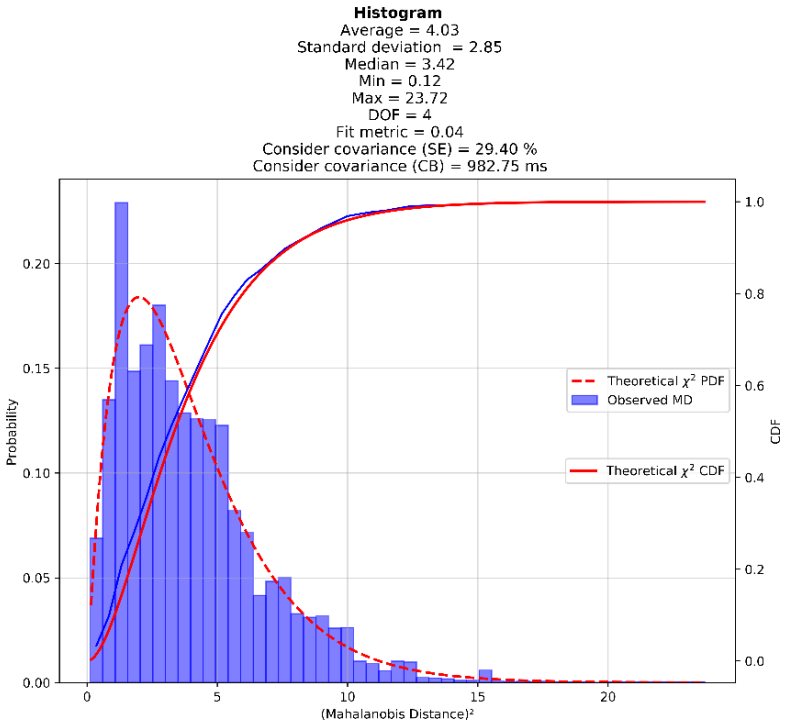

Figure 3.3: Case III-B.

On the contrary, the noise-only covariance no longer represents the uncertainty of the system when dynamic model uncertainty is introduced. Case I-B shows the results of

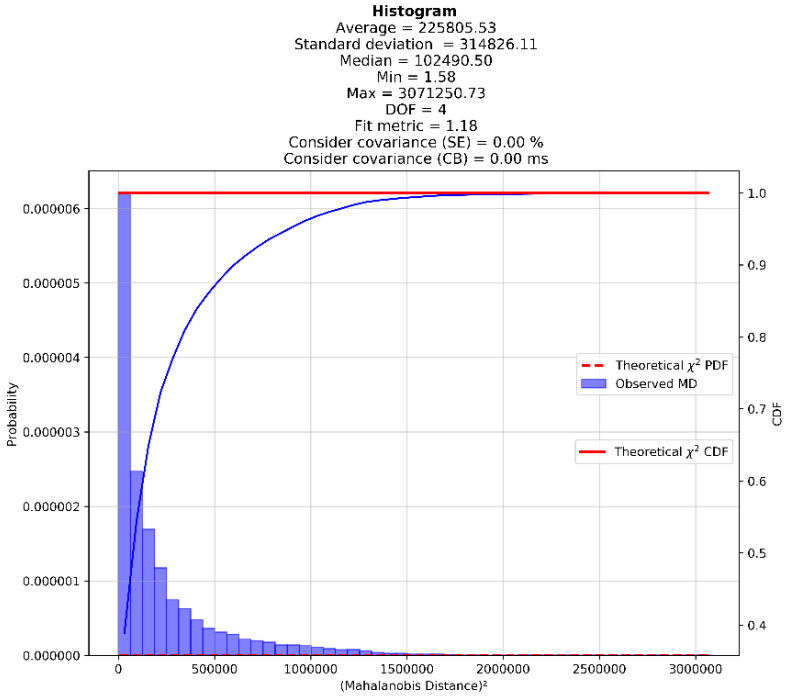

Figure 3.4: Case III-B without *consider parameter* correction.

including both *consider parameter* perturbations simultaneously, performing two-variable optimization at the estimation epoch. As seen in Table 3.4 the methodology is capable of computing *consider parameter* variances within a margin lower than a 10%.

However, we discussed that from an operational perspective it is desirable to extend this analysis into the prediction region. In the second series (II-A, II-B), we establish the analysis epoch at t_0+15, proving that the quality of the results obtained in the previous series can be maintained when propagating up to this time horizon. Additionally, we introduce the usage of *operational reference orbits* in the case II-B. Thus, we include a new layer of realism by not relying on an absolutely true representation of the reference orbit, but rather on the result of an OD process with an associated covariance matrix. As was observed in [88], obtaining appropriate results using the *operational reference orbit* is of high relevance in operational scenarios, allowing the methodology to function using only the observations, not requiring other external information sources.

The third series of cases extend the analysis epoch from a single one to a full interval spanning for 14 days between t_0+7 and t_0+21. Table 3.4 shows the most relevant subcases, combining both *consider parameters* and comparing against reference and operational orbits. Mahalanobis distances are calculated at specific points within this period, at time steps of one day. The main leap forward in this series is that a singular optimized *consider parameter* variance is able to recover the χ^2 behavior of the squared Mahalanobis distance population for a wide propagation interval, obtaining *consider parameter* variances very similar to the introduced perturbations as can be seen in Table 3.4 and recovering the χ^2 behavior as can be observed in Figure 3.3. Again, accurate results are obtained independently on the orbit used to obtain the orbital differences. Besides the fact that adding more comparison epochs increases the analyzed population samples, specific

disturbances associated to a certain point in the orbit can be smoothed by including Mahalanobis distances from a wider range of analyzed epochs.

Figure 3.4 corresponds to the same case scenario as in Figure 3.3, but in this case maintaining the noise-only covariance for the Mahalanobis distances computations. We find that the values of the distribution are far from resembling the χ^2 behavior. This figure has been included to show the inability of the noise-only covariance to represent the uncertainty of the system when model uncertainty is present. The high values of the distribution indicates that, without the *consider parameter* variances correction, the covariance is overly-optimistic and the observed orbital differences are much larger than the standard deviation present in the covariance.

The fourth series of tests does not introduce new elements into the methodology. It serves to prove that the model is sensitive to lower perturbation levels which are aligned with those suggested by the literature. Figure 3.5 contains the fitting results of the last test case, IV-A, which is representative of the full complexity of the methodology proposed in this work. Again, the differences between the input perturbation and the results of the *consider parameter* variances is lower than a 10%, showing that the methodology is able to recover the theoretical χ^2 behavior and thus improve the covariance realism.

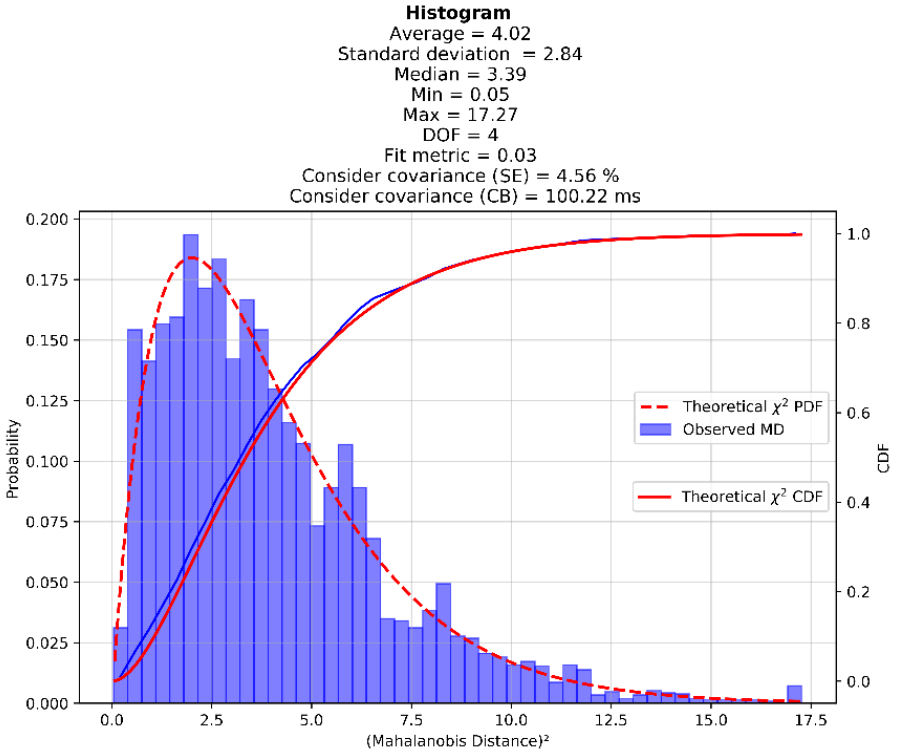

Figure 3.5: Case IV-A.

3.4.3 Containment analysis

To obtain a physical interpretation and a proper visual representation of the effectiveness of the proposed covariance determination method for improving the covariance realism, covariance containment tests, such as the one proposed in [43], are provided in this

section. To evaluate whether the covariance is representative of the orbital differences (i.e. realistic), the Mahalanobis distance can be used as a metric to see the number of points that lay inside a $k-\sigma$ ellipsoid ($k = 1, 2, 3, 4$) and compare it against the theoretical expected fraction for a multivariate Gaussian distribution of as many Degrees Of Freedom (DoF) as components of the state vector used for the Mahalanobis distance. In all tests presented previously, only position and the SRP coefficient of the state vector were included in the Mahalanobis distance computation. Gaussianity tests of the orbital differences were performed (Michael's normality test), to ensure the fulfillment of Gaussian assumptions in the proposed methodology, though those results have been omitted for conciseness. Table 3.5 summarizes the evolution of the containment metric at different epochs, comparing both noise-only and consider covariance matrices versus the 4 DoF theoretical containment results. The results found in Table 3.5 were obtained using the optimum *consider parameter* variances found in the results of case III-B. The results of this test case are chosen for this analysis due to a high resemblance to an operational scenario, as it maintains a realistic amount of data, it uses the *operational reference orbit* for comparison and achieves sufficient accuracy.

Table 3.5: Containment tests

Epoch [days]	**Without consider parameter correction [%]**				**With consider parameter correction [%]**			
	1σ	2σ	3σ	4σ	1σ	2σ	3σ	4σ
t_0+4	0	0	0.25	0.51	8.33	57.07	92.68	99.75
t_0+6	0	0	0.25	0.51	8.84	56.82	92.42	99.49
t_0+8	0	0.25	0.25	0.25	8.84	56.31	93.18	99.75
t_0+10	0	0.25	0.25	0.25	8.33	56.82	92.93	99.75
t_0+12	0	0.25	0.25	0.25	7.58	57.32	93.69	99.75
t_0+14	0	0.25	0.25	0.25	8.61	57.47	93.92	100
t_0+16	0	0	0.25	0.25	8.61	58.73	93.92	100
t_0+18	0	0	0.25	0.25	8.61	58.99	93.92	100
t_0+20	0	0	0	0.25	9.11	58.99	93.92	99.75
Average	**0**	**0.11**	**0.22**	**0.31**	**8.54**	**57.61**	**92.96**	**99.80**
Theoretical (4 DoF)	**9.00**	**59.40**	**93.90**	**99.70**	**9.00**	**59.40**	**93.90**	**99.70**

It is clear from Table 3.5 that the proposed methodology leads to an improvement in covariance containment when model uncertainty is present. The results at all epochs are close to the theoretically expected ones, particularly for 3σ and 4σ. There are several implications of these results. Firstly, the average containment along the complete propagation interval resembles closely its theoretical expectation. Recalling the operational goal of the methodology, this shows that a unique *consider parameter* variance is able to improve substantially the covariance realism in the interval of interest for GEO scenarios. Secondly, the degree of similarity of the containment in all sigma ellipsoids indicates that the consider covariance is not over-sized, showing that the proposed methodology is able to tackle the model uncertainty properly and maintain the traceability of its sources. On the contrary, it is directly observed the lack of covariance

realism in the absence of *consider parameter* correction when model errors are present. Noise-only covariance matrices are too optimistic and fail to represent the PDF of the state. Another way to visualize this phenomenon can be found in Figures 3.6 and 3.7, where we compare the amount of orbital differences included in the 3σ ellipsoid (in green) in both cases: with *consider parameter* and without *consider parameter*, respectively. The orbital differences are shown in the relative frame TNW (in-track, normal and cross-track directions)

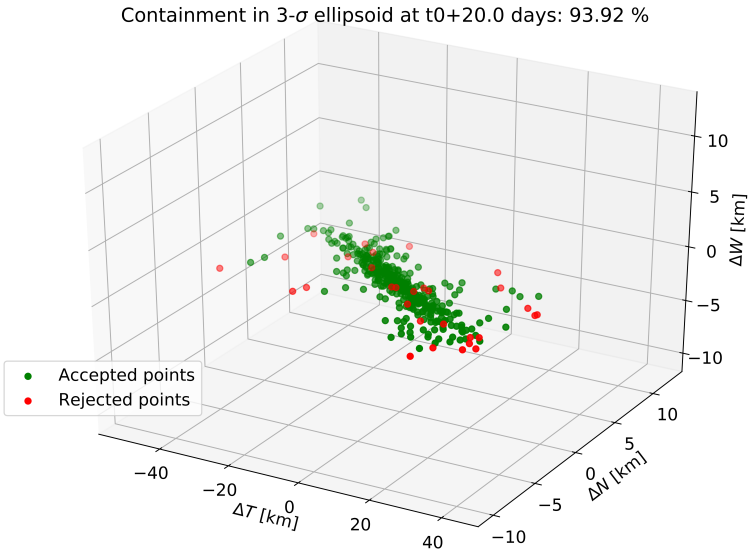

Figure 3.6: Orbital differences 3σ containment at $t_0 + 20$ days using the determined consider covariance.

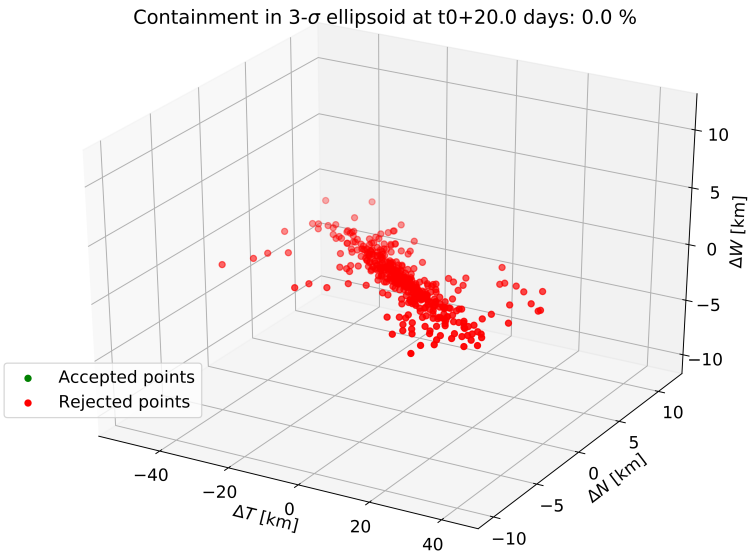

Figure 3.7: Orbital differences 3σ containment at $t_0 + 20$ days without any *consider parameter* correction.

Figure 3.6 shows that the orbital differences are larger in the in-track direction. The consider covariance is elongated in such direction, representing the actual distribution.

The ellipsoidal shape is not easily discerned in Figure 3.6 due to the significantly larger standard deviation of the in-track component. It is clearly observed that the *consider parameter* methodology correction with our determined variance elongates the ellipsoid in the in-track direction, which is the one showing a higher dispersion.

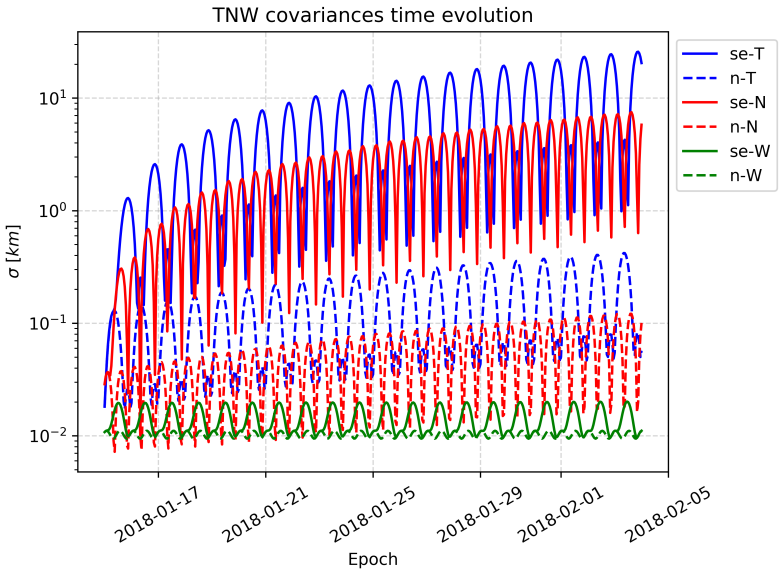

Figure 3.8: Covariance evolution in TNW frame from estimation epoch up to 21 days of propagation for a sample orbit comparing 2 cases: without applying any correction ("n" prefix), with a SRP *consider parameter* variance of 29.4% ("se" prefix).

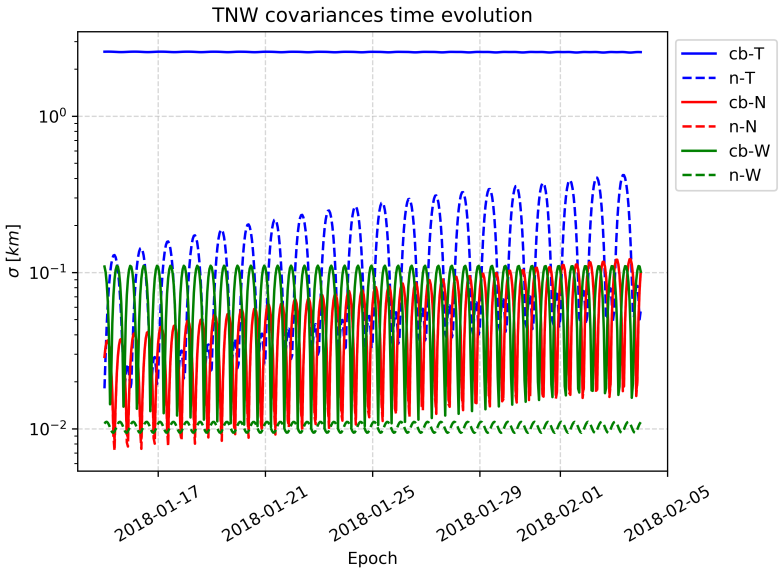

Figure 3.9: Covariance evolution in TNW frame from estimation epoch up to 21 days of propagation for a sample orbit comparing 2 cases: without applying any correction ("n" prefix), with a clock bias *consider parameter* variance of 982.75 ms ("cb" prefix).

For further analysis, Figures 3.9, 3.8 and3.10 are included to show the effect on the position covariance that enables the *consider parameter* correction, focusing on a single orbit and

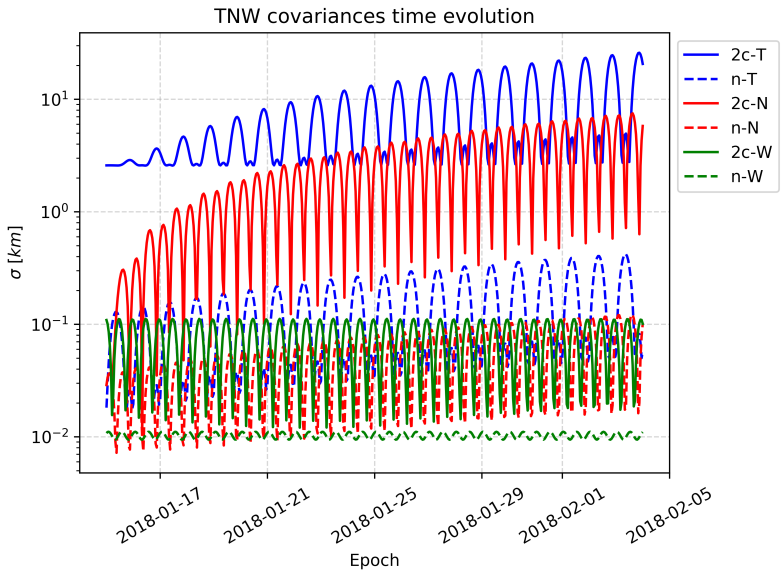

Figure 3.10: Covariance evolution in TNW frame from estimation epoch up to 21 days of propagation for a sample orbit comparing 2 cases: without applying any correction ("n" prefix), with both consider *consider parameter* variances applied simultaneously ("2c" prefix).

separating the contribution of each of the *consider parameters* included in the present analysis. The figures compare the standard deviation of the noise-only covariance and the consider covariance in the three main directions of the local TNW reference frame. Again, the optimum *consider parameter* variances obtained in case III-B (29.4% and 982.75 ms for SRP and clock-bias *consider parameter* standard deviations, respectively) have been used for consistency.

SRP model correction causes a fast covariance growth in in-track and normal directions as compared to the noise-only, mildly affecting the out-of-plane component as can be seen in Figure 3.8. However, at t_0 its effects are barely visible in the state covariance. This is caused by the *consider parameter* correction, which at t_0 for the SRP is mostly applied to the SRP coefficient variance, and is transmitted to the state via the linear propagation of the ESTM (which includes the complete augmented state with the SRP coefficient), due to the correlation between the SRP coefficient term and the state vector. This causes the observed growth in the in-track and normal directions.

Clock bias correction, on the contrary, provokes a remarkable growth of the in-track covariance at t_0 without any further time evolution, as observed in Figure 3.9. This is expected due to the nature of the clock bias perturbation, which is only affecting the measurement model, being observed mostly at the output of the estimation. It is concentrated in the in-track component, since any error in the observation time is directly translated into an uncertainty in the satellite position in the direction of the motion. For this reason the in-track covariance appears constant in the CB-only case, since the orbital oscillations from the noise-only covariance are several orders of magnitude smaller.

When both corrections are combined (Figure 3.10), the clock bias provides not only a higher initial value of the in-track covariance, but also a lower uncertainty limit for this direction along the orbit oscillations. Again, the growth of both in-track and normal

directions with time is dominated by the SRP correction.

3.5 Conclusions and future work

The results shown in this work indicate that the presented covariance determination methodology is capable of accurately capturing the model error present within the dynamics of an RSO on a simulated SST scenario. It has been successfully applied to GEO, considering SRP and sensor time bias uncertainty. We have tested the robustness of the model by enforcing large perturbation levels, while also ensuring that sensitivity to lower values is maintained. The deviation between the uncertainty introduced as perturbation inputs and the determined *consider parameters* has remained lower than a 11% throughout the development of this work. Additionally, successful results have been obtained when estimated orbits are used as reference to compute the Mahalanobis distance, indicating the operational suitability of the methodology for operational scenarios. Relevant metrics for covariance realism assessment such as the covariance containment tests have shown that the proposed methodology is able to determine a realistic covariance, applicable to the complete propagation region of interest in GEO and without over-sizing.

The presented methodology allows to maintain the traceability of the different sources of uncertainty, being capable of determining the uncertainty accordingly in different *consider parameters*. Regarding the impact of the corrections induced by the retrieved *consider parameter* variances on the covariance matrices, it was observed that the time bias uncertainty accumulates in the in-track component at estimation epoch, but does not introduce a significant degree of growth rate in the long term. On the contrary the SRP uncertainty correction, though small at t_0, increases the growth rate in the in-track and normal direction with time.

The next natural step is to use real data from a GEO RSO to further study the capabilities of the methodology. However, the efforts carried out towards realistic simulated scenarios, and the real data results of previous lines of research suggest that the applicability of the proposed methodology for GEO in a real scenario is possible [88]. Further research is under development regarding the optimization process. Robust statistics widely used for the comparison of CDFs such as Cramer-von-Mises or Kolmogorov-Smirnov are being tested as cost functions to retrieve the optimum *consider parameter* variance, allowing also to determine bounds for variances that are statistically consistent to a χ^2 behavior. Additional analysis needs to be performed to increase the number of *consider parameters* for different regimes, intending to quantify as much as possible all sources of uncertainty. Although the work presented here focused on covariance realism, analyzing the two first moments of the state PDF, the impact of the proposed methodology in terms of uncertainty realism by retaining higher order moments of the distribution must be considered. This is crucial for highly non-linear environments where the Gaussian assumptions upon which this methodology is based are stressed.

It is worth reminding that the *consider parameters* methodology assumes a constant error model for its derivation, even though having a certain variance. More complex noise models such as purely Gaussian, Ornstein-Uhlenbeck, Gauss-Markov or other time and space correlation processes are also a current line of research, focusing on how to adapt or generalize the *consider parameters* methodology to more complex representation

of the orbit uncertainty sources. Another relevant line of work is connected to the characterization of the methodology accuracy, exploring the minimum amount of orbital data required to achieve a successful model error estimation. The less data is required, a smaller time-region can be faithfully analyzed, which can allow to capture seasonal variability in the model uncertainties. This is relevant, for instance, in solar weather cycles. Finally, parameterization and bench-marking to select appropriate *consider parameter* corrections as a function of the orbital regimes and space conditions to improve catalog covariance realism is a relevant future goal to improve SST products quality.

Acknowledgments

This project has received funding from the “Comunidad de Madrid" under “Ayudas destinadas a la realización de doctorados industriales" program (project IND2020/TIC-17539).

4

Catalog-based Atmosphere Uncertainty Quantification

4.0 Scientific contribution and context

This paper represents the logical continuation of the work of the previous publications considering SST purposes. In previous Chapters, the *Covariance Determination* methodology was consolidated and validated in LEO and GEO environments, for multiple and combined uncertainty sources, and without requiring external data. Therefore, the next questions to answer were: can this be applied to a catalog of objects? Can it be used to estimate uncertainty models common to the complete catalog?

These questions are addressed in this paper, where a subset of objects with different ballistic coefficients and at different altitudes in a LEO environment is simulated. Each object is exposed to drag model error perturbations, whose variance depends on the altitude, chosen from a realistic analysis of historical atmospheric density dispersion. Then, the objective is to improve the *Covariance Determination* methodology to be able to estimate the parameters that define an altitude-dependent law of the atmospheric density uncertainty. This comes with significant challenges, namely adapting the optimization cost function for multiple objects and uncertain parameters while in a complex simulation environment with correlation and limited data. The paper shows that the *Covariance Determination* methodology is able to estimate the parameters of the altitude-varying density uncertainty, proving that it is able to combine successfully and efficiently the information from multiple objects of a catalog and estimate common models. By grouping catalog uncertainty in transversal models as in this paper, it would be possible to achieve significant covariance realism improvements by applying the quantified uncertainty to the complete catalog, while estimating the model with a reduced subset of control objects. Though a remarkable covariance realism improvement was shown in most objects, those at the lowest altitudes started to show signs of non-linearities, which required normality tests and indicated the need for improvements at lower altitude orbits.

Although the methodology of this paper shares a large fraction of its contents introduction and methodology with previous works, it is further focused on atmospheric density models and their uncertainty, with also some details about stochastic models with correlation.

A. Cano[1,2], **A. Pastor**[1], **J. Míguez**[2], **M. Sanjurjo-Rivo**[2], **D. Escobar**[1],
[1]GMV, 11 Isaac Newton, 28670 Tres Cantos, Madrid, Spain,
[2]Universidad Carlos III de Madrid, 30 Avenida Universidad, 28911 Leganés, Madrid, Spain,
The Journal of the Astronautical Sciences (2023) 70: 42
10.1007/s40295-023-00403-w

Due to the ever-increasing space objects population, Space Situational Awareness (SSA) products and services have become the cornerstone for the safety and sustainability of spacecraft operations. Most of these services rely on the characterization of the uncertainty of the system, which is known as Uncertainty Quantification (UQ). In many applications the uncertainty of the orbit state is represented by the covariance matrix, obtained from an Orbit Determination (OD) process. However, typical OD processes usually consider the measurements noise as the only source of uncertainty. An unrealistic characterisation of the uncertainty of dynamical and observations models leads to a degradation of the realism of the covariance, and jeopardizes spacecraft operations.
In this work, we apply our recent methodology for covariance realism improvement, based on the consider parameter theory of batch least-squares methods, to a catalog scenario to derive the uncertainty of the atmospheric drag model. This methodology infers the variance of consider parameters based on the observed distribution of the Mahalanobis distances of the orbital differences between predicted and estimated orbits, which theoretically should follow a chi-square distribution under Gaussian assumptions. Empirical Distribution Function (EDF) statistics such as the Cramer-von-Mises or the Kolmogorov-Smirnov distances are used to determine optimum variances of such parameters for covariance realism.
The main objective of this work is to adapt and test the previously developed methodology to a LEO catalog scenario, in which the evolution of the density uncertainty for multiple objects can be analyzed together by modeling such uncertainty as a consider parameter. Thus, instead of estimating the variances of the consider parameters tailored to a single object during a long period, the objective of this work is to determine variances of parameters of a parametric model for the atmospheric density uncertainty, improving the covariance realism for different clusters of cataloged objects (i.e. different altitudes or ballistic coefficient). Altitude-dependent models of the atmospheric density uncertainty, based on statistical analysis of historic space weather data, are applied for realistic simulations together with space-correlated density perturbations. Results are presented focusing on the physical interpretation of the determined consider parameter model variances and their effectiveness for improving the covariance realism of the considered catalog of objects.
Keywords: uncertainty realism, covariance realism, catalog uncertainty, space situational awareness, covariance determination, Mahalanobis distance, chi-square distribution

4.1 Introduction

In the current over-populated space environment, the provision of Space Situational Awareness (SSA) and Space Traffic Management (STM) services and products is becoming the cornerstone for safe and efficient spacecraft operations. Many of these services, such as conjunction risk assessment, maneuver detection, fragmentation analysis or catalog build-up and maintenance require reliable estimations of the state of the Resident Space Objects (RSOs) and their associated uncertainty. The quality of this uncertainty

is generally measured by how closely it represents reality, also known as uncertainty realism.
Under the assumption that the state of an orbiting object can be represented by Gaussian random variables, the Probability Distribution Function (PDF) of a state can be reduced to its two first statistical moments (i.e., mean and variance). Despite of these strong assumptions, most operational scenarios represent the RSO state with its mean state and covariance matrix, the main outputs of typical Orbit Determination (OD) processes. Though the latter is only a necessary but not sufficient condition for uncertainty realism, in this framework uncertainty realism is reduced to covariance realism. This uncertainty representation avoids handling more complex PDF representations of the state, being a recurrent choice for SSA operational scenarios where data scarcity and the large number of objects have increased the complexity of the system. Nonetheless, covariance realism still requires an unbiased estimation and covariance consistency in terms of size, shape and orientation.
Typical OD processes, based on batch least-squares algorithms, normally consider the measurements noise as the only source of uncertainty [23], giving the covariance of the estimated state the name of noise-only covariance [56]. However, dynamic or measurement models uncertainty sources are typically disregarded. This leads to a lack of realism in such covariance matrices, being overly optimistic, thus jeopardizing SSA products reliability. This lack of covariance realism is caused by an improper characterization of some of the uncertainty sources present in the underlying models and parameters used to represent the orbital motion [28, 84].
Therefore, it is crucial for SSA activities and the future sustainability of the space environment to improve the modeling and characterization of the RSO uncertainty, which is the goal of Uncertainty Quantification (UQ). Among the many aspects of UQ, this work focuses on the so-called inverse problem, this is, the characterization of the discrepancies between observations of a system and the models used to represent it [11]. Consequently, effective UQ methods that improve the modeling of the uncertainty result in an enhancement of the uncertainty realism.
A widely explored option to characterize the inherent uncertainty of the space environment is the introduction of stochastic dynamic models or process noise, modeling the uncertainty of the system as Brownian motion, Ornstein-Uhlenbeck or Gauss-Markov processes [57, 59]. Process noise techniques, mainly used in filtering applications, also consist in adding certain noise terms to the system dynamics to account for unmodelled uncertainty sources. Their main drawback is the estimation of the noise to be introduced in the system. For these reasons, process noise estimation via calibration processes are required to maintain a physical interpretation of the uncertainty [49, 50]. For instance, in [55], a physically-based estimation of a process noise matrix that models the drag uncertainty is proposed and applied to a batch estimation. In [60, 61, 85], the concept of empirical covariance matrices is proposed. The goal is to include the residuals of the orbit determination process for the estimation of the covariance, adapting faster to noise time variations than process noise techniques. However, the physical interpretation of the uncertainty sources cannot be unveiled with this technique.
Another approach is the parameter uncertainty, which models the uncertainty of the system as uncertain parameters whose distribution impacts the state uncertainty

evolution. Depending on the type and observability of the parameter, its impact on the system time-evolution can be included [11]. An example of uncertain parameters methods is the *consider parameters* theory. It consists in expanding the state space with additional parameters in the dynamic or measurement models. These parameters intend to represent specific and tailored sources of uncertainty, and are devised to follow a certain model with its corresponding uncertainty, in this case, a Gaussian distribution with null mean (to get an unbiased estimation) and certain variance. Even though it has been classically applied to batch estimation, this formulation can be also combined with filtering algorithms such as the Schmidt-Kalman filter [52, 53]. Due to the correlation between those parameters and the dynamics, the state uncertainty evolution is affected by the additional variance of the considered parameters, providing a physically-based and traceable source for the modeled uncertainty. However, the *consider parameters* theory suffers from the same drawback as process noise techniques: realistic noise values or variances of such parameters are not normally known. Overly optimistic, or oversized, variances may fail to model the uncertainty of parameters in the estimation and subsequent propagation of the covariance, not achieving covariance realism.

There are other techniques to improve the realism of the uncertainty of the state without focusing on the modeling and estimation of the different sources of uncertainty. The representation of the state in slowly-varying set of elements allows to maintain Gaussianity for longer propagation arcs and thus reduce the realism degradation, such as mean orbital elements [68, 86] or non-linear reference frames [73]. Covariance inflation techniques are also applied in many operation centers such as the Space Operations Center (CSpOC) [11], using scaling factors for the covariance to improve its realism. Some authors propose the use of such factors based on matching the initial position uncertainty with the velocity error [66]. Others explore the use of the Mahalanobis distance of the orbital differences to find global covariance scaling factors [67]. Even though these methods can be effective under some assumptions, they do not allow to study the physical meaning of the correction.

In previous works, we developed *Covariance Determination*, a methodology to improve covariance realism during orbit determination and propagation, based on the *consider parameters* theory, orbital differences between estimated and predicted orbits and the χ^2 distribution [88, 92, 93]. The core of the method is that, under Gaussian assumption, the difference between both orbits projected into the covariance space (i.e. Mahalanobis distance), must follow a χ^2 distribution. Thus, the variance of the *consider parameters* can be determined via statistical comparison between the observed Mahalanobis distance distribution and the expected one, i.e., a χ^2 distribution. That is, our methodology follows the uncertain parameter approach of UQ, modeling specific uncertainty sources with the *consider parameters* theory. If the variance of such parameters is properly inferred with the proposed methodology, the *consider parameters* theory correction acts as a covariance inflation technique, but according to the physical sources of uncertainty that are included, hence improving the realism of the covariance. In previous works, the proposed methodology has been validated and tested in simulated scenarios for LEO [92] and GEO [93], with different sources of uncertainty analyzed, as well as with real data [88]. However, previous studies were focused on a single RSO analysis, with an assumed constant variance of the *consider parameter* models.

In the present work, the goal is to apply the *Covariance Determination* methodology of [92] in a LEO catalog-like scenario. In this orbit regime, the drag force becomes of high relevance for the orbit dynamics, turning into the dominant perturbation for low of altitudes. In addition, this force is subjected to several sources of uncertainty that are normally disregarded in nominal batch least-squares OD processes. Firstly, in SSA applications for non-collaborative objects, the drag coefficient, mass and area of the RSO is subject to a high level of uncertainty [56]. Secondly, the atmospheric density is also an uncertain parameter, both due to the lack of knowledge in the density models (presenting variations of even a 10-20% between them [32, 91]) and also due to its dependence on the solar activity prediction. For all these reasons, the evolution of the drag uncertainty and the atmospheric density as a function of the altitude, RSO characteristics or solar activity is subject to many studies [32, 34, 35, 54, 57, 59, 94].

Therefore, this work expands the previously developed methodology of [92] to estimate parameters that define the variation of the atmospheric density uncertainty in a catalog of RSOs. To this end, we apply a statistical analysis of historical space weather data to derive a parametric law for the evolution of the density uncertainty with altitude, for a given period of high solar activity, based on the work developed in [17, 27]. Using this law, a simulation with several objects at different altitudes is carried out, applying realistic and altitude-correlated perturbations derived from the uncertainty evolution law. Finally, the *Covariance Determination* methodology is applied simultaneously to all objects with the objective of estimating the parameters that define the evolution of the density uncertainty.

The remainder of the paper is structured as follows: Section 4.2 describes the methodology of the analysis. This includes a summary of the *Covariance Determination* methodology principles in Subsection 4.2.1, the development of the catalog-based adaptation and the historical statistical analysis for the atmospheric density standard deviation in Subsection 4.2.2, and finally a description of the simulation environment in Subsection 4.2.3. Next, Section 4.3 presents the results of the analysis. Finally, Section 4.4 summarizes the main conclusions and future work.

4.2 Methodology

This section describes the methodology of this work. First the main aspects of the *Covariance Determination* method are outlined. Then, the altitude-dependent model for the atmospheric density uncertainty is developed. Finally, the details of the simulation process are explained.

4.2.1 Covariance determination method principles

This section summarizes the background of the *Covariance Determination* methodology developed in [92].

Consider parameters theory

The *Covariance Determination* method is based on the *consider parameters* theory, whose complete description can be found in [23, 28]. Let us define first the estimated parameters vector used in a batch least-squares process as

$$\mathbf{y_{est}} = \begin{pmatrix} \mathbf{r}(t_0) \\ \mathbf{v}(t_0) \\ \mathbf{p}(t_0) \end{pmatrix} \in \mathbb{R}^{n_y}, \tag{4.1}$$

being $\mathbf{r}(t)$, $\mathbf{v}(t)$ and n_y the position, velocity and estimated state dimension, respectively. The vector of dynamical parameters, either applied to the force or the measurement models, corresponds to $\mathbf{p}(t)$. A common dynamical parameter in LEO is the drag coefficient (C_d). Let us represent the considered parameters that are modeled in the system in a *consider parameter* vector as

$$\mathbf{y}_c = \begin{pmatrix} c_1 \\ \vdots \\ c_{n_c} \end{pmatrix} \in \mathbb{R}^{n_c}, \tag{4.2}$$

where n_c is the number of *consider parameters*. They are defined to follow a Normal distribution of the form

$$c_i \sim \mathrm{N}\left(0, \sigma_i^2\right) \quad \text{with} \quad i = 1, \cdots, n_c. \tag{4.3}$$

The *consider parameters* theory models the parameters with zero mean to keep the expected value of the estimation unbiased [28]. On the contrary, the covariance of the estimation is affected by the variance of such parameters. The consider covariance is then

$$\mathbf{P}_c = \mathbf{P}_n + \left(\mathbf{P}_n \mathbf{H}_y^T \mathbf{W}\right) \left(\mathbf{H}_c \mathbf{C} \mathbf{H}_c^T\right) \left(\mathbf{P}_n \mathbf{H}_y^T \mathbf{W}\right)^T, \tag{4.4}$$

where $\mathbf{H_y}$ and $\mathbf{H}_c$ correspond to the Jacobian of the observations with respect to the estimated parameters and *consider parameters*, respectively. The weighting matrix $\mathbf{W}$ contains the expected noise of each measurement and the possible correlation among them. The so-called noise-only covariance $\mathbf{P}_n$ represents the nominal estimation output of a batch least-squares estimation, i.e., the inverse of the normal equations matrix

$$\mathbf{P}_n = \left(\mathbf{H}_y^T \mathbf{W} \mathbf{H}_y\right)^{-1} \in \mathbb{R}^{n_y \times n_y}. \tag{4.5}$$

Finally, $\mathbf{C}$ is defined as

$$\mathbf{C} = \begin{pmatrix} \sigma_1^2 & \cdots & 0 \\ \vdots & \ddots & \vdots \\ 0 & \cdots & \sigma_{n_c}^2 \end{pmatrix}, \tag{4.6}$$

containing the variances of the *consider parameters*, where no correlation between them is assumed. Equation (4.4) can be written as

$$\mathbf{P}_c = \mathbf{P}_n + \mathbf{K} \mathbf{C} \mathbf{K}^T \in \mathbb{R}^{n_y \times n_y}, \tag{4.7}$$

with

$$\mathbf{K} = \mathbf{P}_n \left(\mathbf{H}_y^T \mathbf{W} \mathbf{H}_c\right) \in \mathbb{R}^{n_y \times n_c}. \tag{4.8}$$

Therefore, the consider covariance is obtained as the noise-only covariance plus a covariance correction, which depends linearly on the *consider parameter* variances. The objective of the *Covariance Determination* methodology is to find the variances of the *consider parameters* such that realistic covariance estimations are obtained.
We restrict our analysis to linear regimes and Gaussianity assumption. More complex and accurate uncertainty propagation methods are out of the scope of this work. Additionally, linear propagation methods are common in many SSA scenarios due to its reduced complexity, lower computational cost, and suitability for relatively short propagation intervals. The consider covariance can be linearly propagated as

$$\mathbf{P}_c(t) = \mathbf{\Psi}(t, t_0)\mathbf{P}_c(t_0)\mathbf{\Psi}(t, t_0)^T, \tag{4.9}$$

where $\mathbf{\Psi}(t, t_0)$ is the extended transition matrix, which connects the position and velocity at any time t with respect to the initial state and dynamic parameters at time t_0. It contains the state transition and sensitivity matrices, and can be computed via numerical integration of the variational equations of motion of the system [28]. The length of the propagation arcs where such linear and Gaussian assumptions hold can vary significantly depending on the RSO characteristics or altitude. To assess whether such assumptions are valid during the simulations, Gaussianity tests are applied. Michael's normality test has been chosen for the work presented here [82, 83].

Variance estimation for consider parameters

To determine the unknown variance of the *consider parameters* that improve the consider covariance realism, we resort to the properties of the Mahalanobis distance and the χ^2 distribution under Gaussian assumptions. The Mahalanobis distance (d_M) is a well-known statistical metric that describes how far a state $\mathbf{y}(t)$ is from a certain reference $\mathbf{y}_{ref}(t)$, projected into the covariance space [78]. The squared Mahalanobis distance is defined as

$$d_M^2 = \left(\mathbf{y} - \mathbf{y}_{ref}\right)^T \left(\mathbf{P} + \mathbf{P}_{ref}\right)^{-1} \left(\mathbf{y} - \mathbf{y}_{ref}\right), \tag{4.10}$$

where $\mathbf{P}$ and $\mathbf{P}_{ref}$ are the covariance matrices of the state and the reference, respectively. Both matrices are computed using Equation (4.9), from different estimation processes. In Equation (4.10), it is assumed that both variables $\mathbf{y}$ and $\mathbf{y}_{ref}$ are uncorrelated. This same assumption, applied in other studies such as in [11] or [79], is not easily guaranteed in many scenarios, for instance, when the same sensor network is shared for both estimations. In the case of the *Covariance Determination* process described here, such correlation is mitigated by ensuring that the computed reference orbit does not share any observation with the orbit state under analysis. The process to generate such reference orbits is described in Section 4.2.3, though further details can be found in [92]. Combining Equation (4.7) with Equation (4.10), the squared Mahalanobis distance can be expressed as

$$d_M^2(t) = \Delta\mathbf{y}(t)^T \left(\mathbf{\Psi}(t, t_0)\left(\mathbf{P}_n + \mathbf{K}\mathbf{C}\mathbf{K}^T\right)\mathbf{\Psi}(t, t_0)^T + \mathbf{P}_{ref}(t)\right)^{-1} \Delta\mathbf{y}(t), \tag{4.11}$$

where $\Delta\mathbf{y}(t) = \mathbf{y}(t) - \mathbf{y}_{ref}(t)$. Therefore, Equation (4.11) allows to compute the Mahalanobis distance at any epoch along the propagation arc as a function of the *consider parameter* variances, present in matrix $\mathbf{C}$.

Bearing this in mind, the *Covariance Determination* concept is as follows. Firstly, the χ^2 distribution is defined as the sum of squared Normal distributions [76]. In that case, if the Mahalanobis distance between the state and its reference is computed with a well-characterized covariance (i.e. realistic), the squared Mahalanobis distance should follow χ^2 distribution under Gaussian assumptions. Therefore, it is possible to use Equation (4.11) to determine the variance of the *consider parameters* such that the observed squared Mahalanobis distance distribution resembles the expected theoretical behavior of the χ^2 one. This is done by the minimization of an Empirical Distribution Function (EDF) metric, which can be used to determine the resemblance between two Cumulative Distribution Function (CDF). Among the multiple options available in the state-of-the-art [11, 76], two well-known EDF metrics have been chosen and tested in [92], the Kolmogorov-Smirnov and Cramer-von-Mises metrics.

Finally, it is necessary to define which orbit is to be used as reference for the Mahalanobis distance computation of Equation (4.11). As described in [92], the propagation arc of each orbit is compared against the estimation arc of a newer orbit, since the error of propagating a certain estimation is expected to be larger than the estimation error, bounded by observations. To summarize, the *Covariance Determination* methodology consists in, given a population of orbits, find the variance of the *consider parameters* that lead to consider covariance matrices that are representative of the dispersion observed in the orbital differences, by means of the minimization of an EDF metric.

4.2.2 Catalog atmospheric density uncertainty

The objective of this work is to apply the *Covariance Determination* methodology to estimate not only the uncertainty of a singular RSO, but to estimate the evolution of the atmospheric model uncertainty as a function of the altitude in a catalog. This section describes the rationale behind the input uncertainty in the simulations carried out and how this uncertainty is estimated for a catalog of objects.

Space weather statistical analysis

To test the performance of the methodology, a representative atmospheric density uncertainty as a function of altitude has been used. The applied atmospheric density uncertainty model is based on the work carried out in [27] and [17]. In these works, the uncertainty of the atmospheric density is assessed by analyzing the effect of the solar proxies dispersion in the density output of the NRLMSISE00 model. Historical space weather proxies from 1957 up to 2020 (from Celestrak [95]) are processed to select different solar activity strata (in terms of F10.7 solar flux) and identify epochs of reference for each stratum with moving-averaged proxies, as can be seen in Figure 4.1.

Next, at each reference epoch and solar activity strata (each point of Figure 4.1), an artificial joint random distributions is built, considering the correlation between geomagnetic and solar activity in the surrounding months of the reference epochs. In parallel, a 3-dimensional grid of latitude, longitude and altitude is constructed. Then, 1000 samples of each joint distribution (i.e. one per point in Figure 4.1) are drawn and provided as input to the NRLMSISE00 model at each point of the 3-dimensional grid. The atmospheric density outputs are aggregated, and a standard deviation is obtained for each node, solar activity stratum and reference date. Finally, the maximum standard deviation

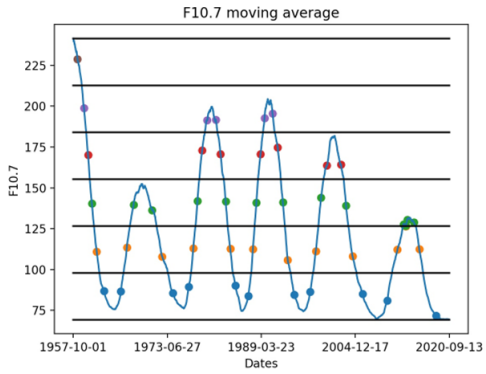

Figure 4.1: Example of 6 different solar activity strata and their reference epochs, from [17].

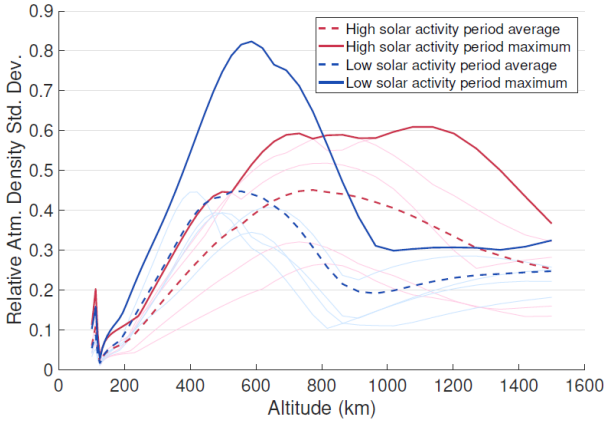

Figure 4.2: Averaged and maximum uncertainty curves for periods of high and low solar activity (solid lines) and original ones for each period of both strata (glassy lines), from [27].

for each altitude and solar activity is stored, retaining as a conservative measure the maximum standard deviation in the latitude/longitude grid of each altitude.
Figure 4.2, from [27], depicts the evolution of relative density standard deviation with altitude, in a two-strata analysis of low or high solar activity. The glassy lines correspond to the uncertainty curves at different reference epochs, for both activity levels. The solid lines correspond to the maximum uncertainty values between all reference dates, whereas dashed lines represent the average value. The relative standard deviation of the density is larger for low solar activity periods. In both periods of low and high solar activity levels, the standard deviation shows a linear growth between approximately 300 km and 500 km, followed by growth rate decrease around 600 km for low activity, and 700 km for high activity. In the work presented here, the high solar activity average standard deviation curve (dashed red line of Figure 4.2) has been chosen to represent the evolution of the density standard deviation in the simulations.

Altitude parametrization

Once it has been explained how a statistically representative evolution of the density standard deviation with altitude has been chosen, this subsection describes how the model of atmospheric drag uncertainty is parameterized and how the *Covariance Determination* methodology is adapted to estimate the evolution of the uncertainty with altitude.
First of all, it is necessary to define the *consider parameter* model for the atmospheric drag. The classical drag acceleration equation including the aerodynamic model *consider parameter* is defined as:

$$\mathbf{a}_{\text{drag}}(t) = -\frac{1}{2}\rho(t)\frac{C_d A}{m}\|\mathbf{v}_{\text{rel}}(t)\|^2 \frac{\mathbf{v}_{\text{rel}}(t)}{\|\mathbf{v}_{\text{rel}}(t)\|}(1+c_{AE}), \tag{4.12}$$

where $\rho(t)$ is the atmospheric density, A the cross-sectional area, m the object mass, C_d the drag coefficient and $\mathbf{v}_{rel}(t)$ is the relative speed vector of the object with respect to the atmosphere. Finally c_{AE} is the *consider parameter*, defined to follow Equation (4.3) as

$$c_{AE} \sim \mathrm{N}\left(0, \sigma_{AE}^2\right). \tag{4.13}$$

Its objective is to model the error in the atmospheric density and ballistic coefficient, this is, containing C_d, mass and cross-sectional area uncertainty. Since this work is focused on the uncertainty arising from the atmospheric density, mass and cross-sectional areas are assumed to be fixed and known quantities. It is worth mentioning that, in the case of real data where the other sources of error in the ballistic coefficient are present, the proposed methodology is expected to remain valid for batch processing. The main reason is that all drag force errors are accumulated into the ballistic coefficient estimation, and the proposed model for c_{AE} would characterize all sources combined. Despite the fact that the proposed methodology is not able to discriminate between the uncertainty contribution of the atmospheric density or the ballistic coefficient, it would still be applicable to characterize the overall uncertainty with the objective of improving the realism of the covariance.

Now, the objective is to characterize the altitude evolution of the atmospheric density standard deviation by means of the *consider parameter* variance. To this end, the *consider parameter* standard deviation is parameterized as follows

$$\sigma_{atm}(h) = \sigma_{AE}(h, a, b, c) = a + bh + ch^2, \tag{4.14}$$

where h is the altitude. A second-order polynomial has been chosen among other families of fitting functions or polynomials based on a trade-off between accuracy and simplicity. Figure 4.3 depicts the dataset for the density standard deviation curve in the averaged high solar activity (dashed red line of Figure 4.2), with a numerical fit to the polynomial of Equation (4.14). The Root Mean Square (RMS) error of the fitting suggests that the polynomial used is satisfactory. The results of this fitting are used as reference values in the simulated scenario, namely: $a_{tg} = -3.72 \cdot 10^{-1}$, $b_{tg} = 2.06 \cdot 10^{-3}$, $c_{tg} = -1.29 \cdot 10^{-6}$,

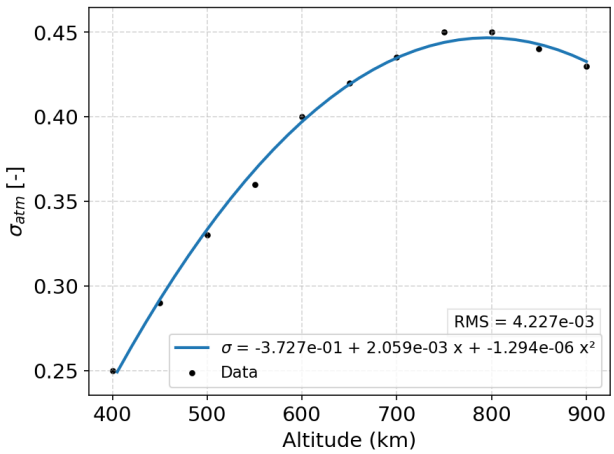

Figure 4.3: Atmospheric density standard deviation data set and second-orbder polynomial fit.

By combining the model of Equation (4.14) with Equation (4.11) for a single *consider parameter*, the Mahalanobis distance is obtained as a function of the parameters of the model (a, b, c). Thus, the problem at hand consists in the estimation of the parameters (a, b, c) that define $\sigma_{AE}(h, a, b, c)$ in the catalog scenario. In other words, the objective is to determine the parameters of the atmospheric density uncertainty model so that, at all altitudes, the population of Mahalanobis distances follow a χ^2 distribution, increasing

the realism of all covariance matrices. To validate the performance of the *Covariance Determination* method to estimate such parameters, the results obtained with the fit of Figure 4.3 are used as target values, as explained further in Section 4.2.3.

4.2.3 Simulation environment

Previous sections have described the evolution of the standard deviation of the atmospheric density, based on statistical analysis of historic space weather data. The ability and performance of the *Covariance Determination* methodology to characterize such density uncertainty model is assessed via simulations, whose details are explained in this section. The goal here is to maintain a simulation environment as realistic as possible, compatible with the described hypothesis and models, and representative of the current state of the LEO environment.

Simulation scheme

As discussed in Section 4.2.1, the proposed *Covariance Determination* methodology requires a population of Mahalanobis distances in order to estimate the variance of the *consider parameter*s. Each Mahalanobis distance sample from Equation (4.11) is retrieved from an orbit determination and propagation process. During the OD process, the noise-only covariance of the estimation is computed along with all components of matrix $\mathbf{K}$, which allows to compute the consider covariance at estimation epoch. However, the Mahalanobis distance must be evaluated at a propagation epoch so that the impact of errors in the atmospheric density can be observed as state vector differences. For this reason, the estimated state is propagated forward in time, obtaining in the process matrix $\mathbf{\Psi}$ to propagate the covariance linearly. The simulation scheme is as follows, analogous to all RSOs:

1. **Reference orbit**: a initial state is propagated forward in time with the dynamic model of Table 4.1. The length of the propagation will be determined by the amount of simulated data desired for the analysis. Previous studies of the *Covariance Determination* methodology have shown that an accuracy of 15% can be maintained with approximately 300 samples of a single object [88, 92]. Thus, the reference propagation has been set to obtain 300 ODs. This propagation does not contain any model error in the atmospheric density.
2. **Monte Carlo iterations**: the following sequence of steps is repeated in a similar fashion to a Monte Carlo scheme. Between each iteration, the reference state (taken from the *Reference orbit*), is shifted forward. Also, each iteration will use different density and measurements perturbations, as further described in Section 4.2.3.
   (a) **Perturbed orbit**: the reference state is propagated backwards 7 days in time, a common length for LEO OD arcs. During this propagation with the dynamic model of Table 4.1, a sample error of the atmospheric density is introduced, as described further in Section 4.2.3. This perturbation is applied as constant for the orbit time-span, as defined in the *consider parameters* theory.
   (b) **Measurements generation**: from that perturbed orbit, measurements are generated from ground-based radars with typical SSA radar noise (Table 4.2). During this process, real observability conditions are considered.

(c) **Orbit determination**: with the synthetic measurements, an OD is performed in a 7 days arc. The estimation epoch (t_0) is automatically set to the epoch of the last observation.

(d) **Orbit propagation**: the estimated state is propagated forward 10 days.

The last 2 steps (2.c and 2.d) are intended to resemble an operational scenario of orbit determination and propagation with correlated measurements. More detailed information about this simulation process can be found in [92].

As it has been mentioned in Section 4.2.1, Equation (4.11) requires an orbit to be used as reference. In this work, as concluded previously in [92], the applied estimated reference orbit consists in taking as reference, for orbit i under analysis, the orbit estimated in the Monte Carlo iteration $i+7$. The main reasons are two: firstly, in an operational environment, precise orbits are generally not available, specially for non-collaborative objects such as space debris; secondly, the error within the OD arc is expected to be bounded by the observations, and lower than the error during prediction (propagation). In order to reduce correlation between them, the orbit under analysis and the estimated reference orbit do not share any measurement. Note that the covariance of the latter orbit ($\mathbf{P}_{ref}$ in Equation (4.11)) is also affected by model errors, and thus the *consider parameter* correction is also applied to it.

Simulation setup

This subsection gathers the main characteristics of the simulation scenario. The details of the dynamic model applied for the high-fidelity numerical propagation are included in Table 4.1. The measurement Gaussian noise applied during the simulation of measurements is described in Table 4.2. Finally, the characteristic of the simulated radars are shown in Table 4.3.

Table 4.1: Dynamical model

Reference frame	J2000 ECI
Gravity field	16x16
Third body perturbations	Sun & Moon
Polar motion and UT1	IERS C04 08
Earth pole model	IERS 2010 conventions
Earth precession/ nutation	IERS 2010 conventions
Atmospheric density model	NLRMSISE-00
Solar radiation pressure model	Cannonball
Drag model	Cannonball
Solar radiation pressure area	Constant area
Drag area	Constant area

Table 4.2: Measurement noise

Measurement type	σ	**Units**
Two-way range	10	m
Two-way range rate	300	mm/s
Azimuth and elevation	1	deg

Table 4.3: Characteristics of simulated radars

Field of view		Pyramidal asymmetric
Line of sight (southwards pointing)	**Azimuth**	180 deg
	Elevation	75 deg
Aperture	**Azimuth**	±43 deg
	Elevation	+15°/-10 deg
Geodetic coord radar 1 (Spain)	**Longitude**	-5.5911 deg
	Latitude	37.16643 deg
	Height	0.1423 km
Geodetic coord radar 2 (Germany)	**Longitude**	7.12961 deg
	Latitude	50.61657 deg
	Height	0.2929 km
Observation spacing		5 seconds

Altitude correlated noise

On the one hand, we are modeling the atmospheric drag density error according to Equation (4.13), each orbit determination and propagation affected by a sample of such distribution, acting as a constant perturbation. On the other hand, the modeled atmospheric density uncertainty evolves solely as a function of altitude for a certain level of solar activity, according to the chosen model for the space environment. Since, under such hypothesis, two objects at the same altitude and time-frame should be affected by the same error in the density model, it would be physically incoherent to apply a completely different perturbation to objects at the same or nearby altitude at the same interval of analysis. Consequently, an altitude-correlated noise sequence is applied.
To achieve a zero-mean correlated noise sequence for the density error, an auto-regressive function with space correlation of order 1 has been applied in the simulations [58], as described next. First the perturbation of the density at a certain time step n as a function of the altitude is defined as $\rho_p(h_n)$. let us assume that the correlation of two perturbations at two consecutive altitudes $\rho_p(h_n)$ and $\rho_p(h_{n-1})$, in discrete form, is as

$$r_\rho(h_n, h_{n-1}) = \mathrm{E}\left[\rho_p(h_n)\,\rho_p(h_{n-1})\right] = r_0(h_n)\, e^{-\alpha|h_n - h_{n-1}|}, \tag{4.15}$$

where $r_0(h_n) = \mathrm{E}\left[\rho_p(h_n)^2\right]$ is the power of the non-stationary perturbation. In this case, we want the power of the noise to coincide with the atmospheric density variance deviation at each altitude, that is,

$$r_0(h_n) = \sigma^2_{atm}(h_n) = (a_{tg} + b_{tg} h_n + c_{tg} h_n^2)^2. \tag{4.16}$$

The spatial correlation of Equation (4.15) can be guaranteed with the auto-regressive model of order 1, AR(1), as

$$\rho_p(h_n) = a(n)\rho_p(h_{n-1}) + u(n), \tag{4.17}$$

with

$$a(n) = \frac{r_0(h_n)}{r_0(h_{n-1})} e^{-\alpha|h_n - h_{n-1}|}, \tag{4.18}$$

$$u(n) \sim \mathrm{N}\left(0, \sigma_u^2(n)\right) \text{ and } \sigma_u^2(n) = r_0(h_n)\left[1 - \frac{r_0(h_n)}{r_0(h_{n-1})} e^{-2\alpha|h_n - h_{n-1}|}\right], \tag{4.19}$$

where $\alpha = 1/h_\alpha$ $[1/km]$ represents the inverse of the altitude scale of correlation, which determines the strength of the correlation (h_α). $u(n)$ is the Gaussian component of the noise, with variance $\sigma_u^2(n)$, that also depends on the power noise and is inversely proportional to the correlation. With this noise model, the perturbation at each altitude is correlated with the noise at the previous altitude by means of the factor $a(n)$, governed by the correlation scale α. The stronger the correlation (i.e., the smaller α), the smaller the Gaussian component $u(n)$ in the noise sequence. The choice of α and its estimation is a planned future line of research. However, in the work presented here, the value of $h_\alpha = 300$ km was selected, to have a scale of correlation of approximately 1/3 of the altitude span covered in the simulation. In order to generate the input sequence of noise, the parameters obtained from the fit to the statistical data in Figure 4.3 are used to define $r_0(h_n)$, as indicated in Equation (4.16).

Figure 4.4 shows the correlated density perturbation sequence (in relative terms) for ten different OD arcs. For each of the OD time-spans, the applied perturbations at each altitude level is represented. It can be noted how for certain OD arc, the perturbations at consequent altitudes show a certain level of correlation, despite maintaining a Gaussian component. Figure 4.4 shows only ten OD arcs, for visualization purposes. If all perturbations at the same altitude and all OD arcs were analyzed, those perturbations would follow a Normal distribution with a standard deviation from Equation (4.16), maintaining the proper uncertainty input for the simulations.

RSO population

In this subsection, a brief description of the objects that have been used in the simulations is provided. The goal is to represent the LEO population for the catalog analysis under the previously described methodology. Recalling the definition of the *consider parameter* variance as a function of altitude (Equation (4.14), objects at the same epoch and similar altitudes would suffer the same atmospheric density error. Therefore, under such model, it is only necessary to include an RSO per altitude in the catalog simulation, since according to such (strong) assumption, the uncertainty estimated would be representative for all objects at that altitude. The process to generate the RSO population has been the following:

1. Starting from SpaceTrak TLE LEO catalog [96], we retain objects of nearly-circular orbits and whose altitude is between 400 and 900 km.
2. Each objects is provided with a ballistic coefficient randomly selected from a distribution of typical values in the LEO catalog
3. An altitude grid of 15 km width, from 400 km up to 900 km is built. A single object inside each altitude grid is stored, filtering for Ballistic coefficients in the range 10-40.

Figure 4.5 depicts the RSO population meeting conditions 1 and 2 of the above list (blue dots), and the finally chosen RSOs (red dots), with a total of 35 randomly selected objects.

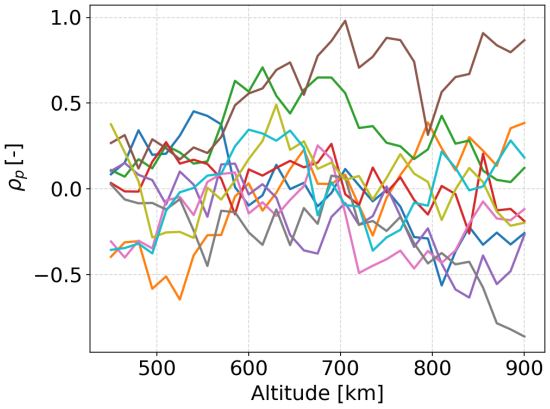

Figure 4.4: Relative density perturbation as a function of altitude for 10 different OD arcs.

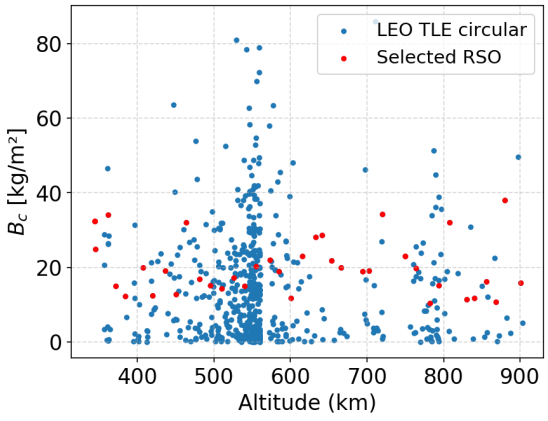

Figure 4.5: All RSOs in circular LEO orbits with assigned ballistic coefficients (blue dot) and the selected RSOs for the analysis (red dots).

4.3 Results

This sections presents and discusses the results of the catalog-based *Covariance Determination* in the described simulated scenario. Before presenting the final results, there are some intermediate Gaussianity analysis worth mentioning. If the orbital differences are not normally distributed, the uncertainty of the system cannot be represented by a covariance matrix. In this simulated scenario, where objects have different ballistic coefficients and altitudes, the time of validity for the linearity and Gaussian assumptions varies significantly, for instance, between altitudes lower than 500 km and those above 800 km. To mitigate this problem, the epochs of analysis for the orbital differences have been set between $t_0 + 1$ and $t_0 + 3$ days (where t_0 refers to the estimation epoch).

In addition to this, Michael's normality tests, were applied to the orbital differences of each object. It is one of the most suited tests for orbital differences analysis due to its powerful tail outlier rejection capabilities [77]. It provides a visual representation of the acceptable Gaussianity region in a percentile plot, and points laying outside can be visually identified. Figure 4.6 show the Michael's test results separating the orbital differences components in RIC local frame (radial, in-track, cross-track [56]), but aggregating all objects and epochs of analysis. It is seen that many points lay outside the normality region in the radial and cross-track directions. On the contrary, normality is preserved on the in-track direction, as seen in Figure 4.6c. Upon these results, the radial and cross-track directions were discarded from the computations of the Mahalanobis distance, shifting from a 3 DoF to a 1 DoF expected χ^2 distribution. Despite maintaining only the in-track component, this direction should enable to capture atmospheric density errors, since the in-track direction is aligned with the velocity vector, direction in which the atmospheric drag acts on the objects.

The final results are gathered in Figure 4.7, which compares the statistical curve of the atmospheric density uncertainty (blue line) with the curve estimated using the catalog-based *Covariance Determination* method (orange line). Figure 4.7 also contains the input noise reconstruction curve at each altitude (green points), as well as it's second-order

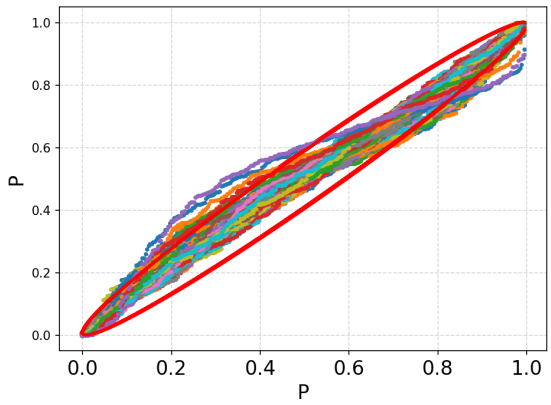

(a) Radial

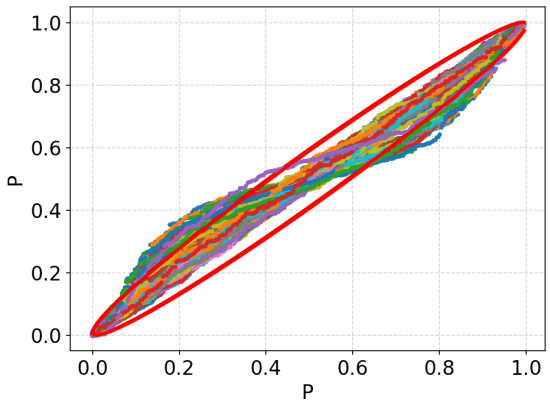

(b) Cross-track

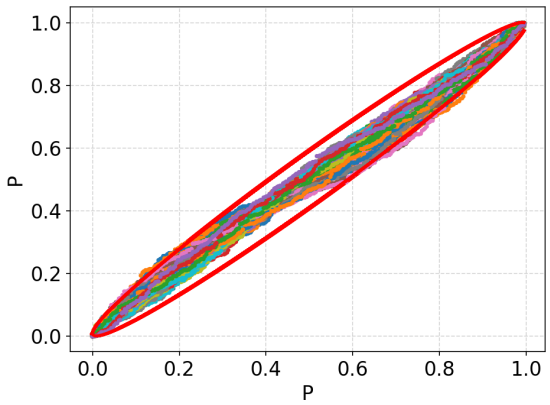

(c) In-track

Figure 4.6: Michael's test results for the orbital differences for all objects and analysis epochs in RIC local frame. The axis represent probability percentiles. Each color depicts a different object. The red ellipsoid shows the limiting boundary for a sample to pass the normality test.

polynomial fit (dashed green line). The individual *consider parameter* standard deviations obtained by analyzing each object individually are represented as orange dots. The estimated coefficients of the parametric function can be found in Table 4.4, comparing the results with the second-order fits to the model and input reconstruction. In addition, the RMS of the differences between the estimated curve and both the model and the input reconstruction is also showed.

It can be noted in Figure 4.7 that the input reconstruction does not follow exactly the statistical model for the density standard deviation. The reason is the amount of samples (orbits) used per altitude grid. Each orbit per altitude level will be subjected to a sample perturbation. Thus, the input model is perfectly reconstructed with the perturbations only for a sufficiently high number of samples. However, in this case 300 orbits per altitude level were selected. This choice was a trade-off between data quantity and accuracy, bearing in mind the operational applicability of the methodology. The green curve converges to the blue one with increasing the amount of samples. The individual results of each object are shown for reference. It is seen that the uncertainty recovered for the objects individually is subject to a certain error, as was expected due to the 300

samples choice. Regarding the estimated parameters with the *Covariance Determination* methodology, the difference with respect to the density uncertainty model varies between 20% and 40%, as shown in Table 4.4. Even though this difference appears to be significant, the resulting curve of atmospheric density standard deviation with altitude is similar to the model one, as can be seen by comparing both curves in Figure 4.7 and in the RMS value of 0.0096 of Table 4.4.
Moreover, regarding the differences between the estimated parameters and the resulting ones from a second-order fitting to the reconstructed input in Table 4.4, the accuracy of the method in this case is improved up to a range of 14%-23% in terms of parameters, and an RMS of 0.0086. This is an indicator of the performance of the methodology to characterize the input uncertainty, even though this latter does not follow precisely the chosen model due to the samples limitation. Additionally, in both cases, the RMS results of comparing the models in Table 4.4 correspond to less than 2.2% of the maximum standard deviation, indicating a satisfactory accuracy in terms of atmospheric density standard deviation. It is seen how, when estimating the uncertainty evolution parameters using all the data from the selected catalog, the resulting curve is similar to a best-fit for the individual objects results, allowing a mitigation of individual errors and outliers of the objects in the catalog.

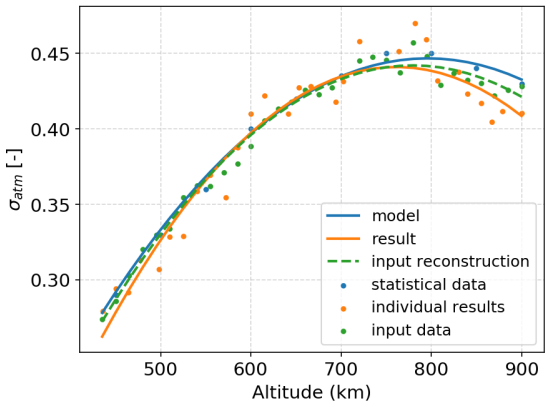

Figure 4.7: σ_{AE} evolution results.

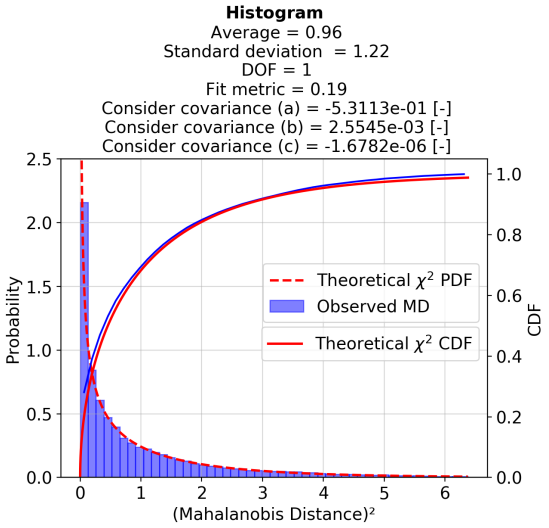

Figure 4.8: Optimized squared Mahalanobis distance distribution for all objects. 1 Degree of Freedom (in-track), analysis window between t_0+1-t_0+3.

Figure 4.8 shows the final distribution of the squared Mahalanobis distance samples, coming from all orbits of all objects in the considered catalog, when applying the estimated constants of the *consider parameter* variance. As discussed previously, only 1 DoF is considered in the optimization, the in-track component. A satisfactory match between the squared Mahalanobis distance CDF and PDF and the χ^2 distribution can be appreciated in Figure 4.8, confirmed with the metric of the fitting process, where Cramer-von-Mises test statistic was used. A metric of 0.19 is obtained, shown at the header of Fig 4.8, whereas the upper limit for the Cramer-von-Mises test statistic to reject the null hypothesis is 1.167. Thus, the test determines that the observed distribution, after the *consider*

Table 4.4: Results of the atmospheric density standard deviation parameters

	a [-]	b [-]	c [-]	RMS [-]
Estimated	$-5.31 \cdot 10^{-1}$	$2.55 \cdot 10^{-3}$	$-1.68 \cdot 10^{-6}$	-
Input reconstruction	$-4.29 \cdot 10^{-1}$	$2.24 \cdot 10^{-3}$	$-1.43 \cdot 10^{-6}$	-
Model	$-3.72 \cdot 10^{-1}$	$2.06 \cdot 10^{-3}$	$-1.29 \cdot 10^{-6}$	-
Difference w.r.t input [%]	23.90	13.84	17.5	0.0080
Difference w.r.t model [%]	42.74	23.78	30.23	0.0096

parameter correction, provides a strong match with the χ^2 distribution, in this case with a significance level of 0.25.

It is important to remark that all samples, coming from orbital differences of distinct objects and orbits, can be treated as part of the same distribution thanks to the Mahalanobis distance. When affected by the same perturbation in density, the error in position will depend significantly on the object altitude, position, ballistic coefficient. Nonetheless, the evolution of the covariance is also proportional to those factors. This normalization of the errors allows all Mahalanobis distances to belong to the same distribution, provided that the model errors are properly characterized and under certain assumptions such as Gaussianity and linearity, as previously discussed. Analogously, the covariance will also adapt for different orbit visibility and geometry factors that impact the OD process.

The results of the Cramer-von-Mises test is a marker of the covariance realism improvement that is obtained with the *Covariance Determination* methodology in the considered catalog of objects. However, this realism improvement is only ensured in the in-track direction. Even though this component of the state vector in local reference is the most affected by atmospheric density errors, it is necessary to assess the improvement in realism in all position components. For this purpose, covariance containment tests, as proposed in [43], allow for a clear physical insight and visual representation of the level of realism of the covariance. To evaluate if the covariance is representative of the orbital differences, the Mahalanobis distance can be used as a metric to see the amount of points that lay inside a $k\sigma$ ellipsoid ($k = 1, 2, 3, 4$) and compare it against the expected fraction for a multivariate Gaussian distribution of the same number of DoF. In this case, the interest lay in assessing the containment in full position (i.e., 3 DoF) that is achieved with the parameters that were estimated with the catalog-based *Covariance Determination*. Figures 4.9a and 4.9b show the visual representation of the containment test for two different objects in the analyzed catalog, for a 3σ containment. Each of the points correspond to orbital differences between estimated and predicted orbits, for different ODs and up to 3 days of propagation. Figure 4.9a corresponds to an object at a high altitude (830 km), showing a 3σ containment of 96.59%. Such containment is similar to the 97.1% value of 3σ theoretical containment for a 3 DoF multivariate Gaussian distribution. The samples of orbital differences are less dispersed in the in-track direction as compared to Figure 4.9b. The latter corresponds to the object in a worse scenario, that is, at low altitude (477 km) with a low ballistic coefficient, showing a 3σ containment of 92.03%. In fact, non-linearity is building up in Figure 4.9b, where the so-called banana-shape of the orbital differences start to appear. As a consequence, the containment in Figure 4.9b is

lower than in its counterpart of Figure 4.9a. Consequently, extreme care must be taken in terms of linearity and Gaussian assumptions when a catalog of objects is analyzed. Table 4.5 presents the average containment tests results for the complete catalog in two different cases: with the noise-only covariance (i.e. without any model error correction) and with the consider covariance (i.e. the resulting covariance when applying the *consider parameter* variance obtained with the *Covariance Determination* process). An average containment similar to their expected fractions at the different $k\sigma$ levels is seen, which indicates an overall covariance realism improvement for the catalog as compared to the containment obtained with the noise-only covariance, which fails to model the uncertainty of the system in the presence of dynamic model errors. In fact, the similarity between the containment tests and the theoretical expectations at all σ level indicates that the *Covariance Determination* methodology does not oversize the covariance matrices.

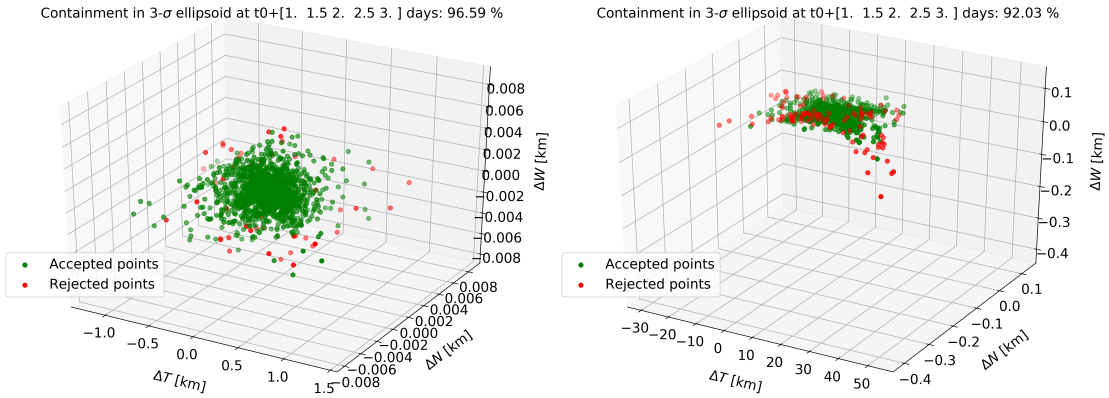

(a) Object # 6, at 830 km altitude

(b) Object # 27, at 477 km altitude

Figure 4.9: Covariance containment test at 3σ level for 3 DoF, using the optimum estimated parameters results. Theoretical 3σ containment for a multivariate Guassian distribution of 3 DoF is 97.1% [43].

Table 4.5: Average covariance containment tests (in %) for selected catalog of objects

	1σ	2σ	3σ	4σ
Noise-only covariance	0.25	1.40	2.87	4.37
Consider covariance	19.20	72.93	96.64	99.80
Theory (3DoF)	19.90	73.90	97.10	99.87

4.4 Conclusions and future work

The goal of the presented work was to extend the *Covariance Determination* methodology to a catalog scenario, in which the evolution with altitude of the atmospheric density uncertainty could be estimated. To this end, a parametric, altitude-dependent function of the density standard deviation has been applied as *consider parameter* model, switching the *Covariance Determination* process to the estimation of the parameters that define such model by considering a catalog of objects. In line with the statistical analysis of historic space weather data and its impact on density estimation, a second-order polynomial was chosen to model the evolution of relative density standard deviation with altitude, and the resulting uncertainty curve for a high solar activity period was used as reference model for the simulations. The validation of the methodology was carried out in a simulated environment, having several orbit determination and propagation steps for each object in the chosen catalog, adding space-correlated perturbations to the atmospheric density according to the reference second-order model.

The *Covariance Determination* methodology was able to estimate the parameters of the input model, obtaining an RMS of the residuals between both parametric curves below 2.2% of the maximum atmospheric density standard deviation. The estimated atmospheric density model is close to the chosen theoretical model except at high altitudes, due to a deviation in the input perturbations caused by a limited amount of samples. Nonetheless, the *Covariance Determination* method has showed a satisfactory ability to estimate parameters affecting multiple objects of a catalog. As a result of the properties of the Mahalanobis distance, the information of all objects could be treated as samples of the same distribution, allowing to determine properly the parameters of the density uncertainty. Due to departure from Gaussian assumptions after 3 days of propagation at low altitudes, the radial and cross-track components of the position differences were discarded from the computation of the Mahalanobis distance. However, the remaining in-track component is the direction where most of the density-related errors are expected to impact in the orbit, since the in-track direction is aligned with the velocity. The squared Mahalanobis distance distribution, after estimating the parameters of the uncertainty, presented a large similarity with the χ^2 distribution, confirmed by the Cramer-von-Mises statistic, which is an indicator of realism of the covariance. The averaged covariance containment results showed an improvement of the covariance realism in the catalog.

Regarding future work, a clear line of improvement is to analyze the sources of the non-Gaussianity in the radial and cross-track directions, to understand their origin and to be able to include them in the analysis. Moreover, the simulations must be extended to a larger amount of samples per altitude, in order to confirm the convergence of the methodology to the chosen atmospheric density model. Additionally, alternative state representations and covariance propagation techniques that are able to maintain Gaussianity for longer propagation arcs are to be investigated, such as in curvilinear coordinates or mean orbital elements. This is expected to provide better conditioned covariance matrices that improve the behavior of the squared Mahalanobis distance distribution. It is also necessary to move towards more complex models for the dynamic model uncertainty, as opposed to the *consider parameters* theory with constant parameters. In this regard, time or space correlated noise models such as Ornstein-Uhlenbeck or Gauss-Markov processes are to be analyzed, adapting the principles of the *Covariance*

Determination method to the estimation of the parameters that define such stochastic models. Finally, it is relevant to remark that the presented results correspond to simulated data. Further validation with real data is required to re-assess the performance of the methodology in terms of covariance over-sizing and realism metrics, which are crucial to develop more flexible and complete methodologies to capture the uncertainty in real space environments.

Acknowledgments

This project has received funding from the “Comunidad de Madrid" under “Ayudas destinadas a la realización de doctorados industriales" program (project IND2020/TIC-17539), and from Agencia Estatal de Investigación of Spain (project PID2021-125159NB-I00 TYCHE).

5

Atmospheric drag uncertainty quantification for orbit determination and propagation via Stochastic Consider Parameters

5.0 Scientific contribution and context

Considering the achievements in previous publications, there were still two major gaps to cover. First, the *consider parameters* are, though effective, an overly simplified characterization of uncertainty sources such as the atmospheric drag. Second, the limited access to real data prevented a formal validation of the *Covariance Determination* method in an operational environment. These main gaps are addressed in this paper.

The main contribution of this paper is the novel model of Stochastic Consider Parameters (SCP), which combines, the benefits of the *consider parameters* theory with a stochastic model with time correlation for the atmospheric drag, closer to its expected behavior. Then, the SCP model is combined in the framework of the *Covariance Determination* methodology to estimate the stochastic noise parameters of the drag model. This is applied in LEO with real data from the Spanish Space Surveillance and Tracking Radar (S3TSR), validating the covariance realism improvement capabilities and comparing it against the classic *consider parameters* models.

The SCP model and its quantification methodology have been developed throughout subsequent works prior to its culmination in this paper. First, Monte Carlo simulations to understand the impact of stochastic models with correlation in covariance propagation were studied in [17]. Then, the first prototype of the SCP model for covariance propagation was validated in [18], whose results are summarized in Appendix B. Finally, a preliminary version adapting the SCP model to OD with several simulation results was proposed in [97]. Therefore, the consolidation of the SCP model and its validation with real observations in this paper is considered a satisfactory closure of the objectives of the thesis. Nonetheless, further research applying the SCP model to real range-rate observations and improvements in Gaussianity maintenance can be found in Appendix B.

A. Cano[1,2], **M. Sanjurjo-Rivo**[2], **J. Míguez**[2], **A. Pastor**[1], **D. Escobar**[1],
[1]GMV, 11 Isaac Newton, 28670 Tres Cantos, Madrid, Spain,
[2]Universidad Carlos III de Madrid, 30 Avenida Universidad, 28911 Leganés, Madrid, Spain,
Advances in Space Research (2024) Submitted for publication

The efficiency and sustainability of spacecraft operations is a growing challenge due to the accelerated increase of the space objects population. Thus, the quality of Space Traffic Management (STM) and Space Situational Awareness (SSA) services is essential to ensure the sustainability of the space environment. The quality of such services relies not only on an accurate knowledge of the Resident Space Object (RSO) state, but also on its associated uncertainty. However, there is a lack of accurate and cost-effective methodologies for Uncertainty Quantification (UQ) in the context of SSA, where a large number of objects are maintained in the catalogs.

The atmospheric drag is one of the largest sources of uncertainty in Low Earth Orbits (LEO). Stochastic models have been widely proposed in the literature to represent its aleatoric nature. However, the introduction of stochastic dynamics increases the complexity of orbit propagation and determination. On the other side, classical implementations to characterize the uncertainty from dynamical models in batch least-squares orbit determination such as the consider parameters theory fail to represent the stochastic nature of the atmospheric drag uncertainty, despite maintaining a tractable level of complexity.

This work presents the validation with real data of the Stochastic Consider Parameters (SCP) model, a methodology developed for uncertainty quantification via covariance estimation applied to batch least-squares orbit determination and propagation that allows considering the effect of stochastic time-correlated errors to improve the covariance realism efficiently. To estimate the parameters that govern the stochastic noise, the SCP model is combined with a previously developed uncertainty quantification method. In this work, real radar observations from the Spanish Space Surveillance Radar (S3TSR) are used to test the covariance realism improvement of the SCP method for several RSOs at different altitudes with respect to deterministic constant error models. The results analyze the physical interpretation of the estimated noise parameters with real data, while also evaluating key metrics to assess covariance realism such as Cramer-von-Mises metric and covariance containment.

Keywords: uncertainty quantification, uncertainty realism, stochastic noise, atmospheric drag, consider parameters, real measurements

5.1 Introduction

Space Traffic Management (STM) and Space Situational Awareness (SSA) services are becoming the cornerstone for the sustainability of space activities given the current and future population of orbiting objects. Reliable knowledge of the RSO's state and associated uncertainty is required for successful catalog build-up and maintenance given the increasing demand for services such as conjunction risk assessment, manoeuvre detection, fragmentation analysis, or re-entry prediction. The quality of these services depend significantly on how well the uncertainty of the state is characterized, that is, on the Uncertainty Realism.

In most SSA operational environments and applications, the covariance matrix is historically used to represent the RSO state uncertainty, retaining only up to the second

moment of the Probability Density Function (PDF), in a trade-off between accuracy, complexity, and computational efficiency. This choice is expected to be representative of the uncertainty of the system under the assumptions of Gaussianity and linearity, allowing to reduce the problem of Uncertainty Realism to Covariance Realism. The covariance matrix has been historically used in SSA systems as a trade-off between accuracy and computational efficiency, especially given the current catalog sizes. However, the covariance matrix is able to characterize the uncertainty of the RSOs only if the linearity and Gaussianity of the system is ensured, and if appropriate uncertainty quantification techniques are applied to characterize the multiple sources of uncertainty affecting the space environment.

Batch least-squares algorithms are one of the most common orbit determination methods in SSA systems. This family of algorithms provides the best-fit estimation for the state, given a set of observations and under a certain dynamic and measurements model. The covariance of the state is a nominal output of these processes, where the expected measurement noise is typically the only source of uncertainty [23] (i.e. Noise-only Covariance [56]). The generation of such covariance while not requiring any prior information of the state uncertainty is one of the reasons why batch estimation methods are widely used in SSA. However, uncertainty in the dynamics and measurements models cause the noise-only covariance to lack realism.

Atmospheric drag is one of the largest sources of uncertainty in Low Earth Orbits (LEO) due to its dependency on the RSO characteristics and environmental factors such as the space weather. Its aleatoric behavior has been widely studied in the literature. Several stochastic noise models have been proposed for the solar flux, from white noise and Brownian motion [54, 55], to Ornstein-Uhlenbeck processes with a tendency to mean values [57, 59, 98]. Other studies explore variations of Ornstein-Uhlenbeck that include spatial or temporal correlation such as Gauss-Markov models, which have shown improvement in covariance realism in Kalman filter estimation [51]. Other authors propose stochastic machine learning techniques for the prediction of the drag coefficient and its uncertainty, trained with well-known objects such as the CHAllenging Minisatellite Payload (CHAMP) satellite [99, 100]. In [101], other stochastic machine learning models for drag uncertainty are enhanced with Gauss-Markov processes, being later combined in an ensemble approach to improve the realism of their uncertainty distribution.

However, operational applications implementing stochastic models for atmospheric drag uncertainty in SSA are not common since the introduction of stochastic dynamics significantly increases the complexity of orbit determination processes, requiring for instance state space augmentation or modifications in the deterministic equations of motion and their integration, among other possibilities. Other alternatives that are able to characterize complex PDFs such as Monte Carlo methods or Particle Filters lead to large computational costs when facing large populations [65]. In filtering applications, a common alternative for uncertainty realism are process noise techniques which consist in adding certain noise terms to the system dynamics to account for un-modeled uncertainty sources [11]. However, to determine the amount of noise, non-physical calibration processes are required [49, 50].

Focusing on batch estimation methods, a classical method for uncertainty modeling is

the *consider parameters* theory [23], characterizing the uncertainty sources by including uncertain parameters in the dynamics or measurements models. Although mostly applied to batch estimation, this formulation has been combined with filtering algorithms as in the Schmidt-Kalman filter [52, 53]. The *consider parameters* theory maintains the physical traceability of the modeled uncertainty, it is conveniently compatible with operational systems, and can be applied to improve the realism of the covariance as shown in previous works [92, 93, 102]. Nonetheless, classical parameter uncertainty methods present two main drawbacks. First, they fail to represent the stochastic nature of the atmospheric drag uncertainty. Second, realistic values of the uncertainty of the model parameters are not known, as in the case of process noise techniques. Therefore, a cost-effective methodology is needed that allows to model the stochastic nature of the atmospheric drag while at the same time being able to quantify the uncertainty of the model parameters to improve the realism of the covariance.

The contribution of this work to improve the covariance realism process is twofold. Firstly, it presents a methodology to model stochastic uncertainty in orbit propagation and batch least-squares orbit determination, named as Stochastic Consider Parameters (SCP). Secondly, a method to quantify such stochastic uncertainty is proposed as an extension of a previously developed methodology, named *Covariance Determination*.

The Stochastic Consider Parameters model allows estimating the effect of stochastic time-correlated errors to improve the covariance realism efficiently, avoiding the integration of stochastic dynamics or Monte Carlo methods. The objective is to combine the aforementioned advantages of the *consider parameters* theory with a stochastic model that is able to represent the behavior of the atmospheric drag. In that line, an autoregressive function of order 1, AR(1) [58], is chosen to model the stochastic drag, controlled by an unknown power of the noise and unknown correlation time scale. Then, the noise sequence is discretized to characterize each noise realization as a consider parameter, where the properties of the variational equations are exploited to compute efficiently their impact on the estimated and propagated covariance. The presented formulation is agnostic to the uncertainty source modeled and avoids the integration of stochastic equations of motion, being able to represent perturbation models ranging from purely Gaussian noise to constant error, depending on the correlation time scale.

However, as in the *consider parameters* theory or process noise algorithms, realistic values of the noise parameters are not known, in this case, the noise power and correlation time scale. Thus, the SCP theory is combined with a previously developed uncertainty quantification methodology, named as *Covariance Determination* [92, 93, 102], that allows the estimation of the variance of parameters that model the uncertainty in dynamical and measurements models. This *Covariance Determination* methodology is based on the observed distribution of the Mahalanobis distance of the orbital differences between estimated and predicted orbits, which should follow a χ^2 distribution under Gaussian assumptions. The variance of the uncertain parameters is estimated by minimizing an Empirical Distribution Function (EDF) test statistic between the observed Mahalanobis distance distribution and the χ^2 distribution.

The SCP method was first introduced in [97] to model the atmospheric density uncertainty in a simulation environment. This work presents the consolidation, validation and performance analysis of the SCP model and *Covariance Determination* method with real

radar measurements from the Spanish Space Surveillance Radar (S3TSR). Sentinel 3A, a satellite whose precise ephemeris are publicly available [103], is used for validation of the methodology prior to benchmarking with other RSOs at different altitudes. The results focus on the physical interpretation of the estimated noise parameters and the improvement in covariance realism using metrics such as Cramer-von-Mises Empirical Distribution Function (EDF) metric, and covariance containment. Additionally, the performance of the SCP method is compared against constant consider parameter models, as developed in previous works [92].
The work is structured as follows. Section 5.2 explains the methodology of the SCP model and summarizes the *Covariance Determination* methodology. Section 5.3 describes the radar characteristics and data processing chain. The results are presented and discussed in Section 5.4. Finally, the most relevant conclusions are summarized in Section 5.5.

5.2 Methodology

This section describes the Stochastic Consider Parameter model and summarizes the *Covariance Determination* methodology developed in previous works. The classical *consider parameters* theory formulation is briefly revisited, followed by the definition of the correlated stochastic model for the atmospheric drag error and how to map their effect into the estimation and propagation of the covariance matrix.

5.2.1 Consider Covariance Formulation

Let us define the extended state vector of an RSO as

$$\mathbf{y_{ext}(t)} = \begin{pmatrix} \mathbf{r}(t) \\ \mathbf{v}(t) \\ \mathbf{q}(t) \\ \mathbf{c}(t) \end{pmatrix} \in \mathbb{R}^{n_x+n_q+n_c}, \tag{5.1}$$

composed of the state vector $\mathbf{x}(t) = (\mathbf{r}(t), \mathbf{v}(t))$ of size n_x, estimated parameters $\mathbf{q}(t)$ of size n_q and the *consider parameters* of our analysis $\mathbf{c}(t)$, of size n_c, with uncertain variance. We define n_y as the amount of parameters estimated during the OD process, this is: $n_y = n_x + n_q$. The covariance matrix is a nominal product of the batch least-squares estimation, the so-called noise-only covariance $\mathbf{P}_n$. It consists in the inverse of the normal equations matrix as [28]:

$$\mathbf{P}_n = \left(\mathbf{H}_y^T \mathbf{W} \mathbf{H}_y\right)^{-1} \in \mathbb{R}^{n_y \times n_y}, \tag{5.2}$$

where matrix $\mathbf{H}_y \in \mathbb{R}^{n_m \times n_y}$ represents the partials of the measurements with respect to the estimated state, and $\mathbf{W} \in \mathbb{R}^{n_m \times n_m}$ corresponds to the weighting matrix, being n_m the amount of measurements. In the *consider parameters* theory, uncertain parameters are added into the dynamic or measurements models to characterize the uncertainty of the system. Such parameters are defined to follow a Normal distribution of the form [28]

$$c_i \sim \mathrm{N}\left(0, \sigma_i^2\right), \tag{5.3}$$

where σ_i^2 represents the variance of the consider parameter. Finally, the *consider covariance* at estimation epoch is defined as [28]

$$\mathbf{P}_c = \mathbf{P}_n + \mathbf{K}\mathbf{C}\mathbf{K}^T \in \mathbb{R}^{n_y \times n_y} \tag{5.4}$$

$$\mathbf{K} = \mathbf{P}_n \left(\mathbf{H}_y^T \mathbf{W} \mathbf{H}_c\right) \in \mathbb{R}^{n_y \times n_c}, \tag{5.5}$$

Where matrix $\mathbf{H}_c \in \mathbb{R}^{n_m \times n_c}$ corresponds to the partials of the measurements with respect to the *consider parameters*, where the i^{th} row accounts for the partial derivative of each measurement with respect to the consider parameters as follows:

$$\mathbf{H}_{ci} = \frac{\partial \mathbf{h_i}(t_i)}{\partial \mathbf{c}(t)} = \frac{\partial \mathbf{h}_i(t_i)}{\partial \mathbf{x}(t_i)} \cdot \frac{\partial \mathbf{x}(t_i)}{\partial \mathbf{c}(t)} \in \mathbb{R}^{1 \times n_c} \tag{5.6}$$

where t_i is the measurement epoch, $\frac{\partial \mathbf{h}_i(t_i)}{\partial \mathbf{x}(t_i)}$ represents the partial of the measurement with respect to the state at the measurement time, and $\frac{\partial \mathbf{x}(t_i)}{\partial \mathbf{c}(t)}$ is the so-called sensitivity matrix. This latter corresponds to the partial derivative of the state at t_i with respect to the consider parameters, and can be obtained through the integration of the variational equations similarly to the case of dynamic parameters such as the ballistic coefficient, as derived in [28].
Finally, $\mathbf{C}$ is defined as

$$\mathbf{C} = \begin{pmatrix} \sigma_1^2 & \cdots & 0 \\ \vdots & \ddots & \vdots \\ 0 & \cdots & \sigma_{n_c}^2 \end{pmatrix}, \tag{5.7}$$

containing the variances of the *consider parameters*, where no correlation between them is assumed in the classical *consider parameter* theory. It is important to note that this theory models the error present on each OD as constant during the estimation and propagation arcs. That is, c_i is a constant-error model for each OD under analysis, but defined to follow Equation (5.3) when a sufficient amount of ODs are analyzed, with the variance of each consider parameter represented in matrix $\mathbf{C}$.

5.2.2 Drag Force with Stochastic Noise

The stochastic time-correlated drag acceleration model to be applied in the system dynamics is as follows:

$$\boldsymbol{a}_{\text{drag}}(t) = -\frac{1}{2}\bar{\rho}(t)\frac{C_D A}{m} v_{rel}(t)^2 \frac{\boldsymbol{v}_{rel}(t)}{\|\boldsymbol{v}_{\text{rel}}(t)\|}(1 + p(t)), \tag{5.8}$$

where C_D is the drag coefficient, A the cross-sectional area, m the object mass, v_{rel} the relative speed of the object with respect to the atmosphere and $\bar{\rho}(t)$ corresponds to the mean atmospheric density at a certain position and epoch, obtained in this work with the NRLMSISE-00 model. The ballistic coefficient term ($C_D A/m$) is normally estimated as a constant value for the estimation and propagation arc in batch processes. Even though it is known to undergo variations in cross-sectional area and drag coefficient, this is a common assumption in most SSA operational scenarios for non-collaborative objects. Finally, $p(t)$ corresponds to the normalized stochastic perturbation, which represents deviations in the density, but also absorbs errors in the modeling of the ballistic coefficient.

Separated models could be proposed for object-related uncertainty sources (i.e. ballistic coefficient) and for environment-related sources (i.e. atmospheric density). However, as further discussed later, the nature of the proposed uncertainty quantification method is based on information from orbital differences. Thus, uncertainty models applying to the same perturbing force are not trivial to decouple, as was seen in [92]. The analysis of separated stochastic models for object and environment drag uncertainty that still allows their differentiation through orbital differences is out of the scope of this paper, though it is a future research under consideration.

To introduce a zero-mean correlated noise sequence for the perturbation error, an autoregressive function with time correlation of order 1 AR(1) is proposed [58], which can be considered as a discrete version of a Gauss-Markov process. The previously mentioned Ornstein-Uhlenbeck noise, another variation of Gauss-Markov process, allows for a tendency to a mean value. However, we propose the AR(1) model with zero mean to represent perturbations around a mean drag force.

First, let us assume that the correlation of two perturbations at two consecutive time steps $p(t_n)$ and $p(t_{n-1})$, in discrete form, is exponential as follows

$$r_p(t_n, t_{n-1}) = \mathbb{E}[p(t_n)\, p(t_{n-1})] = r_0(t_n)\, e^{-\frac{1}{\tau}|t_n - t_{n-1}|} \tag{5.9}$$

with

$$r_0(t_n) = \mathbb{E}\left[p(t_n)^2\right] = \sigma^2_{AE}(t_n), \tag{5.10}$$

where $r_0(t_n)$ is the power of the non-stationary perturbation, and is defined as the variance of the relative atmospheric drag uncertainty $\sigma^2_{AE}(t_n)$, in this case absorbing uncertainty in density and ballistic coefficient. The correlation of Equation (5.9) can be guaranteed with the AR(1) model, as

$$p\left(t_n, \sigma^2_{AE}, \tau\right) = a(n, \tau) p(t_{n-1}) + u(n, \sigma^2_{AE}, \tau), \tag{5.11}$$

with

$$a(n, \tau) = \frac{r_0(t_n)}{r_0(t_{n-1})} e^{-\frac{1}{\tau}|t_n - t_{n-1}|}, \tag{5.12}$$

$$u(n, \sigma^2_{AE}, \tau) \sim \mathrm{N}\left(0, \sigma^2_u(n, \sigma^2_{AE}, \tau)\right) \tag{5.13}$$

$$\sigma^2_u(n, \sigma^2_{AE}, \tau) = r_0(t_n)\left[1 - \frac{r_0(t_n)}{r_0(t_{n-1})} e^{-2\frac{1}{\tau}|t_n - t_{n-1}|}\right], \text{and} \tag{5.14}$$

$$p(t_0) = u(0) \sim \mathrm{N}(0, r_0(t_0)) \tag{5.15}$$

Thus, the noise at each step is related to the previous noise by the correlation factor $a(n)$ and has a Gaussian term $u(n)$. The strength of the correlation is controlled by τ, which represents the time scale of the correlation. The variance of the Gaussian term, $\sigma^2_u(n)$, is also proportional on the power noise but decreases with the correlation time scale. In other words, the stronger the correlation in the noise, the smaller the Gaussian term becomes. It can be noted from Equation (5.12) and Equation (5.13) that two limiting cases appear. Assuming constant power noise ($r_0(t_n) = r_0(t_{n-1})$), in the limit when the correlation time scale tends to infinity ($\tau_\alpha \approx \infty$) we find $\sigma^2_u(n) = 0$; $p(t_n) = p(t_{n-1})$. That is, the stochastic noise reduces to a constant noise model. On the opposite side,

when the correlation time scale tends to very small values ($\tau_\alpha \approx 0$) we end up with $\sigma_u^2(n) = r_0^2(t_n)$; $a(n) = 0$; $p(t_n) = u(n)$. That is, a purely Gaussian noise. These limits are relevant to understand the maximum and minimum impact that the stochastic noise can achieve in the covariance time evolution as a function of the correlation time scale. Further analysis of the limiting values of this stochastic model can be found in [18].

5.2.3 Stochastic Noise Discretization

Most batch least squares estimation algorithms, based on linearization, define the dynamic and *consider parameters* as constant throughout the estimation arc and the posterior propagation of the state, as in the case of the ballistic coefficient. This constant-error model is not completely representative of parameters such as the atmospheric density or ballistic coefficient that are known to vary during the estimation and propagation arcs. To build the SCP model within batch estimation methodology, we define the discrete noise sequence for the atmospheric drag as a series of constant parameters being applied sequentially, where the discretization time is a parameter of choice, although for accurate modeling the discretization grid should be much finer than the typical time scale of variation of the model represented. This is depicted in Figure 5.1, where each realization from the stochastic noise would be active between consecutive time steps. Hereafter, we refer to each discrete noise perturbation from the stochastic model as *stochastic parameter* (p_i).

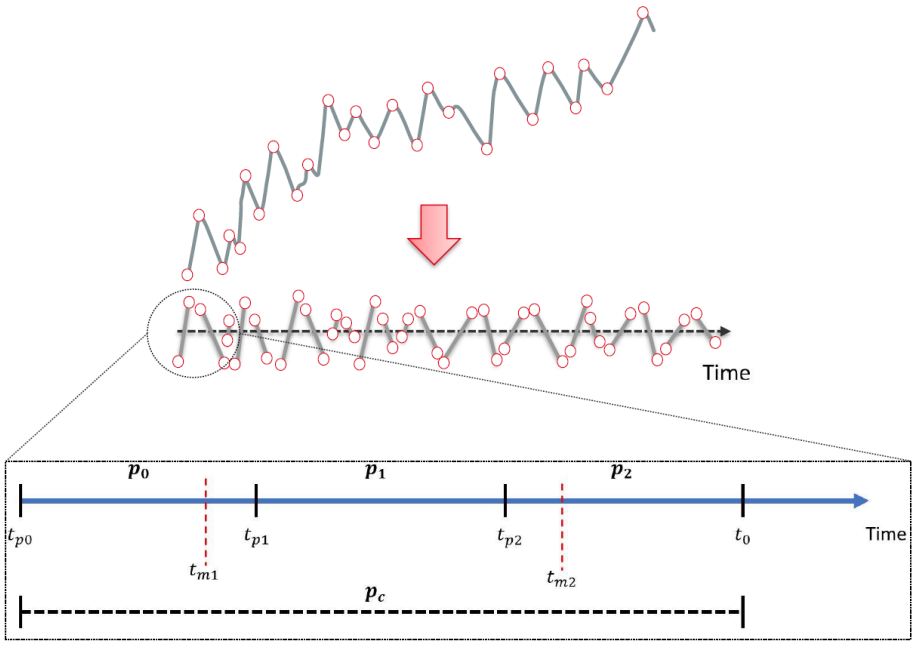

Figure 5.1: Parameters application timeline showing the stochastic parameter application times t_{pi} and the time of the measurements t_{mi}.

Batch estimation methods are able to map efficiently the impact of constant model parameters into the evolution of the state and its covariance by means of the sensitivity matrix. This is obtained through the integration of the variational equations, whose computational burden increases significantly with the number of parameters. Therefore, solving the variational equations for the huge number of stochastic parameters becomes

impractical for the nominal estimation and propagation arcs in SSA. Nonetheless, the properties of the variational equations can be exploited to mitigate this issue because each stochastic parameter represents the same physical variable (i.e. a perturbation in the drag), only applied at different epochs. As shown in [18], it can be proven from the properties of the variational equations that the partial derivatives of the state with respect to any of the stochastic parameters can be derived from the partial derivatives of a global dynamic parameter (p_c) applied during the complete estimation or propagation arc, shown Figure 5.1. Please refer to Appendix B for a complete derivation. The sensitivity matrix for each stochastic parameter is then as follows:

$$\frac{\partial \mathbf{x}(t)}{\partial p_i} = \begin{cases} \frac{\partial \mathbf{x}(t)}{\partial p_c} - \frac{\partial \mathbf{x}(t)}{\partial \mathbf{x}(t_{pi})} \frac{\partial \mathbf{x}(t_{pi})}{\partial p_c} & t_{pi} <= t <= t_{pi+1} \\ \frac{\partial \mathbf{x}(t)}{\partial \mathbf{x}(t_{pi+1})} \left(\frac{\partial \mathbf{x}(t_{pi+1})}{\partial p_i} \right) & t > t_{pi+1} \\ 0 & t < t_{pi} \end{cases} \tag{5.16}$$

where $\frac{\partial \mathbf{x}(t)}{\partial \mathbf{x}(t_r)}$ represents the state transition matrix from any reference time t_r to time t, and $\frac{\partial \mathbf{x}(t)}{\partial p_c}$ is the sensitivity matrix of p_c, that is, the partial derivatives of the state with respect to the global parameter at time t. Thus, by solving the variational equations for a single global parameter, the sensitivity matrix of each stochastic parameter can be retrieved as a function of its start and stop time (t_{pi} and t_{pi+1}, respectively). Firstly, the contribution of the stochastic parameter to the state and covariance is null before its start time. During the time it is applicable, its partial derivative corresponds to the difference between the global parameter sensitivity and the linear propagation of the global parameter sensitivity from the start epoch to time t via the state transition matrix. Once the parameter is not active, the sensitivity matrix at the stop time is propagated forward with the state transition matrix.
Thus, Equation (5.16) allows to compute the sensitivity matrix of all stochastic parameters efficiently and with negligible impact to most operational orbit determination systems where the state transition and sensitivity matrices are computed natively. Since this work focuses on atmospheric drag uncertainty, the global parameter p_c is chosen to be the ballistic coefficient.

5.2.4 Consider Covariance with Correlated Stochastic Parameters

Up to now, it has been described how to compute the sensitivity matrix of multiple, constant parameters for the discretized stochastic drag model. Thus, it remains to explain how to include the correlation between each of the stochastic parameters and the new formulation for the *consider covariance*. Recalling Equation (5.11), the term $u(n)$ follows the required Gaussian distribution for a *consider parameters* under the following assumptions:

- Constant discretization time step: $\Delta t_n = |t_n - t_{n-1}|$
- Constant noise power: $r_0(t_n) = r_0(t_{n-1})$

The discretization time is to be chosen as a trade-off between computational cost and accuracy to the pure stochastic model, as further discussed later. However, the constant noise power assumption implies that the drag uncertainty, in relative terms, is constant.

This is a delicate assumption, since the atmospheric density uncertainty is known to depend strongly on the altitude of the RSO and the solar and geomagnetic activity as studied in previous works [17, 27]. Therefore, the boundaries of the methodology are limited to such assumption of constant power of the noise, which is not expected to remain perfectly constant in real environments. However, the analysis and optimization processes carried out in this work are focused on RSOs whose orbits are nearly circular, and on time frames where the solar and geomagnetic activity did not suffer extreme relative changes. Further analysis on the sensitivity of the methodology to such assumptions and its performance when they are not valid are out of the scope of this paper, but it is a planned line of research.

Therefore, the power of the stochastic noise is assumed constant for an object orbiting at a constant altitude for a given solar activity period. In that case, Equation (5.11) can be written as a linear product in matrix form for the complete set of stochastic parameters as:

$$\mathbf{p} = \mathbf{A}\mathbf{u}, \tag{5.17}$$

with

$$\mathbf{p} = \begin{pmatrix} p_0 \\ \vdots \\ p_n \end{pmatrix}; \ \mathbf{u} = \begin{pmatrix} u_0 \\ \vdots \\ u_n \end{pmatrix}; \ \mathbf{A} = \begin{pmatrix} 1 & \cdots & 0 \\ \vdots & \ddots & \vdots \\ b_{ij} & \cdots & 1 \end{pmatrix} \in \mathbb{R}^{N\times N}, \tag{5.18}$$

where $N = n+1$ is the number of stochastic parameters, which corresponds to the number of time steps in the noise sequence. Finally, $b_{ij} = \prod_{j+1}^{i} a(\tau)$; $\forall\ i > j$ where i and j represent the row and column of the matrix, respectively. Therefore, the set of stochastic parameters is decomposed as the set of Gaussian terms u_i and their correlation inside matrix $\mathbf{A}$.

If we define $\mathbf{u}$ as our new set of consider parameters ($\mathbf{u} = \mathbf{c}$), or in this case, stochastic consider parameters, then we have that

$$\frac{\partial \mathbf{x}(t)}{\partial \mathbf{c}} = \frac{\partial \mathbf{x}(t)}{\partial \mathbf{p}} \frac{\partial \mathbf{p}}{\partial \mathbf{c}} = \frac{\partial \mathbf{x}(t)}{\partial \mathbf{p}} \mathbf{A}. \tag{5.19}$$

Equation (5.19) can be applied within matrix $\mathbf{H_c}$, required for the formulation of the *consider covariance*. The last term of Equation (5.6) with the stochastic consider parameter model results in

$$\frac{\partial \mathbf{x}(t_i)}{\partial \mathbf{c}} = \left[\frac{\partial \mathbf{x}(t_i)}{\partial p_i}, \cdots, \frac{\partial \mathbf{x}(t_i)}{\partial p_{n_c}} \right] \cdot \mathbf{A} \in \mathbb{R}^{n_x \times N}, \tag{5.20}$$

where now $\mathbf{c}$ is a vector of *stochastic consider parameters* of size N, and the partial derivatives of each stochastic parameter p_i are computed as developed in Eq (5.16). Therefore, the *consider covariance* with the SCP formulation is of the form:

$$\mathbf{P}_c = \mathbf{P}_n + \mathbf{K}_{CA}\mathbf{A}\mathbf{C}(\mathbf{K}_{CA}\mathbf{A})^T \in \mathbb{R}^{n_y \times n_y} \tag{5.21}$$

$$\mathbf{K}_{CA} = \mathbf{P}_n \left(\mathbf{H}_y^T \mathbf{W} \mathbf{H}_{CA} \right) \in \mathbb{R}^{n_y \times N}, \tag{5.22}$$

where N is the number of stochastic parameters included in the OD arc. The partials of the measurements with respect to the stochastic parameters, $\mathbf{H_{CA}}$, is computed by

combining Equation (5.20) and Equation (5.6), where each row (i.e. the contribution of each measurement) is

$$\mathbf{H}_{CA_i}(m_i, t_m) = \frac{\partial \mathbf{h_i}(t_m)}{\partial \mathbf{x}(t_m)} \cdot \frac{\partial \mathbf{x}(t_m)}{\partial \mathbf{p}} \in \mathbb{R}^{n_m \times N}, \tag{5.23}$$

where t_m corresponds to the epoch of measurement m_i, which can lay between the application times of the stochastic parameters as depicted in Figure 5.1. Finally, the matrix of the consider parameter variances is now as follows:

$$\mathbf{C} = \begin{pmatrix} r_0 & \cdots & \cdots & 0 \\ \vdots & \sigma_u^2(r_0, \tau, \Delta t_n) & & \vdots \\ \vdots & & \ddots & \vdots \\ 0 & \cdots & \cdots & \sigma_u^2(r_0, \tau, \Delta t_n) \end{pmatrix} \in \mathbb{R}^{N \times N}, \tag{5.24}$$

where r_0 is the previously defined power of the noise, and $\sigma_u^2(r_0, \tau, \Delta t_n)$ is the variance of the consider parameters, both of them being constant under the previously discussed assumptions. The variance of the first consider parameter, i.e. the first perturbation, corresponds to r_0 as defined by Equation (5.15).

To summarize, the stochastic noise model for the drag uncertainty is discretized in stochastic consider parameters whose effect in the *consider covariance* is mapped with the above equations as a function of the power of the noise r_0 and the correlation time scale τ. It is important to note that the computation of matrix $\mathbf{H_{CA}}$ in Equation (5.15) suffers from the curse of dimensionality with the number of stochastic consider parameters. For the discretization scheme to converge to the theoretical stochastic model, the number of stochastic parameters should tend to infinite. This trade-off has been analyzed in previous works by comparing the accuracy of the SCP model with respect to Monte Carlo simulations with stochastic drag dynamics, as a function of the discretization interval [18]. In that analysis, a stochastic parameter application interval of 5 minutes was found to be a satisfactory trade-off between computational cost and accuracy. Thus, this time interval has been used in the work presented here for both the estimation and propagation arcs.

5.2.5 Linear covariance propagation with SCP

Previous sections have developed how to compute the *consider covariance* at estimation epoch, with the SCP model. However, most SSA services are focused on the prediction arcs, where the errors in the dynamics are dominant. Therefore, it is necessary to define how to propagate the covariance matrix with the SCP model outside the estimation arc. Linear covariance propagation is based on the integration of the variational equations [28]. Its solution is the Extended State Transition Matrix $\mathbf{\Psi}$ [92], which is composed of the state transition matrix $\mathbf{\Phi}$ and the sensitivity matrix S, as shown in Equation (5.25). In the case of the SCP model, the proposed atmospheric drag model is applicable not only to the estimation arc, but also to any posterior propagation arc. Thus, the linear propagation of the *consider covariance* under the stochastic drag model proposed is

$$\begin{aligned} \mathbf{P}_c(t) &= \boldsymbol{\Psi}(t,t_0)\mathbf{P}_{c_{ext}}(t_0)\boldsymbol{\Psi}(t,t_0)^T = \\ &= \begin{pmatrix} \boldsymbol{\Phi}(t,t_0) & \mathbf{S}(t) \\ \mathbf{0} & \mathbf{I} \end{pmatrix} \begin{pmatrix} \mathbf{P}_c & \mathbf{0} \\ \mathbf{0} & \mathbf{C}_{prop} \end{pmatrix} \boldsymbol{\Psi}(t,t_0)^T, \end{aligned} \tag{5.25}$$

where $\mathbf{P}_c$ is obtained with Equation (5.21), having the same size as the estimated parameters and matrix $\mathbf{S}(t)$ is now composed of:

$$\mathbf{S}(t) = \left[\frac{\partial \mathbf{x}(t)}{\partial \mathbf{d_p}} \quad \frac{\partial \mathbf{x}(t)}{\partial \mathbf{p}} \mathbf{A} \right]. \tag{5.26}$$

The former term of Equation (5.26) represents the sensitivity matrix of any other dynamic parameters $\mathbf{d_p}$ applied during the orbit determination and propagation (i.e. ballistic or solar radiation pressure coefficient). The latter term is computed as previously developed in Equation (5.16). Finally, $\mathbf{C}_{prop}$ is a matrix containing the variance of the *stochastic consider parameters* to be applied during propagation, which in this case is analogous to Equation (5.24) except for the first element, which corresponds to $\sigma_u^2(r_0, \tau, \Delta t_n)$ instead of r_0 since the parameters during the propagation arc are already correlated to the parameters applied during the estimation arc. The size of $\mathbf{C}_{prop}$ is determined by the number of stochastic parameters considered during the propagation arc, which depends on the discretization step and the length of the propagation arc.

5.2.6 Covariance Determination Method Summary

Previous sections have described how to compute the *consider covariance* and its linear propagation with the proposed SCP model, as a function of the power of the noise and the correlation time scale. The objective now is to estimate the values of those parameters that govern the noise in order to improve the realism of the covariance. Previous works have developed a methodology, named *Covariance Determination*, that is able to estimate the variance of consider parameters to model the uncertainty in the space environment [92, 93, 104]. In this work, this framework is combined with the SCP model to estimate the parameters of the stochastic noise using real measurements. For completeness, the concepts of the *Covariance Determination* methodology are summarized next.

The Mahalanobis distance (d_M) is a well-known statistical metric that describes how far a state $\mathbf{y}(t)$ is from a certain reference $\mathbf{y}_{ref}(t)$, projected into the covariance space [78]. The squared Mahalanobis distance is defined as

$$d_M^2(t) = \Delta\mathbf{y}(t)^T \left(\mathbf{P_c}(t) + \mathbf{P}_{ref}(t) \right)^{-1} \Delta\mathbf{y}(t), \tag{5.27}$$

where $\Delta\mathbf{y}(t) = \mathbf{y}(t) - \mathbf{y}_{ref}(t)$ represents the orbital differences between the state and its reference, whereas $\mathbf{P_c}(t)$ and $\mathbf{P}_{ref}$ are the covariance matrices of the state and the reference, respectively, being $\mathbf{P_c}(t)$ computed by means of Equation (5.25). In Equation (5.27), it is assumed that both variables $\mathbf{y}(t)$ and $\mathbf{y}_{ref}(t)$ are uncorrelated. This common assumption [11, 79], is not easily guaranteed in many scenarios, for instance, when the same sensor network is shared for both estimations.

Hence, the Mahalanobis distance is obtained as a function of the variance of the stochastic consider parameters, which in the case of the SCP model are controlled by the power

of the noise r_0 and the time scale of the correlation τ. Bearing this in mind, the Covariance Determination concept is as follows. If the dispersion of the orbit state is well characterized by its covariance matrix (i.e. realistic), then the distribution of Mahanalobis distances of the state should behave as a χ^2 distribution, defined as the sum of squared Normal distributions [76]. In that case, Equation (5.27) can be applied within an optimization process to find the optimum noise parameters that lead the Mahalanobis distance distribution to resemble the χ^2 distribution. This can be achieved by minimizing an Empirical Distribution Function (EDF) metric, generally used to assess the similarity between two Cumulative Distribution Functions (CDFs). Cramer-von-Mises (CvM) EDF metric has been chosen among other options available in the literature [11, 76], where a metric larger than 1.16 rejects the null hypothesis of the test distribution being drawn from the reference distribution with a significance level of 0.001. This cost metric is minimized following a heuristic optimization process based on the Differential Evolution algorithm [90]. The final *Covariance Determination* process with the SCP model is summarized in Algorithm 2 in Appendix B.

Regarding the computation of the Mahalanobis distance, position orbital differences in TNW local orbital frame are used. The velocity terms of the covariance are discarded for two main reasons. First, numerical instabilities appear during the computation of the Mahalanobis distance due to ill-conditioning of the Cartesian position-velocity cross-terms after approximately 4 days of propagation, as seen in [69]. Second, other authors propose similar metrics based only on position uncertainty arguing that the latter is the most relevant one in high-velocity collision risk assessments, which account for the majority of encounters in LEO. Thus, TNW position orbital differences are used hereafter, which also alleviates Gaussianity maintenance as described in [69]. Nonetheless, velocity covariance terms are maintained for the linear covariance propagation during the optimization process, as they are relevant to the mapping of the dynamic parameter uncertainties into the state uncertainty during propagation.

Then, it is necessary to describe the population of orbital differences $\mathbf{\Delta y}$ to characterize the distribution of the state. Firstly, the interest is placed on propagation epochs, since the impact of errors in the estimation of dynamic parameters is not properly observed in the orbit state until enough propagation time has elapsed, which will depend on the relevance of the dynamic parameter in the dynamics of motion. In this work, the orbital differences under analysis are selected in the propagation range between $t_0 + 3$ days and $t_0 + 6$ days, where t_0 corresponds to the epoch of the last measurement in the OD arc (estimation epoch). This interval of analysis was selected as a trade-off for all analyzed LEO objects, aiming to have enough propagation time while still remaining under linear and Gaussian assumptions. Secondly, a sufficient number of orbits are required in order to obtain reliable and converged results. This was further analyzed in [92], where approximately 50 orbits was deemed sufficient under data scarce scenarios. Thirdly, it is crucial to define which orbit is to be used as reference for the Mahalanobis distance computation of Equation (5.27). In SSA operations, there is a very limited availability of precise ephemeris information, only reserved to a few operational spacecraft. Even though their availability is leveraged in this work for complete validation of the methodology, the SCP model and the *Covariance Determination* method must be prepared for the common case where no external source of precise ephemeris is available. Bearing this in mind, the *Covariance*

Determination method is designed to compare the propagation arc of each orbit against the estimation arc of a newer orbit, since the error of propagating a certain estimation is expected to be larger than the estimation error, bounded by observations. This is exemplified in Figure 5.2 and called hereafter as *Operational Reference* orbit. To avoid correlation in the orbital differences, the *Covariance Determination* method ensures that the computed reference orbit does not share any observation with the orbit state under analysis. Previous works [92, 97, 102] with simulated data have proven that this choice of reference orbit is able to provide similar accuracy to using precise ephemeris, though this is further discussed in the results of this work.
It is worth mentioning that the proposed *Covariance Determination* methodology is not able to adapt to sudden changes in the environment that have a significant impact on the uncertainty, such as solar or geomagnetic storms. Due to the requirement of multiple orbits as input, which can span several months, this methodology models uncertainty in the overall period of analysis, providing an averaged quantification of the uncertainty that can be useful for catalogs while not being able to respond to abnormal events.
Finally, it is relevant to point out that a constant model consider parameter for the range bias uncertainty is applied for all the RSOs under analysis in this work. The reason is that, when dealing with real measurements, there is some uncertainty in the measurements biases that needs to be modeled and estimated in order to achieve covariance realism at estimation epoch, since the uncertainty of the atmospheric drag is not mapped into the position uncertainty until enough propagation time is elapsed. In the case of S3TSR, the most relevant information is contained in the range measurements, and thus, a constant-model consider parameter is applied and estimated during the *Covariance Determination* process. Please refer to [92] for further details about measurements model consider parameters.

5.3 S3TSR data processing

This section describes the characteristics and processing chain of the real measurements used for the validation and analysis of the presented methodology.

5.3.1 S3TSR radar

The available data corresponds to measurements from the Spanish Space Surveillance and Tracking Radar (S3TSR). Located in Morón (Spain), provides range, range-rate, azimuth, and elevation measurements. Further details about the radar characteristics can be found in [105]. The extent of the available data is from June of 2019 up to March 2020, even though maintenance and other unavailability periods do not allow to have continuous coverage of the complete time interval. Furthermore, the data period corresponds to the transition from solar cycle 24 to cycle 25, with low and relatively stable solar and geomagnetic activity.

5.3.2 RSOs under analysis

The main characteristics that define the orbit of the analyzed RSOs are shown in Table 5.1. They correspond to defunct rocket bodies or large space debris objects with enough radar cross-section to maximize the number of measurements in the available time interval.

The only exception is the case of Sentinel 3A (NORAD ID 41335), which has been selected for calibration and initial validation purposes due to the public availability of precise ephemeris.

Table 5.1: RSOs characteristics

NORAD ID	**41335**	**27665**	**21610**	**33066**	**27371**	**43520**
Altitude [km]	810	800	760	660	520	430
SMA [km]	7180,8	7175,5	7133,6	7041,2	6917,7	6848,1
Eccentricity [-]	1,3E-03	6,0E-04	1,3E-03	1,0E-03	1,8E-03	6,5E-04
Inclination [deg]	98,5	39,7	98,5	48,5	38,0	34,9
RAAN [deg]	323,3	109,7	133,9	162,3	354,6	315,1
Argument of pericentre [deg]	109,7	148,7	123,4	48,7	105,2	28,8
OD arc length [days]	7	7	7	7	6	4,5

5.3.3 Orbit determination and propagation

In SSA operations, orbit determinations are launched routinely upon the reception of new measurements in order to update the RSO orbit in the catalog. Such estimations are propagated into the future to provide other services such as collision avoidance. Due to the goal of operational applicability of the methodology described in this work, an analogous process to routine operations is followed to process the S3TSR data:

- **Orbit determination**: a batch least-squares algorithm is applied with a Gauss-Newton solver during a fixed arc length. The estimated parameters are position, velocity, ballistic coefficient and solar radiation pressure coefficient. The estimation epoch (t_0) is selected as the epoch of the last observation that entered the estimation arc. The dynamic model used is described in Table 5.2. The length of the arc is selected according to the orbital regime of the RSO under analysis, in a trade-off that aims to maximize the amount of data used while at the same time ensuring that the linearization of the dynamics holds. The selected arc lengths, derived from operational experience, are shown in Table 5.1.
- **Orbit propagation**: the estimated state is propagated forward 8 days, with the same dynamical model.
- **Outliers filtering**: estimations with too few data, or with manoeuvres on the estimation or propagation arcs need to be filtered out.

The orbit determination and propagation process is launched daily until spanning the whole interval of available data.

5.3.4 Operational reference orbit

Once all the orbits (estimations and propagations) have been generated, it is necessary to select the appropriate *Operational reference orbit* in order to execute the *Covariance Determination* algorithm with the SCP model, as previously discussed. The choice of each *Operational Reference* orbit for each propagated orbit is crucial for a successful characterization of the uncertainty in the system. Two main factors are to be considered for this choice:

Table 5.2: Reference dynamical model

Reference frame	GCRF
Gravity field	32x32
Third body perturbations	Sun & Moon
Polar motion and UT1	IERS C04 08
Earth pole model	IERS 2010
Earth precession/ nutation	IERS 2010
Atmospheric density model	NLRMSISE-00
Solar radiation pressure model	Cannonball
Drag model	Cannonball
Solar radiation pressure area	Constant area
Drag area	Constant area

- Orbit coverage: depending on the desired interval of analysis to perform the *Covariance Determination* process, the *Operational Reference* must cover the interval inside its orbit determination arc. In this work, the interval of analysis has been chosen from $t_0 + 3$ to $t_0 + 6$ of the orbit under analysis, where linearity and Gaussianity assumptions are expected to hold for all analyzed objects.
- Correlation: the correlation between the propagated orbit and the *Operational Reference* must be kept to the minimum. For this purpose, it is necessary to avoid that both orbits share any measurements between them.

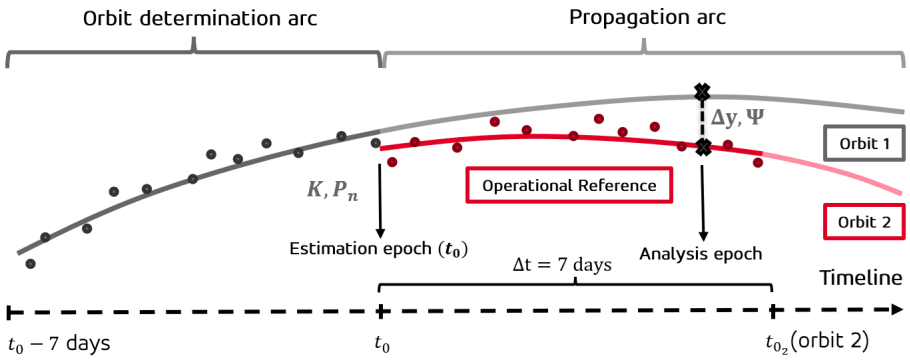

Figure 5.2: Orbit determination and propagation diagram with the definition of the *Operational Reference orbit.*

5.4 Results

5.4.1 Validation with Sentinel-3A

The reason for choosing Sentinel-3A to validate the proposed methodology is the availability of precise ephemeris that can be used as ground truth reference for the computation of the Mahalanobis distance. The goal now is to perform the *Covariance Determination* algorithm in 2 different ways: comparing the performance of the SCP model versus the constant consider parameter model, and comparing the results between using precise ephemeris as reference orbit or using the already defined *Operational*

Reference orbits. These results are summarized in Table 5.3, where a total of 55 orbits are available for analysis due to the aforementioned filtering process and radar unavailability. Please note that in the case of using the *Operational Reference* orbits, the amount of orbits is lower since there are cases where an appropriate estimated reference could not be found.

Table 5.3 shows the optimum parameters found during the *Covariance Determination* process (σ_{AE}, τ), the Cramer-von-Mises (CvM) metric result and the corresponding 3σ covariance containment during the optimization arc, which in this case is between t_0+3 and t_0+6 days of propagation for all RSOs. A CvM metric lower than 1.16 indicates that the samples (squared Mahalanobis distance) of the test distribution are drawn from the reference distribution (χ^2) with a 99.9% confidence interval [76]. The covariance containment metric consists in measuring the number of samples laying inside different $k\sigma$ ellipsoids and compare it against the expected fraction for a multivariate Gaussian distribution of the same number of Degrees of Freedom (DoF). Containment levels similar to the theoretical multivariate Gaussian distribution are indicative of covariance realism. For brevity, the results discussed here are focused on the 3σ containment where the theoretical fraction of samples containment is 97.1% for a 3 DoF distribution, finding similar conclusions at the different sigma levels. The 3 DoF correspond to position orbital differences, in the TNW local orbital frame (In-track, Normal, Cross track). The in-track axis is defined as tangential to the orbit and parallel to the velocity. The normal axis is placed in the orbit plane, perpendicular to the in-track axis, and the cross-track axis is perpendicular to the orbit plane [56]. Finally, the covariance containment metric is showed in the last two columns of Table 5.3 for two different cases: applying the *Covariance Determination* method correction, or using the noise-only covariance.

Table 5.3: Stochastic consider parameters results for Sentinel 3A

Reference orbit	N_{orb}	σ_{AE} [%]	τ [s]	τ [days]	σ_{RB} [-]	**CvM**	**3σ Containment [%]**	
							Corrected	**Noise-only**
Precise ephem.	55	54.43	-	-	0.69	0.19	95.48	69.61
Operational Ref.	51	44.19	-	-	0.51	0.04	94.72	71.92
Precise ephem.	55	59.97	73633	0.85	0.45	0.06	96.03	69.61
Operational Ref.	51	61.92	106200	1.23	0.28	0.03	95.61	71.92

The first two rows of Table 5.3 correspond to the case of constant consider parameter model, not showing an estimation for the correlation time scale (τ). The last two rows correspond to the *Covariance Determination* results when applying the SCP model. The estimated standard deviation of the range bias σ_{RB} is normalized with the expected accuracy of the sensor.

Several conclusions are drawn from the results showed in Table 5.3. The low Cramer-von-Mises metric and the 3σ covariance containment levels close to the theoretical 97.1% indicate that a significant covariance realism improvement is achieved with both consider parameter models as compared to the noise-only covariance. However, it can be noted that the Stochastic Consider Parameters model obtains a higher level of realism, achieving a better fit to the χ^2 distribution and a containment closer to the expected multivariate Gaussian distribution. This is better appreciated in Figure 5.3, which depicts the optimum distribution of Mahalanobis distances after the *Covariance*

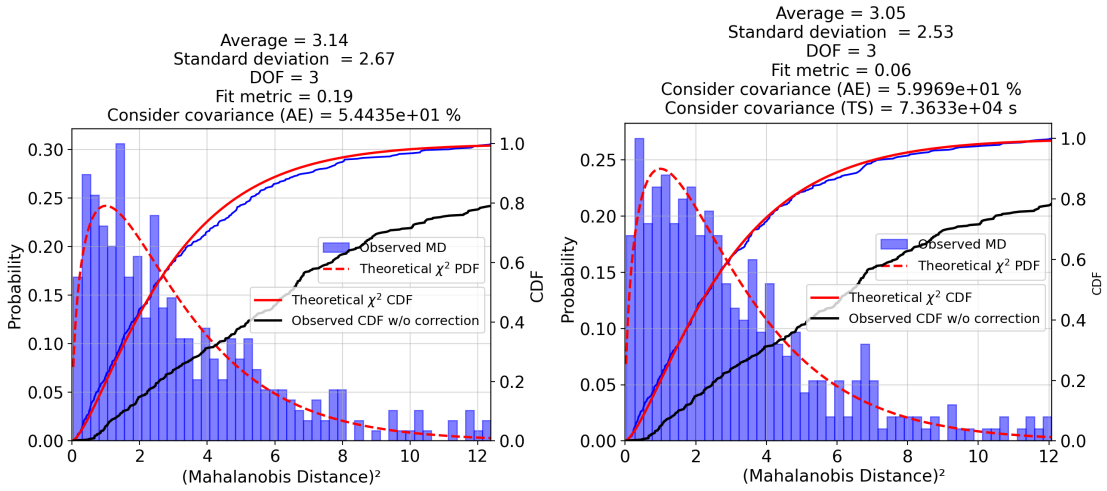

(a) Constant consider parameters model

(b) Stochastic Consider Parameters model

Figure 5.3: Sentinel-3A optimum squared Mahalanobis distance distribution using precise ephemeris as reference, with epochs of analysis between $t_0 + 3$ days up to $t_0 + 6$ days. The blue curve represents the CDF of the Mahalanobis distance distribution. The black curve represents the CDF of the distribution if no covariance correction is applied (i.e. using the noise-only covariance).

Determination process using the constant consider parameters (Figure 5.3a) and the SCP model (Figure 5.3b). The headers of both figures represent the average and standard deviation of the distribution, the number of DoF (TNW position orbital differences), the fit metric (i.e. the Cramer-von-Mises test metric as compared to the $\chi^2(DoF)$ distribution), and the estimated values of the uncertainty. In Figure 5.3a, the estimated uncertainty corresponds to the single consider parameter for drag uncertainty in the case of using the precise ephemeris as reference, corresponding to the first row of Table 5.3. In Figure 5.3b, the estimated uncertainty corresponds to the power of the noise and correlation time scale, corresponding to the third row of Table 5.3. The red curves represent the theoretical PDF and CDF of the χ^2 distribution, and the blue line corresponds to the CDF of the observed squared Mahalanobis distance, after optimization. It is seen how the fit between the blue curve (the observed Mahalanobis distances CDF) and the red curve (χ^2 CDF) is better when using the SCP model, especially at the center of the CDF, as compared to the constant consider parameter model. In addition to this, the black curve in both figures show the CDF of the so-called noise-only covariance, which is far from the desired χ^2 behavior. This is the level of realism achieved by the nominal covariance after a batch estimation with high fidelity dynamics, highlighting the improvement achieved with the *Covariance Determination* process presented here, and especially with the SCP model.

Regarding the optimum values found for the consider parameters and the stochastic noise, they are aligned with the uncertainty expectations in the density and ballistic coefficient of real environments. In the case of the power of the noise for the atmospheric drag, it is expected to absorb errors not only related to the density, but also to the ballistic coefficient estimation of the batch least-squares. The uncertainty between different density models ranges from 10-20% [24, 91], while also large uncertainty in the ballistic coefficient is

expected, especially due to the variations of the cross-sectional area coming from the lack of knowledge of attitude dynamics, common for space debris. As compared to the constant consider parameter model, the SCP model provides a better fit, allocating slightly less uncertainty in the range bias whereas the power of the stochastic noise is increased. However, the increase in the power of the noise is compensated with a correlation scale of the order of 1 day, which is able to better represent the uncertainty observed in the orbital differences.
Finally, it is important to remark that similar optimum parameters are found when using as reference the precise ephemeris or the *Operational Reference* orbits, as seen in Table 5.3. This is crucial to prove that the *Covariance Determination* method is able to maintain the performance and the traceability of the physical sources of uncertainty even when an external, precise source of ephemeris is not available, which is the general case of the space debris problem.

5.4.2 Space debris RSO results

After assessing the feasibility of characterizing the uncertainty of the orbit estimation and propagation using the *Operational Reference* orbits to compute the Mahalanobis distance, this section presents the analysis for the other 5 RSOs considered in this work, for which there are no precise ephemeris available. The results are summarized in Table 5.4. It uses a similar format to the previously described Table 5.3, with the addition of a column for the average of the estimated ballistic coefficients, for reference.

Table 5.4: Space debris RSOs results

Object	$B_c[\frac{m^2}{Kg}]$	N_{orbits}	σ_{AE} [%]	τ[s]	τ[days]	σ_{RB} [-]	CvM	3σ Cont. [%]
27665	0.018	76	65.05	-	-	1.19	0.15	95.8
			40.78	130520	1.51	1.92	0.05	96.59
21610	0.018	44	39.77	-	-	0.83	0.22	96.00
			25.26	441490	5.11	1.41	0.34	96.67
33066	0.012	47	63.73	-	-	0.37	0.79	93.63
			69.78	107060	1.24	0.23	0.49	96.84
27371	0.011	69	28.72	-	-	1.11	0.28	95.43
			38.61	42300	0.49	0.21	0.03	96.32
43520	0.038	15	21.58	-	-	1.78	0.07	88.78
			26.05	14911	0.17	1.81	0.29	93.07

Overall, Table 5.4 shows that both the constant and the SCP models provide a significant covariance realism improvement after the *Covariance Determination* process (further compared against the noise-only covariance in Section 5.4.3). Again, the SCP model results in better Cramer-von-Mises metrics and covariance containment, which indicates a better characterization of the uncertainty.
Figure 5.5 shows the dispersion of the orbital differences in TNW local frame, normalized with the standard deviation of its covariance, for the object 27371 in the propagation arc between $t_0 + 3$ days and $t_0 + 6$ days. The orbital differences laying outside of their corresponding 3σ covariance ellipsoid are depicted as red dots, resulting in the 96.32% of containment shown in Table 5.4. Bear in mind that even though all samples at multiple epochs are plotted together, each orbital difference is compared against its

own corrected covariance by means of Equation (5.27), which allows the evaluation of all orbital differences as part of the same distribution for the *Covariance Determination* optimization. The non-diagonal plots of Figure 5.5 indicate that linearity and Gaussian assumptions are still valid, even though more samples (i.e. orbit determinations and propagation) would be desired. Gaussianity tests such as Michael's normality tests [82] have been carried out for all RSOs to ensure normality. A clear negative correlation is observed between the radial and cross-track orbital differences. This behavior can be expected when only a single sensor is used for the orbit determination, especially when the range measurement is the dominant measurement. Due to the RSO orbit geometry, the uncertainty present in the range measurement can accumulate on the radial or the cross-track direction depending on the portion of the orbit being observed. Thus, this uncertainty can be expected map alternatively in the radial or cross-track directions, leading to a negative correlation that is observed both in the orbital differences and in the covariance, being able to maintain the realism. Even though this correlation is expected to impact the 3 DoF assumption of the χ^2 distribution, ignoring such behavior between the radial and cross-track errors would be detrimental to the covariance realism assessment. The case of the lowest altitude RSO (NORAD 43520) was found to be at the limit of the linearity assumptions, obtaining a worse CvM metric with the SCP model than with the constant consider parameter model, despite having a better covariance containment. Reaching the limits of linearity in combination with a limited population of orbits causes the statistical comparison metric to have high sensitivity and to be less reliable. For these reasons, apart from a larger number of orbits, RSOs at lower altitudes require alternative state representations that allow to maintain Gaussianity for longer propagation arcs. Curvilinear coordinates that adapt better to the orbit curvature [71], or transformations that convert along-track differences into time differences (QtW transformation [73]) can be integrated with the computation of the Mahalanobis distance, being a current line of work.

In relation to the estimated values for the different uncertainty models, a trend of less power of the noise with decreasing altitude is observed, with the exception of object 33066. The reduction of the stochastic noise power with decreasing altitude is an expected phenomena for the density uncertainty, as has been observed after statistical analysis of historic space weather data [18]. Despite a lower relative uncertainty in the density, the larger relevance of the drag force leads to larger absolute uncertainty in the atmospheric drag as altitude decreases. However, as discussed in the results of Sentinel 3A, the stochastic noise model proposed is also absorbing uncertainty of the ballistic coefficient. Regarding the estimation of the stochastic correlation, lower correlation time scales are found for objects 27371 and 43520, the ones at the lowest altitudes of the set. Figure 5.4 shows the contour plot of the Cramer-von-Mises metric for object 27371, in logarithmic scale, as a function of the correlation time scale and noise power. Blue-shaded regions corresponds to Cramer-von-Mises metrics below 1, that is, matches between the observed and the theoretical squared Mahalanobis distance distributions with a confidence interval lower than a 99.9%. A characteristic curve is observed, with an asymptotic tendency at a certain power of the noise for increasing correlation, and inversely for increasing power of the noise. Relevant insights of the SCP model can be gained from the contour of Figure 5.4. For a given uncertainty of the system, similar realism can be achieved with

a trade-off between correlation and power of the noise, which is related to the nature of the stochastic noise model proposed. As the correlation time scale increases, orbit errors are more constant and tend to accumulate upon propagation. Therefore, a reduction in the power of the noise is seen until reaching a limit where the correlation time scales are of the order of the propagation and estimation arcs, equivalent to the constant consider parameter model. Inversely, lower correlation leads to less accumulation in the orbital errors, which requires an increase in the power of the noise in order to characterize the given uncertainty in the system. In the case of object 27371 in Figure 5.4, as the atmospheric drag becomes the main driver of the orbital dynamics, the characteristic frequency at smaller time scales (related to orbital periods and day/night variations) is expected to be better characterized by the stochastic model, finding the optimum noise and time correlation shown in Table 5.4 in the middle of the blue-shaded region. In other RSOs at higher altitudes, the perturbations in the drag of each orbit determination are found to be more correlated in time, acting similarly to a bias for each estimation. Thus the estimated correlation time scales increase as well as the overall relative power of the noise, as previously mentioned. Nonetheless, there are also factors related to the individual RSO characteristics, such as the attitude, that are impacting the estimation of the correlation time scale. Thus, further analysis is required in future works to obtain more insights on the relevance of object-related stochastic noise as compared to the environment-related, with the ultimate goal of being able to estimate noise parameters related exclusively to the environment that could be directly applicable to the complete catalog of objects.

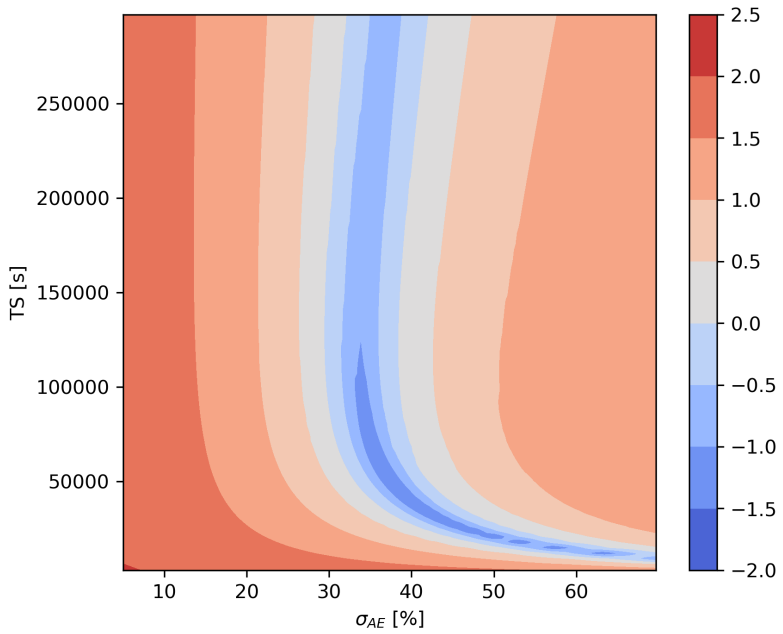

Figure 5.4: Logarithmic contour of the Cramer-von-Mises metric as a function of the correlation time scale τ (vertical axis) and the power of the noise σ_{AE} (horizontal axis) for object 27371, fixing the range bias consider parameter to the estimated value of Table 5.4.

A crucial factor to be considered in SSA operations is the computational cost. On the one side, the SCP method with known noise parameters has been shown to be several orders of magnitude more efficient than Monte Carlo propagation with stochastic dynamics [18]. On the other side, the problem at hand is to estimate the unknown noise parameters, which involves an heuristic optimization process whose cost function (the Cramer-von-Mises test) is built upon the SCP estimation and propagation of several orbits at the same time. The time discretization of the stochastic noise sequence generates a stochastic consider parameter vector size of approximately 3744 elements in the case of OD arcs of 7 days, with 6 days of propagation. Then, at each step of the optimization, Equation (5.27) must be evaluated for each pair of orbit and reference, whose covariances are computed by means of Equation (5.25) and Equation (5.21), the latter suffering from the dimension of the stochastic consider parameter vector. This implies a major increase in the computational cost of the SCP methodology as compared to the constant consider parameter model, going from around 3 minutes to 1 hour (Python implementation with 3 threads). For operational applicability, this significant increment in the computational cost must be traded-off with the observed improvement in the uncertainty modeling. Lighter computations such as the *Covariance Determination* with constant consider parameter models could be applied in the general case of space debris, still achieving a significant improvement in covariance realism, while the SCP model could be applied ad-hoc for high-interest events or a subset of RSOs whose uncertainty is expected to be of the same level as other objects with similar orbits or characteristics. Nonetheless, a large potential for computational time improvement is foreseen for the SCP methodology. On the one side, the estimated time scales of correlation are several orders of magnitude larger than the stochastic parameters time-step selected in this work (5 minutes). Thus, larger intervals could be applied without significant loss of accuracy, which leads to a large reduction in the computational cost. On the other side, the SCP method can benefit from its adequacy for parallelization and implementation in faster computer programming languages.

5.4.3 Covariance realism analysis

Even though the previous results have shown improvements in covariance realism, such results were focused on the optimization interval at the epochs of analysis. Thus, it is customary to analyze the realism of the estimated covariance matrices not only inside that arc, but including the complete propagation arcs of interest in LEO which range between the estimation epoch until around 8 days of propagation.

For this purpose, the 3σ covariance containment is computed every 3 hours between t_0 and $t_0 + 8$ days for all the RSOs analyzed in this work. The results are shown in Figure 5.6 as a box-plot, using 3 different covariance matrix computation methods for each RSO: the constant consider parameter model, the SCP model and the noise-only covariance without applying *Covariance Determination*. The limits of each box represent the first and third quartiles, whereas the green line corresponds to the median value. The upper and lower bars represent the maximum and minimum values, respectively, whereas the circular points correspond to outliers. The 97.1% theoretical 3σ containment for a 3 DoF multivariate Gaussian distribution is depicted as a dashed black line.

A straightforward conclusion drawn from Figure 5.6 is that the noise-only covariance is a poor representation of the orbit uncertainty, especially in the work presented here where

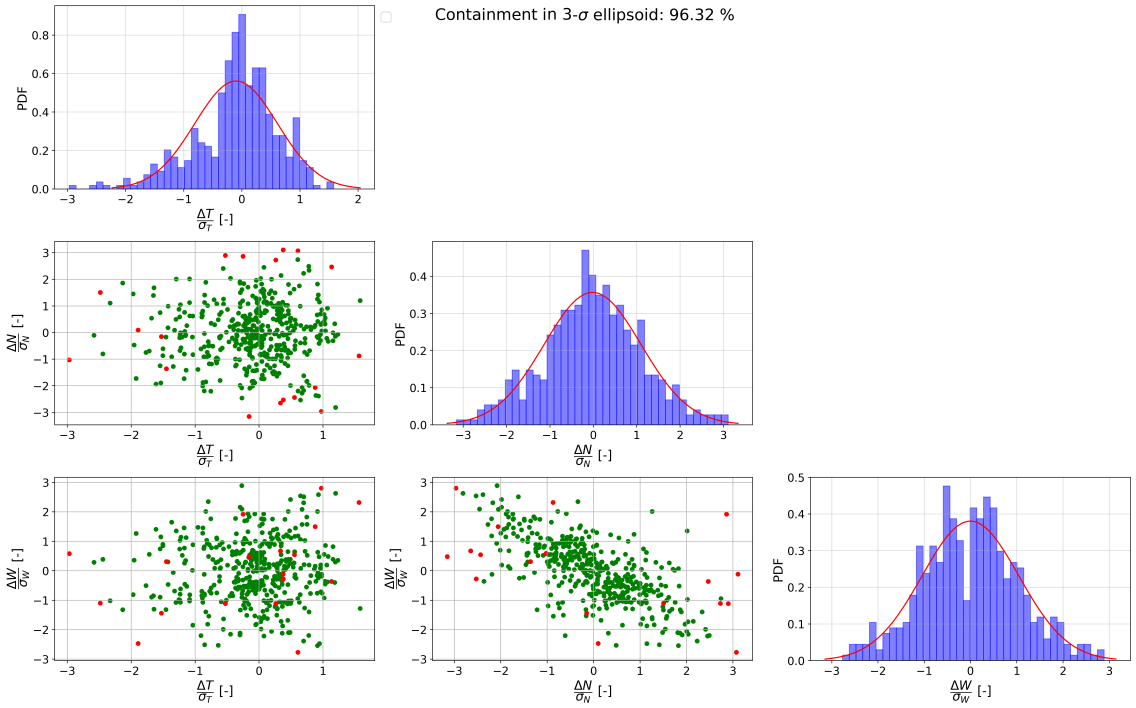

Figure 5.5: Orbital differences, and 3σ Covariance containment in the optimization arc for object 27371 after *Covariance Determination* with SCP model. The orbital differences are shown in TNW local frame, normalized by the standard deviation of the *consider covariance*.

real measurements are used for orbit determination. On the contrary, it is confirmed that both consider parameter models after applying *Covariance Determination* enhance significantly the realism of the covariance matrices with real data for the complete propagation interval. Additionally, the SCP model is seen to outperform the constant consider parameter model in all cases, not only showing median values closer to the theoretical 97.1% but also smaller box sizes, which indicate less dispersion in its covariance containment. Objects 33066 and 43520 show a more degraded realism as compared to the rest of the tested objects. In the case of object 33066, it is attributed to errors in the orbit determination and propagation process that are not completely modeled with the SCP methodology or the range bias uncertainty, which could be related to specific characteristics of the RSO. In the case of object 43520, the median 3σ containment of around 87% indicate that not enough orbits are being analyzed to have a proper estimation of the noise parameters, which is even more problematic with an object at 430 km of altitude where the strength of the non-linearity starts to grow significantly. In fact, the failure of Gaussian assumptions of that object at long propagation epochs such as 8 days leads to a decrease in covariance containment, which is observed as a larger standard deviation in the box-plot of Figure 5.6, especially in the case of constant consider parameter model.

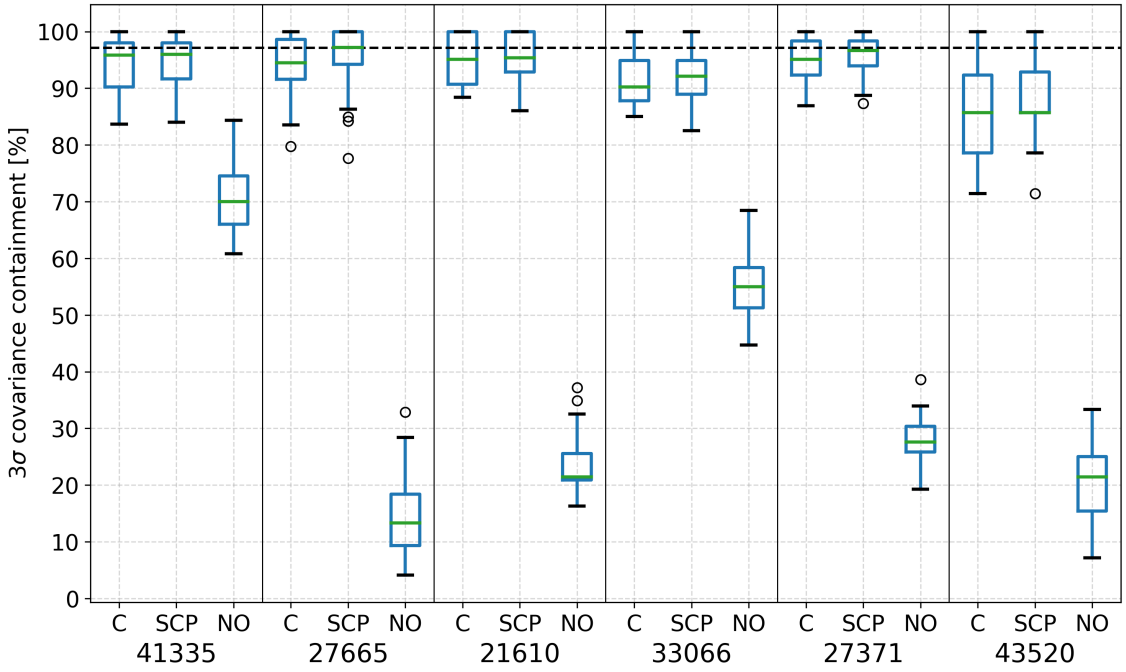

Figure 5.6: Covariance containment boxplot for each RSO from t_0 up to 8 days of propagation. Columns 'C' stand for constant consider parameter model, columns 'SCP' correspond to the stochastic consider parameters model, and columns 'NO' represent the noise-only covariance without applying *Covariance Determination*.

5.5 Conclusions and future work

This work has presented the Stochastic Consider Parameter model, a methodology to characterize the stochastic nature of the atmospheric drag uncertainty and improve covariance realism in batch least-squares estimation and propagation. The main objective was to combine a representative model of the drag uncertainty with the advantages of the *consider parameters* theory in batch estimation. The SCP model has been combined with the *Covariance Determination* method to estimate the parameters of the stochastic noise, i.e. the power of the noise and the correlation time scale. The methodology has been validated and tested with real measurements from the S3TSR Spanish surveillance radar for different RSOs at multiple altitudes.

Sentinel 3A measurements have been used for validation of the methodology due to the availability of precise ephemeris to compute the Mahalanobis distance. Results have shown that the SCP model achieves a high level of covariance realism, being able to improve the Cramer-von-Mises fit and the covariance containment with respect to the constant-error consider parameter model. Moreover, similar performance is obtained for the computation of the Mahalanobis distance when using either precise ephemeris or the *Operational Reference* orbits (estimated orbits), being this a requisite for the application of the SCP model to space debris where no precise ephemeris are available.

The results for the other space debris objects have shown again a high performance of the SCP model for covariance realism improvement at different altitudes, despite the challenge of using real radar measurements. The physical interpretation of the estimated noise parameters and their evolution with altitude and RSO characteristics has been

discussed. A noteworthy advantage of the presented methodology is that it is able to provide quantities for uncertain parameters such as the power of the stochastic noise, its correlation strength, and the range bias uncertainty, which are not commonly available. These estimates can be leveraged in other methodologies such as in the process noise of filtering applications or other uncertainty propagation techniques.
Regarding the covariance realism improvement in the propagation arcs of interest for LEO orbits in SSA, it has been seen that the noise-only covariance is a poor representation of the space environment uncertainty with 3σ containment of up to 70% in the best case scenario. On the contrary, covariance realism improvement techniques such as the SCP model have shown 3σ containment closer to the theoretical 97.1%, indicating a strong capability to improve covariance realism.
However, the improvement in the characterization of the drag uncertainty of the SCP model comes with a significant increase in the computational cost. Despite being able to map efficiently the impact of the stochastic drag model into the covariance, the increased cost to evaluate each Mahalanobis distance results in a longer computational time during the minimization process. This is detrimental to operational applicability due to the large number of RSOs in current catalogs. Lighter computational methods such as the constant consider parameter model could be applied for the general case of RSOs, while applying the more accurate SCP model to high-interest events or subsets of RSOs. Firstly, this would allow to have an overall improvement in the realism of the catalog covariances. Secondly, more accurate services could be provided by improving the characterization of the uncertainty with the SCP model, such as high-risk conjunction events that are being monitored by SSA control centers.
Regarding future work, further tests with real data are necessary to determine key factors for the operational applicability of the SCP method. Larger datasets are required to analyze the sensitivity of the methodology to the number of orbits when real observations are used, as opposed to the sensitivity analysis performed with simulated data in previous works [92]. Additionally, the analysis of longer datasets would provide insights regarding the execution frequencies required to maintain enough realism in operational catalogs. Another future objective is to analyze the performance of longer time-steps for the stochastic parameters discretization, given that the estimated correlation time scales are several orders of magnitude larger. This is expected to improve significantly the computational efficiency of the SCP model. In addition to this, it is needed to investigate the compatibility of the *Covariance Determination* method and SCP model with other authors model and input uncertainty, trying to find synergies and further operational applicability.
Apart from this, even if achieving satisfactory results with real measurements of several RSOs is a relevant conclusion, it is necessary to continue testing this methodology with data from more RSOs to determine the limitations of the SCP model. On the one side, it is needed to distinguish better between the object-related and the environment-related noise estimation. This would allow to derive laws about the evolution of the noise parameters as a function of altitude, solar activity, or object characteristics, with the goal of applying this method in future catalogs of RSO. On the other side, it is necessary to assess the performance of the SCP model and the *Covariance Determination* method when non-linearities arise, especially at lower altitudes. Therefore, further tests focused on

lower altitude objects are required, where alternative state representations like curvilinear coordinates or other non-linear reference frames that maintain Gaussianity further in time can be applied to expand the ranges of applicability of the SCP model. Moreover, Gaussianity tests must be combined with the proposed methodology in order to detect possible departures from such assumptions at lower altitude orbits, being able to switch automatically to more favorable state representations.

Acknowledgment

This project has received funding from the “Comunidad de Madrid" under “Ayudas destinadas a la realización de doctorados industriales" program (project IND2020/TIC-17539). JM acknowledges the support of Spain’s *Agencia Estatal de Investigación* (ref. PID2021-125159NB-I00 TYCHE) funded by MCIN/AEI/10.13039/501100011033 and by ERDF “A way of making Europe”. Moreover, the authors would like to acknowledge the Spanish Space Agency (Agencia Espacial Española - AEE) and in particular Cristina Pérez Hernández for the provision of the S3TSR observations under the S3T program. Finally, special thanks to GMV Precise Orbit Determination department for their support to provide precise ephemeris for Sentinel 3A.

Appendix A: Global parameter discretization

This appendix provides a complete derivation of Equation (5.16), which represent the partial derivatives of the state with respect to each stochastic parameter as a function of time and the partial derivatives of the a single, global parameter. Figure 5.1 depicts an schematic of the discretization process.

The objective is to discretize the global parameter into a number of smaller parameters that are active sequentially in time. First, the system dynamics are defined as

$$\frac{\partial \mathbf{x}(t)}{\partial t} = \mathbf{f}(t, \mathbf{x}, \mathbf{p}); \quad \mathbf{x}(t_0) = \mathbf{x_0}, \tag{5.28}$$

where the dynamics of the system depend on time, the state ($\mathbf{x}$), and the dynamic parameters ($\mathbf{p}$). Linearizing the trajectory, the state transition matrix and sensitivity matrix are defined, respectively, as

$$\mathbf{\Phi}(t, t_0) = \frac{\partial \mathbf{x}(t)}{\partial \mathbf{x_0}} \tag{5.29}$$

$$\mathbf{S}(t) = \frac{\partial \mathbf{x}(t)}{\partial \mathbf{p}} \tag{5.30}$$

where $\mathbf{x_0}$ represent the state at the initial time. Then, the differential equations that describe the time evolution of the state transition and sensitivity matrix follow the equations of motion. These are the variational equations [28], as follows:

$$\frac{\partial}{\partial t}\mathbf{\Phi}(t, t_0) = \frac{\partial \mathbf{f}(t, \mathbf{x}, \mathbf{p})}{\partial \mathbf{x}(t)}\mathbf{\Phi}(t, t_0); \; \mathbf{\Phi}|_{t=t_0} = \mathbf{I} \tag{5.31}$$

$$\frac{\partial}{\partial t}\mathbf{S}(t) = \frac{\partial \mathbf{f}(t, \mathbf{x}, \mathbf{p})}{\partial \mathbf{x}(t)}\mathbf{S}(t) + \frac{\partial \mathbf{f}(t, \mathbf{x}, \mathbf{p})}{\partial \mathbf{p}}; \; \mathbf{S}|_{t=t_0} = \mathbf{0} \tag{5.32}$$

For simplicity, let us assume we have only a single-global parameter to conform the dynamic parameters vector ($\mathbf{p} = p_c$). Now, our objective is to separate the contribution of this parameter, into multiple, sequential parameters applied in different time intervals. To that end, we can define the individual sensitivity matrix of one discrete parameter (p_i) as

$$\mathbf{S_i}(t) = \frac{\partial \mathbf{x}(t)}{\partial p_i}, \tag{5.33}$$

which still has to fulfill

$$\frac{\partial}{\partial t}\mathbf{S_i}(t) = \frac{\partial \mathbf{f}(t, \mathbf{x}, \mathbf{p})}{\partial \mathbf{x}(t)}\mathbf{S_i} + \frac{\partial \mathbf{f}(t, \mathbf{x}, \mathbf{p})}{\partial p_i}; \quad \text{for } t_{pi} < t < t_{pi+1} \tag{5.34}$$

with

$$\mathbf{S_i}|_{t=t_{pi}} = \mathbf{0} \tag{5.35}$$

Where t_{pi} and t_{pi+1} correspond to the start and end epochs of application of the parameter, respectively (see Figure 5.1). Our objective is to obtain the partial derivatives of p_i as a function of the those of p_c, the latter being computed natively in most SSA orbit determination systems (i.e. ballistic coefficient or solar radiation pressure coefficient).

The properties of the variational equations allow to relate sensitivity matrices resulting from the same model, with the only difference being the initial conditions. As both parameters (p_c and p_i) correspond to the same physical phenomena (even if applied in different time intervals), we have that:

$$\frac{\partial \mathbf{f}(t,\mathbf{x},\mathbf{p})}{\partial p_i} = \frac{\partial \mathbf{f}(t,\mathbf{x},\mathbf{p})}{\partial p_c}. \tag{5.36}$$

However, their contribution to the state evolution is not expected to be the same, as p_i is only active between t_{pi} and t_{pi+1}. Nonetheless, the aggregated contribution of all discrete parameters at time t must equal the contribution of the global parameter at time t. Thus, it is required that:

$$\sum_{i=0}^{N} \frac{\partial \mathbf{x}(t)}{\partial p_i} = \frac{\partial \mathbf{x}(t)}{\partial p_c}. \tag{5.37}$$

We define the differences between the partial derivatives of p_i and p_c at time t as $\mathbf{\Delta}(t)$:

$$\frac{\partial \mathbf{x}(t)}{\partial p_c} = \frac{\partial \mathbf{x}(t)}{\partial p_i} + \mathbf{\Delta}(t) \longrightarrow \frac{\partial \mathbf{x}(t)}{\partial p_i} = \frac{\partial \mathbf{x}(t)}{\partial p_c} - \mathbf{\Delta}(t), \tag{5.38}$$

which needs to fulfill Equation (5.35) and Equation (5.37). Then, we propose $\mathbf{\Delta}$ to be the linear propagation of the contribution of the global parameter at the start time of the discrete parameter, that is:

$$\mathbf{\Delta}(t) = \frac{\partial \mathbf{x}(t)}{\partial \mathbf{x}(t_{pi})} \frac{\partial \mathbf{x}(t_{pi})}{\partial \mathbf{p_c}} \text{ for } t_{pi} < t < t_{pi+1}, \tag{5.39}$$

where

$$\frac{\partial \mathbf{x}(t)}{\partial \mathbf{x}(t_{pi})} = \frac{\partial \mathbf{x}(t)}{\partial \mathbf{x_0}} \left(\frac{\partial \mathbf{x}(t_p i)}{\partial \mathbf{x_0}} \right)^{-1} = \mathbf{\Phi}(t,t_0)\mathbf{\Phi}(t_{pi},t_0)^{-1}, \tag{5.40}$$

which leads to:

$$\frac{\partial \mathbf{x}(t)}{\partial p_i} = \frac{\partial \mathbf{x}(t)}{\partial p_c} - \frac{\partial \mathbf{x}(t)}{\partial \mathbf{x}(t_{pi})} \frac{\partial \mathbf{x}(t_{pi})}{\partial p_c} \text{ for } t_{pi} <= t <= t_{pi+1}. \tag{5.41}$$

Therefore, the contribution of a parameter at the stop time of its application ($\frac{\partial \mathbf{x}(t_{pi+1})}{\partial p_c}$) corresponds to the difference between the global parameter at such time, and the linear propagation of the global parameter from the start time ($\mathbf{\Delta}(t_{pi+1})$), which are not equal since the global sensitivity matrix $\frac{\partial \mathbf{x}(t)}{\partial p_c}$ is computed by solving the complete variational equations by numeric integration. On the contrary, at the start time of application ($t = t_{pi}$), we have that:

$$\frac{\partial \mathbf{x}(t_{pi})}{\partial \mathbf{x}(t_{pi})} = \mathbf{I}, \tag{5.42}$$

which leads Equation (5.41) to fulfill Equation (5.35):

$$\mathbf{S_i}(t = t_{pi}) = \frac{\partial \mathbf{x}(t_{pi})}{\partial p_c} - \frac{\partial \mathbf{x}(t_{pi})}{\partial p_c} = \mathbf{0}. \tag{5.43}$$

After the end epoch of the parameter (t_{pi+1}), the parameter does not affect the dynamics, so:

$$\frac{\partial \mathbf{f}(t, \mathbf{x}, \mathbf{p})}{\partial p_i} = \mathbf{0} \text{ for } t > t_{pi+1}, \tag{5.44}$$

which combined with Equation (5.34), concludes that the contribution of the parameter after its end time corresponds to the linear propagation of its contribution from the time it stopped. Inversely, before the start time of the parameter, its impact on the state was null. This leads to the compact form shown in Equation (5.16), as follows:

$$\frac{\partial \mathbf{x}(t)}{\partial p_i} = \begin{cases} \frac{\partial \mathbf{x}(t)}{\partial p_c} - \frac{\partial \mathbf{x}(t)}{\partial \mathbf{x}(t_{pi})} \frac{\partial \mathbf{x}(t_{pi})}{\partial p_c} & t_{pi} <= t <= t_{pi+1} \\ \frac{\partial \mathbf{x}(t)}{\partial \mathbf{x}(t_{pi+1})} \left(\frac{\partial \mathbf{x}(t_{pi+1})}{\partial p_i} \right) & t > t_{pi+1} \\ 0 & t < t_{pi} \end{cases} \tag{5.45}$$

Finally, Equation (5.16) can be readily shown to fulfill Equation (5.37). Focusing on Figure 5.1, let us compute the contribution of all parameters at time t_{m2}, which is found between the start and end times of parameter p_2. There are a total of 3 discrete parameters (p_0, p_1, p_2):

$$\sum_{i=0}^{2} \frac{\partial \mathbf{x}(t_{m2})}{\partial p_i} = \frac{\partial \mathbf{x}(t_{m2})}{\partial p_0} + \frac{\partial \mathbf{x}(t_{m2})}{\partial p_1} + \frac{\partial \mathbf{x}(t_{m2})}{\partial p_2}. \tag{5.46}$$

According to Equation(5.16), we have that:

$$\frac{\partial \mathbf{x}(t_{m2})}{\partial p_0} = \mathbf{\Phi}(t_{m2}, t_{p1}) \left[\frac{\partial \mathbf{x}(t_{p1})}{\partial p_c} - \mathbf{\Phi}(t_{p1}, t_{p0}) \frac{\partial \mathbf{x}(t_{p0})}{\partial p_c} \right]; \tag{5.47}$$

$$\frac{\partial \mathbf{x}(t_{m2})}{\partial p_1} = \mathbf{\Phi}(t_{m2}, t_{p2}) \left[\frac{\partial \mathbf{x}(t_{p2})}{\partial p_c} - \mathbf{\Phi}(t_{p2}, t_{p1}) \frac{\partial \mathbf{x}(t_{p1})}{\partial p_c} \right]; \tag{5.48}$$

$$\frac{\partial \mathbf{x}(t_{m2})}{\partial p_2} = \frac{\partial \mathbf{x}(t_{m2})}{\partial p_c} - \mathbf{\Phi}(t_{m2}, t_{p2}) \frac{\partial \mathbf{x}(t_{p2})}{\partial p_c}. \tag{5.49}$$

Where it can be noted that $\frac{\partial \mathbf{x}(t_{p0})}{\partial p_c} = \mathbf{0}$, since the global parameter (p_c) must satisfy its initial condition for the sensitivity matrix. Combining all parameters, we end up with:

$$\begin{aligned} \sum_{i=0}^{2} \frac{\partial \mathbf{x}(t_{m2})}{\partial p_i} = \frac{\partial \mathbf{x}(t_{m2})}{\partial p_c} - \mathbf{\Phi}(t_{m2}, t_{p2}) \frac{\partial \mathbf{x}(t_{p2})}{\partial p_c} + \mathbf{\Phi}(t_{m2}, t_{p2}) \frac{\partial \mathbf{x}(t_{p2})}{\partial p_c} \\ - \mathbf{\Phi}(t_{m2}, t_{p2}) \mathbf{\Phi}(t_{p2}, t_{p1}) \frac{\partial \mathbf{x}(t_{p1})}{\partial p_c} + \mathbf{\Phi}(t_{m2}, t_{p1}) \frac{\partial \mathbf{x}(t_{p1})}{\partial p_c} \end{aligned}$$

Now, if we notice that $\mathbf{\Phi}(t_{m2}, t_{p2}) \mathbf{\Phi}(t_{p2}, t_{p1}) = \mathbf{\Phi}(t_{m2}, t_{p1})$, then all terms cancel out except for the first one, proving Equation (5.37).

Appendix B

Algorithm 2 *Covariance Determination* with SCP model

Require: A sample of ODs (N_{OD}) and their propagation

Require: For each OD, retrieve matrices $\mathbf{P_n}$, and $\mathbf{K_{CA}}$ from Equation (5.22), Equation (5.23) and Equation (5.16)

Require: For each OD, at each epoch of analysis (t_m) retrieve $\mathbf{\Psi}(t_m, t_0)$ and compute the orbital differences between the predicted and estimated orbit $\Delta\mathbf{y}(t_m)$. Let N_m be the number of analysis epochs for each orbit.

for i = 1:N_{OD} **do** ▷ Heuristic global optimization loop

Given σ_{AE}, τ

Compute matrices $\mathbf{C}$ and $\mathbf{A}$ with Equation (5.24) and Equation (5.18)

Compute $\mathbf{P_C}$ matrix following Equation (5.21)

for m = 1:N_m **do**

Compute $\mathbf{P_C}(t_m)$ matrix following Equation (5.25)

Compute the Mahalanobis distance (d_m) with Equation (5.27), using $\mathbf{P_C}(t_m)$ and $\Delta\mathbf{y}(t_m)$

end for

end for

Let $\mathbf{d}$ be the one-dimensional squared Mahalanobis distances vector, of size $N_{OD} \times N_m$

Minimize: $CvM(\mathbf{d}(\sigma_{AE}, \tau), \chi^2(DoF))$ ▷ Cramer-von-Mises metric between $\mathbf{d}$ and the χ^2 distribution

6

Conclusions and future work

Section 6.1 summarizes the conclusions of this dissertation, considering the objectives of the thesis stated in Section 1.2 and the overall goal. Afterwards, Section 6.2 reviews possible future lines of research.

6.1 Conclusions

The first objective of the thesis, modeling uncertainty in dynamic and measurement models, is considered satisfactorily fulfilled in this dissertation. Regarding the uncertainty associated with errors in the drag model of LEO orbits (*Objective 1.1*), they aret characterized in Chapter 2, modeling ballistic coefficient and atmospheric density uncertainty with a constant *consider parameter*, whereas applying a time-dependent error for the prediction of space weather proxies. Later, Chapter 4 proposes an altitude-dependent model for the evolution of the atmospheric density in a catalog of objects. Finally, Chapter 5 improves the characterization of the aleatoric behavior of the atmospheric drag by developing a stochastic model with time correlation.
Objective 1.2 is covered mostly in Chapter 3, which focuses on uncertainty characterization in GEO orbits and models the errors in solar radiation pressure and cross-sectional area by means of a *consider parameter*. The last sub-objective of the uncertainty modeling was to tackle errors in the measurement models (*Objective 1.3*), and is also considered fulfilled throughout the work of this thesis. Range bias uncertainty, one of the most relevant sources of measurement error in LEO orbits, is modeled both in Chapter 2 and Chapter 5. In GEO regimes, time bias errors are characterized in Chapter 3. It is worth highlighting that the *consider parameter* model of constant variance for the measurement error is agnostic to the chosen bias, as long as it corresponds to an observable quantity. Thus, even though this thesis focuses on the most relevant measurements uncertainty depending on the observing sensor, others such as angular or range-rate biases can be characterized as well. In fact, range-rate bias uncertainty was modeled with real data from GRAVES bi-static radar in the work performed during the research stay at Centre National D'Études Spatiales (CNES) [40], further detailed in Appendix B.
Regarding the second objective of the thesis about the quantification of the modeled uncertainty, it is also considered satisfactorily fulfilled in this dissertation. Concerning *Objective 2.1*, the models proposed in *Objective 1* for LEO orbits are successfully estimated with the *Covariance Determination* methodology, both in the form of classic *consider*

parameter (Chapters 2 and 4) and with the SCP model (Chapter 5). The uncertainty quantification accuracy and the achieved improvement in covariance realism are analyzed first in realistic simulations of operational scenarios, either for singular objects (Chapters 2 and 5), or simultaneously for a catalog subset (Chapter 4). Furthermore, the performance of both the constant-model or stochastic consider parameters is tested with real observations in Chapter 5, showing successful uncertainty characterization and significant covariance realism improvement.

Last, *Objective 2.2* is partially covered in Chapter 3, quantifying the modeled uncertainty in GEO orbits in a simulated environment. However, this dissertation does not include results of the developed methodologies in GEO with real observations, placing the focus on real data applications to the more complex LEO regime. Nonetheless, although not included in this dissertation, the *Covariance Determination* method has been successfully applied to real observations in GEO and MEO orbits in the studies performed in [106].

Apart from the objectives of the thesis and the results already discussed in each of the papers in this dissertation, there are global conclusions worth mentioning. Firstly, it has been shown that classical orbit determination algorithms such as batch-least squares neglect dynamic and measurement model errors, which leads to an underestimation of the uncertainty as has been noted by the low realism level of the noise-only covariance along this thesis. This reinforces the initial statement that SSA services require effective, efficient, and reliable methodologies to improve uncertainty realism. In this regard, the *Covariance Determination* methodology developed throughout this dissertation has shown remarkable capabilities to quantify some of the most relevant uncertainty sources in SST, displaying significant covariance realism improvement with both simulated and real observations. It has been shown as an efficient and versatile methodology, supporting the simultaneous estimation of multiple uncertainty sources in low and high Earth orbits without requiring external information such as precise ephemeris, being also applicable to complete catalogs including space debris. Additionally, the *Covariance Determination* UQ methodology has been designed flexibly to allow more realistic representations of the uncertainty sources, as in the case of the SCP model for the atmospheric drag, which yielded better uncertainty characterization and covariance realism, at the expense of a more complex time-correlated model. Thus, a trade-off between accuracy and efficiency is to be made when choosing the uncertainty models, depending on the available data, the analysis purpose, and ultimately, the provided SSA services.

For all the above reasons, the application of the methodologies developed in this dissertation to current SSA services is gaining interest, being already implemented as part of the European Catalog produced by the European Union Space Surveillance and Tracking (EUSST) consortium [107], as well as being on the operational route for SSA services at the Spanish Space Surveillance and Tracking Operations Center (S3TOC) and CNES. Preliminary studies about the benefits of applying these covariance improvement techniques in conjunction analysis were carried out in [108, 109] during the development of this thesis.

To summarize, the work in this thesis provides a step towards better characterization and quantification of the uncertainty in SST with relevant improvements of covariance realism focusing on operational applicability, which is key for the quality of SSA services and the space sustainability given the current and predicted status of the space environment.

6.2 Future work

Whereas specific limitations and future improvements of the methodologies are discussed in each paper included in this dissertation, the most relevant gaps are gathered here. The first clear line of research is a deeper benchmark of the methodologies developed in this dissertation. This implies further tests with real data in all orbital regimes, with objects of different sizes, shapes, and orbital geometry. For the general application of the *Covariance Determination* method to complete catalogs, it is necessary to analyze the expected computational cost as a function of the catalog size and available data. Alternatively, the catalog could be split into families of objects attending to common characteristics, choosing a few samples of each family for uncertainty quantification and then extrapolating the results to the rest of the family. However, it is needed to investigate how to propose uncertainty models that are representative of complete catalogs, and how accurate is the uncertainty extrapolation to other similar objects. Another current line of research is the application of these methodologies to improve the quality of other SSA services such as conjunction analysis, manoeuvre detection, or re-entry analysis, even though preliminary studies were carried out during this thesis.

Further research is required for highly elliptical orbits. Even though there are no explicit assumptions regarding the eccentricity in the presented uncertainty quantification techniques, it has been generally assumed that the variance of the atmospheric drag is expected to remain constant, for constant altitudes. This assumption would not apply to eccentric orbits, requiring the adaptation of the constant-variance uncertainty models. Piece-wise optimization or other altitude-varying models such as the one proposed in Chapter 4 are options to be investigated.

Moreover, the analysis conducted in this thesis does not extend to orbits below 400 km of altitude, where the drag perturbation breaks the Gaussian and linear assumptions in very short estimation and propagation arcs. To overcome this limitation and reach longer arcs, the combination of the *Covariance Determination* methodology with other state representations is a current line of research, such as non-linear or curvilinear coordinates. For instance, during this thesis, the QtW reference frame has been integrated for the computation of the Mahalanobis distance after linearizing the QtW transformation for the covariance matrix, being able to maintain Gaussianity longer and successfully quantify the uncertainty at lower altitudes [47]. Preliminary results about this current line of research are included in Appendix B, though further testing and validation with real data is required.

Finally, it is needed to continue looking towards more complex representations of the uncertainty. Stochastic models could be applied to represent the aleatoric errors in the SRP force surface area, similar to its application in LEO orbits for the drag force. Other time-varying or altitude dependent uncertainty models for measurement or atmospheric density errors would be also worth exploring, as well as methods to deal with epistemic sources of uncertainty. Nonetheless, the trade-off between accuracy and computational efficiency must always be evaluated in face of the size of space objects catalogs.

A

Other research merits

Publications

The following publication, even though not included in the dissertation, has related topics where the author contributed:

- L. Porcelli, A. Pastor, **A. Cano**, G. Escribano, M. Sanjurjo-Rivo, D. Escobar, P. Di Lizia, 2022, Satellite maneuver detection and estimation with radar survey observations, *Acta Astronautica*, 201, 274–287
  10.1016/j.actaastro.2022.08.021

Conference papers

The following list includes all conference papers prepared and presented by the author of this thesis, whose research outcomes have contributed to define the overall planning of the thesis, some of them leading to the generation of the publications presented in this thesis.

- **A. Cano**, A. Pastor, D. Escobar, 2021, Covariance determination for improving uncertainty realism, *8th European Conference on Space Debris*, Darmstadt, Germany (virtual)
- **A. Cano**, S. Fernández, A. Pastor, D. Escobar, 2021, Improving orbital uncertainty realism through covariance determination in GEO, *22nd Advanced Maui Optical and Space Surveillance Technologies*, Maui, United States (virtual)
- **A. Cano**, P. Gago, A. Pastor, M. Sanjurjo-Rivo, J. Míguez, D. Escobar, 2022, Atmospheric correlation impact in uncertainty propagation, *3rd IAA Conference on Space Situational Awareness*, Madrid, Spain
- **A. Cano**, A. Pastor, J. Míguez, M. Sanjurjo-Rivo, D. Escobar, 2022, Catalogue-based atmosphere uncertainty quantification, *23rd Advanced Maui Optical and Space Surveillance Technologies*, Maui, United States
- **A. Cano**, M. Sanjurjo-Rivo, J. Míguez, A. Pastor, D. Escobar, 2023, Covariance propagation with time-correlated errors, *2nd NEO and Debris Detection Conference*, Darmstadt, Germany
- **A. Cano**, M. Sanjurjo-Rivo, J. Míguez, A. Pastor, D. Escobar, 2023, Stochastic Consider Parameters for covariance realism in orbit determination, *AAS/AIAA Astrodynamics Specialists Conference*, Big Sky, United States

A

- **A. Cano**, M. Sanjurjo-Rivo, J. Míguez, A. Pastor, D. Escobar, 2023, Uncertain parameter estimation for improved realism in SSA products, *2nd International Orbital Debris Conference*, Houston, United States

The following list includes other conference papers where the author of this thesis has contributed significantly during the development of this project, with topics related to the ones of this dissertation. The presenting author of each paper is underlined:

- A. Pastor, G. Escribano, **A. Cano**, M. Sanjurjo-Rivo, C. Pérez, I. Urdampileta, D. Escobar, 2021, Manoeuvre detection and estimation based on sensor and orbital data, *8th European Conference on Space Debris*, Darmstadt, Germany (virtual)
- J. Bravo, J. Lopez, A. Lopez, P. Martınez, J. Miguez, D. Morante, M. Sanjurjo-Rivo, M. Vazquez, **A. Cano**, D. Escobar, E. Villanueva, P. Gago, B. Bastida, S. Lemmens, K. Merz and J. Siminski, 2021, Uncertainty propagation meeting space debris needs, *8th European Conference on Space Debris*, Darmstadt, Germany (virtual)
- L. Porcelli, A. Pastor, **A. Cano**, G. Escribano, M. Sanjurjo-Rivo, D. Escobar, P. Di Lizia, 2022, Satellite manoeuvre detection with radar survey observations, *3rd IAA Conference on Space Situational Awareness*, Madrid, Spain
- F. Hoots, V. Baral, F. Delmas, **A. Cano**, S. Martínez, C. Pérez, M. Hejduk, P. Ramsey, K. Auman, 2023, US-EUSST Data Exchange for Improved Orbital Safety, *24th Advanced Maui Optical and Space Surveillance Technologies Conference (AMOS)*, Maui, United States
- F. Hoots, V. Baral, **A. Cano**, S. Martínez, M. Hejduk, 2024, International Sharing of Satellite Tracking Data For Improved Orbital Safety, *AAS/AIAA Astrodynamics Specialist Conference*, Broomfield, United States

Workshops

The presenting author in underlined:

- **Cano, A.**, Pastor, A., Escobar, D., 2020, Improving covariance realism through consider analysis in orbit determination, *UMD Center for Orbital Debris Education and Research (CODER) Workshop*, virtual
- Sanjurjo Rivo, M., **Cano, A.**, Pastor, A., Escribano, G., Sztamfater, Y., Escobar, D., Míguez, J., López-Santiago, J., Vázquez, M., Águeda, A., 2022, Retos futuros en la vigilancia y seguimiento de objetos espaciales, *IX Congreso Nacional de I+D en Defensa y Seguridad*, Pontevedra, Spain
- **Cano, A.**, Pastor, A., Arias, E., Sáez, D., Míguez, J., Sanjurjo-Rivo, M., Escobar, D., 2022, Covariance determination for uncertainty realism in collision probability estimates, *5th International Workshop on Key Topics in Orbit Propagation Applied to Space Situational Awareness*, Logroño, Spain
- **A. Cano**, V. Baral, E. Delande, M. Sajurjo-Rivo, J. Míguez, D. Escobar, 2024, Covariance realism improvement with GRAVES radar measurements in orbit estimation and propagation, *6th International Workshop on Key Topics in Orbit Propagation Applied to Space Situational Awareness*, Arrás, France

Science outreach

Talks to promote science dissemination:

- **Cano, A.**, Sztamfater, Y., Pastor, A., 2022, Basura y vigilancia espacial: origen, impacto y soluciones, *Semana de la Ciencia 2022*, Madrid, Spain

B

Other research results

This appendix chapter groups relevant results and conclusions from other works carried out during this thesis, which despite not being included as papers in the main body of this dissertation, provide valuable insights and first steps towards future improvements.

Stochastic Consider Parameters model validation with Monte Carlo

The first developments of the SCP model were presented in [18], where the stochastic noise discretization and its impact on linear covariance propagation was validated against Monte Carlo simulations. The main goal was to assess the achievable accuracy of the SCP model as compared to completely non-linear Monte Carlo propagation of the covariance. To this end, the proposed stochastic noise shown in Section **??** was introduced in the equations of motion, and propagated with a high-fidelity orbit propagator. in a parametric analysis for multiple power of the noise and correlation time scales, the reconstructed Monte Carlo covariance was then compared to the one obtained by propagating linearly the covariance SCP method. As a summary, Figure B.1 shows a contour plot of the relative error in the along-track standard deviation (the most affected local orbital direction due to drag effects), having on the horizontal axis the propagation time, and on the vertical axis the correlation time scale (normalized by the orbit period).

It is shown in Figure B.1 that, even using a relatively high discretization time step of 5 minutes, the relative error in the covariance does not reach further than 10% in this simulation. It is worth noting that this error is not only due to the discretization of the noise model, where a constant power of the noise for the stochastic model was not forced in the Monte Carlo propagations, in relative terms. On the contrary, it was left to vary with position, as expected in the space environment, to test the hypothesis of constant relative power of the noise assumed by the SCP model.

Therefore, this work yielded promising conclusions about the stochastic noise discretization and its application to linear covariance propagation. First, overall good accuracy can be achieved with the method as compared to realistic Monte Carlo simulations. Second, this slight lack of accuracy is compensated with a remarkable improvement in the computational cost, being able to map the effect of stochastic noise with a single linear propagation, saving more than 78% of computational time as compared to Monte Carlo runs of only 200 samples. This remarkable improvement in computational

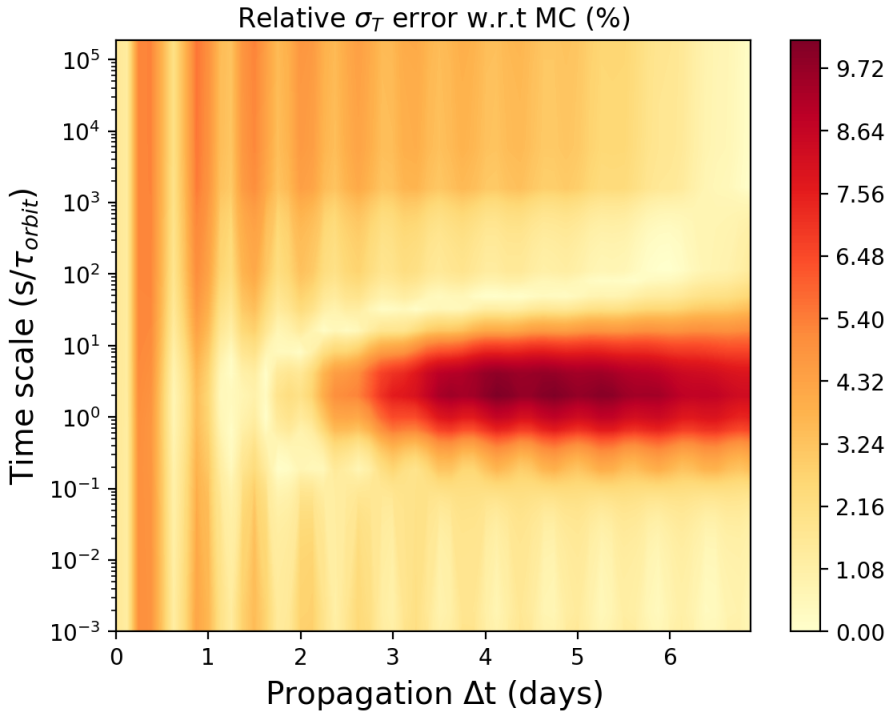

Figure B.1: σ_T relative error contour of the SCP model for propagation versus Monte Carlo, with a discretization time step of 5 minutes. Simulated object at 800 km altitude with a relative power of the noise of $\overline{\sigma}_{atm} = 0.219$. From [18].

cost allows to use the SCP model in combination to the *Covariance Determination* method, being possible to use it for the computation of each Mahalanobis distance during the optimization process.

SCP model with GRAVES radar range-rate measurements

The SCP complete model was further tested with real data at CNES during a research visit, where data from GRAVES bi-static radar was provided. This surveillance radar contributes to EUSST SST sensor network, providing range-rate and angular measurements. The purpose of this study was twofold: on the one hand, to further test the SCP methodology with real data. On the other hand, to analyze the impact of range-rate bias uncertainty and correct it for realism, which was a measurement type whose uncertainty had not been tackled before by the *Covariance Determination* method. As opposed to S3TSR, where range measurements are the principal observable, GRAVES main information source comes from the range-rate measurements. This makes GRAVES data a suitable candidate to test the capabilities of the methodology to model range-rate bias uncertainty.
The results of this study were presented at [40]. The main results for several space debris objects are shown in Table B.1. Regarding the quantified uncertainty, the estimated noise parameters show higher uncertainty with increasing altitude (in relative terms), an expected behavior from previous works [27]. The absolute uncertainty at lower altitudes,

where the drag force is stronger, is expected to be larger. However, in relative terms, it is expected to decrease. The range-rate uncertainty results are normalized with the expected GRAVES sensor accuracy, showing standard deviations of the same order with some exceptions.

Finally, Table B.1 shows the already described covariance containment metric, comparing the performance of the SCP method against the containment when no covariance correction is applied (noise-only covariance). It is clearly seen the uncertainty quantification capabilities of the SCP model with the *Covariance Determination* method, especially as compared to the noise-only covariance. This difference is exacerbated at lower altitude objects, where drag force becomes more dominant. However, the SCP containment does not reach the theoretical expectation of 97.1%. There are two main reasons for this. The main reason is that, during the preliminary calibration process of GRAVES measurements, abnormal residuals were found mostly in the cross-track direction due to epistemic sources of error in the range-rate measurements, possibly due to issues in the ionospheric treatment in GRAVES data post-process prior to their publication. During this study, these errors were analyzed and corrected with empirical models, yielding more accurate orbit determination results. Nonetheless, despite these improvements, orbit inaccuracies still prevent reaching the 97.1% theoretical containment.

Table B.1: Uncertainty quantification results and 3σ covariance containment (theoretical containment of 97.1%). From [40]

NORAD	Altitude [km]	N_{orbits}	σ_{AE} [%]	τ [s]	σ_{RR} [-]	3σ Containment	
						SCP	Noise-only
41335	810	59	69,81	112840	0,60	93,52	48,12
40697	790	21	56,24	499330	0,48	93,53	64,96
27665	800	58	34,62	798450	1,53	87,80	30,53
29110	624	113	13,55	78333	0,63	95,39	0,41
25979	560	115	22,52	8962	4,15	92,27	0,53

Covariance Determination with QtW transformation

Even though the initial distribution of the state usually behaves as a Gaussian distribution, long propagation arcs and the highly non-linear dynamics of the space environment cause the state distribution to depart from Gaussianity. As previously discussed, this can become extremely relevant in data starved systems as in SSA, requiring long propagation arcs between measurement updates, or at low altitude orbits, where the orbital dynamics become highly non-linear.

As previously mentioned, the departure of the state distribution from Gaussianty is largely affected by the reference frame in which the uncertainty is represented. Inertial and cartesian frames present difficulties in characterizing the curvilinear nature of the orbits and their non-linearities, leading to the use of object-centered local frames. However, they are not enough to maintain Gaussianity for large initial covariance matrices or long propagation arcs, especially at low altitude orbits.

This supposes a limitation to the *Covariance Determination* methodology, which applies the TNW orbital frame. To extend the validity of the methodology to lower altitudes, the QtW non-linear reference frame was combined with the *Covariance Determination* method, as outlined in [47]. This reference frame is introduced during the computation of the Mahalanobis distance. First, the orbital differences between the orbit under analysis and its reference are transformed to QtW coordinates with the full non-linear transformation as described in [73]. Then, an analytical Jacobian of the transformation is derived in order to rotate the covariance matrix from TNW to QtW frame, as described in [47].
To test the capabilities of the QtW frame to extend the range of validity of the *Covariance Determination* method, an object at 450 km of altitude with a ballistic coefficient of 0.02 was simulated during 3 months of sequential orbit determinations and propagations, introducing a 20% of uncertainty in the drag force, and 15 meters of uncertainty in the range measurements bias, similarly to the simulations carried out in Chapter 2. Then, the *Covariance Determination* method with constant consider parameters model is applied, analyzing the range of propagation between 4 and 6 days, to allow for non-linearities to add up. Figure B.2 depicts the 3σ covariance containment results when using the TNW frame, whereas Figure B.3 shows the results when applying the QtW transformation.
In Figure B.2, a final containment of 69,3% is achieved, being able to appreciate the appearance of the non-linearities in the T-N frame, the commonly known as banana-shape of the orbital differences due to the orbit curvature. This leads to a breakup of the Gaussian assumptions, and a large degradation of the covariance realism and containment. On the contrary, Figure B.3 shows a covariance containment of 93.38%, a significant improvement as compared to the TNW frame. Furthermore, it is seen that the orbital differences present a Gaussian behavior. However, the theoretical value of 97.1% is not reached either in the QtW frame, in this case, probably due to the errors introduced within the covariance rotation of the QtW Jacobian transformation. Though this is something to bear in mind for the application of this QtW frame, these results are an indicator of the benefits of the QtW frame transformation for covariance realism in cases of high non-linearities in the system.

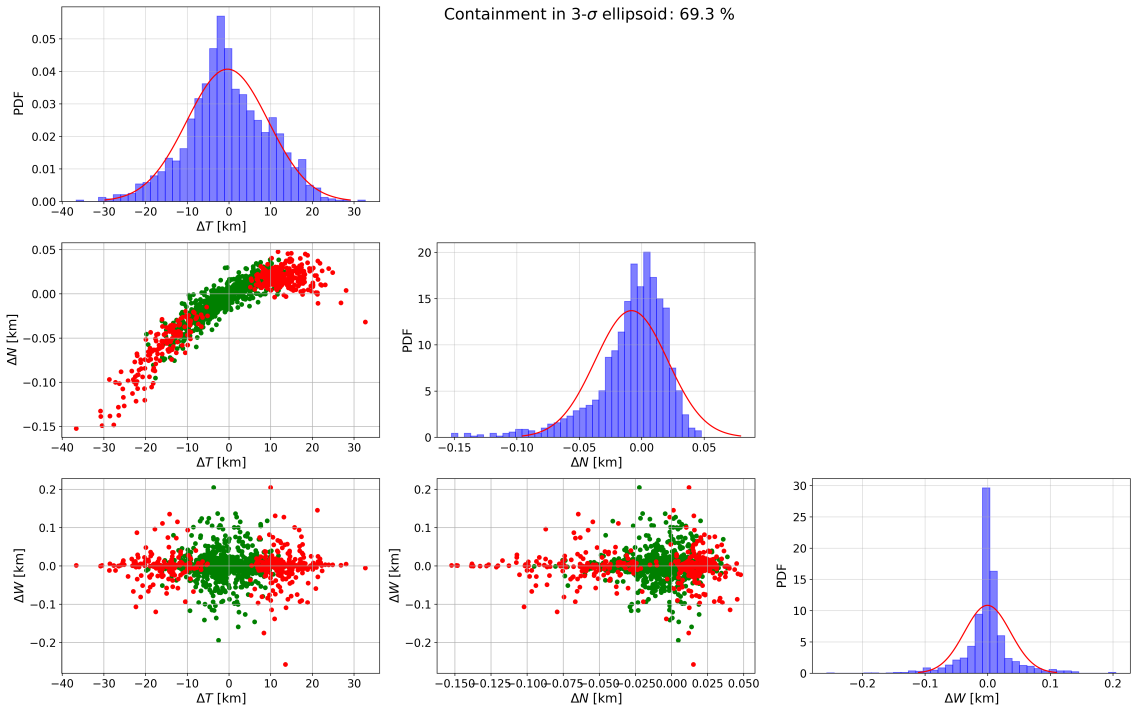

Figure B.2: Orbital differences and covariance containment in TNW frame after applying *Covariance Determination* at a 450 km of altitude object.

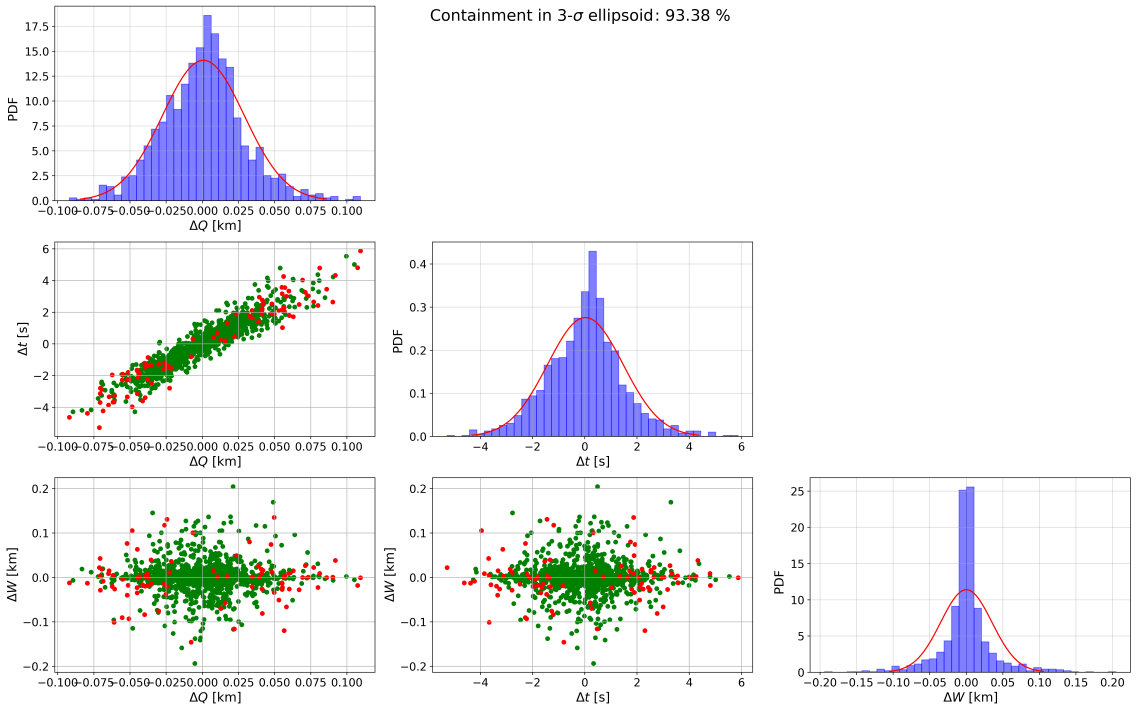

Figure B.3: Orbital differences and covariance containment in QtW frame after applying *Covariance Determination* at a 450 km of altitude object.

Bibliography

[1] A. Concini and J. Toth, "The future of the european space sector", *European Comission*, 2019.

[2] E. S. D. Office, "Esa's annual space environment report", ESA, Tech. Rep., 2024.

[3] K. Hae-Dong, "Key definitions of the inter-agency space debris coordination committee (iadc)", IADC, Tech. Rep., 2015.

[4] D. J. Kessler and B. G. Cour-Palais, "Collision frequency of artificial satellites: The creation of a debris belt", *Journal of Geophysical Research*, vol. 83, pp. 2637–2646, A6 Jun. 1978.

[5] Inter-Agency Space Debris Coordination Committee (IADC), "IADC space debris mitigation guideline", Inter-Agency Space Debris Coordination Committee (IADC), Tech. Rep., 2002.

[6] UNCOPUOS, "Technical report on space debris", United Nations Committee on the Peaceful Uses of Outer Space (UNCOPUOS), Tech. Rep., 1999.

[7] UNOOSA, "Space debris mitigation guidelinesof the committee onthe peaceful uses of outer space", United Nations Office for Outer Space Affairs, Tech. Rep., 2010.

[8] E. S. D. M. W. Group, "Esa space debris mitigation requirements", ESA, Tech. Rep., 2023.

[9] A. Pastor, D. Escobar, M. Sanjurjo-Rivo, and A. Águeda, "Correlation techniques for catalogue build-up and maintenance with radar and optical survey measurements", in *1st International Orbital Debris Conference (IOC)*, ser. 0, Sugar Land, United States, Dec. 2019.

[10] A. Pastor, M. Sanjurjo-Rivo, and D. Escobar, "Track-to-track association methodology for operational surveillance scenarios with radar observations", *CEAS Space Journal*, 2022.

[11] A. B. Poore *et al.*, "Covariance and Uncertainty Realism in Space Surveillance and Tracking", Numerica Corporation Fort Collins United States, Tech. Rep., Jun. 2016.

[12] K. Hill, K. Alfriend, and C. Sabol, "Covariance-based uncorrelated track association", in *AIAA/AAS Astrodynamics Specialist Conference and Exhibit*, American Institute of Aeronautics and Astronautics, Aug. 2008. DOI: 10.2514/6.2008-7211.

[13] R. Vazquez *et al.*, "Manoeuvre detection for near-orbiting objects", in *8th European Conference on Space Debris*, T. Flohrer, S. Lemmens, and F. Schmitz, Eds., vol. 8, 2021.

[14] J. Montilla *et al.*, "Manoeuvre detection in low earth orbit with radar data", *Advances in Space Research*, 2022. DOI: 10.1016/j.asr.2022.10.026.

[15] A. Pastor *et al.*, "Manoeuvre detection and estimation based on sensor and orbital data", in *8th European Conference on Space Debris*, T. Flohrer, S. Lemmens, and F. Schmitz, Eds., vol. 8, Darmstadt, Germany (remote): ESA Space Debris Office, Apr. 2021.

[16] L. Porcelli *et al.*, "Satellite manoeuvre detection with radar survey observations", in *3rd IAA Conference on Space Situational Awareness (ICSSA)*, Tres Cantos, Spain, Apr. 2022.

[17] A. Cano *et al.*, "Atmospheric correlation impact in uncertainty propagation", in *3rdInternational Conference on Space Situational Awareness(ICSSA)*, ICSSA, Apr. 2022.

[18] A. Cano, M. Sanjurjo-Rivo, J. Miguez, A. Pastor, and D. Escobar, "Covariance propagation with time-correlated errors", in *2nd NEO and Debris Detection Conference*, 2023.

[19] C. Sabol, K. Hill, K. Alfriend, and T. Sukut, "Nonlinear effects in the correlation of tracks and covariance propagation", *84:69–80*, vol. 84, pp. 69–80, Mar. 2013. DOI: 10.1016/j.actaastro.2012.08.023.

[20] D. T. Hall, L. G. Baars, and S. J. Casali, "A multistep probability of collision computational algorithm", in *AAS/AIAA Astrodynamics Specialist Conference*, 2023.

[21] M. R. Akella and K. T. Alfriend, "Probability of collision between space objects", *Journal of Guidance, Control, and Dynamics*, vol. 23, pp. 769–772, 2000, ISSN: 0731-5090. DOI: 10.2514/2.4611.

[22] J. L. Foster and H. S. Estes, "A parametric analysis of orbital debris collision probability and maneuver rate for space vehicles", Johnson Space Center, Tech. Rep., 1992.

[23] B. D. Tapley, B. E. Schutz, and G. H. Born, *Statistical Orbit Determination*. San Diego, California: Elsevier Academic Press, 2004.

[24] D. A. Vallado and D. Finkleman, "A critical assessment of satellite drag and atmospheric density modeling", *Acta Astronautica*, vol. 95, pp. 141–165, Feb. 2014. DOI: 10.1016/j.actaastro.2013.10.005.

[25] M. Vasile, "Satellite dynamics and space missions", in Springer International Publishing, 2019, pp. 291–328, ISBN: 978-3-030-20633-8. DOI: 10.1007/978-3-030-20633-8_7.

[26] Y.-z. Luo and Z. Yang, "A review of uncertainty propagation in orbital mechanics", *Progress in Aerospace Sciences*, vol. 89, pp. 23–39, Feb. 2017. DOI: 10.1016/j.paerosci.2016.12.002.

[27] J. B. Aguado *et al.*, "Uncertainty propagation meeting space debris needs", in *8th European Conference on Space Debris*, 2021.

[28] O. Montenbruck and E. Gill, *Satellite Orbits: Models, Methods and Applications*. Berlin: Springer-Verlag Berlin Heidelberg, 2000, p. 369, ISBN: 978-3-540-67280-7. DOI: 10.1007/978-3-642-58351-3.

[29] J. M. Picone, A. E. Hedin, D. P. Drob, and A. C. Aikin, "NRLMSISE-00 empirical model of the atmosphere: Statistical comparisons and scientific issues", *Journal of Geophysical Research: Space Physics*, vol. 107, no. A12, SIA 15–1–SIA 15–16, Dec. 2002. DOI: 10.1029/2002ja009430.

[30] A. Marcos and et al, "Satellite drag models: Current status and prospects", in *AAS/AIAA Astrodynamics Specialist Conference*, Victoria, Canada, 1993.

[31] D. E. Doornbos, *Thermospheric Density and Wind Determination from Satellite Dynamics*. Springer Science & Business Media, 2012.

[32] D. A. Vallado and T. Kelso, "Earth orientation parameter and space weather data for flight operations", in *Advances in the Astronautical Sciences*, AAS 13-373, vol. 148, 2013.

[33] D. R. Weimer, "A comparison of the jb2008 and nrlmsise-00 neutral density models.", *GEM Meeting at Fall AGU 2014*, 2004.

[34] J. M. Leonard, J. M. Forbes, and G. H. Born, "Impact of tidal density variability on orbital and reentry predictions", American Geophysical Union, Tech. Rep., 2012.

[35] F. A. Marcos *et al.*, "Towards next level satellite drag modeling", in *AIAA Guidance, Navigation, and Control Conference*, 2010.

[36] R. Anderson, G. Born, and J. Forbes, "Sensitivity of orbit predictions to density variability", *Journal of Spacecraft and Rockets*, vol. 46:1214–1230, Aug. 2009. DOI: 10.2514/6.2008-6443.

[37] R. L. Anderson, C. P. Guignet, G. H. Born, and J. M. Forbes, "Effect of density model time-delay errors on orbit prediction", *Journal of spacecraft and rockets*, vol. 50, no. 5, Oct. 2013. DOI: 10.2514/1.A32368.

[38] A. Hattori and T. Otsubo, "Time-varying solar radiation pressure on Ajisai in comparison with LAGEOS satellites", *Advances in Space Research*, vol. 63, no. 1, pp. 63–72, 2019, ISSN: 0273-1177. DOI: https://doi.org/10.1016/j.asr.2018.08.010.

[39] A. Cano, "Orbital uncertainty analysis for covariance realism enhancement in orbit determination", M.S. thesis, GMV/Universidad Carlos III de Madrid, 2020.

[40] A. Cano *et al.*, "Covariance realism improvement with graves radar measurements in orbit estimation and propagation", in *6th International Workshop on Key Topics in Orbit Propagation Applied to Space Situational Awareness*, Arrás, France, 2024.

[41] J.-W. Lee and R. Pogge, "Long-term variation of the shutter delay time of y4kcam of the ctio 1.0 m telescope", *Journal of the Korean Astronomical Society*, vol. 49, no. 6, pp. 289–293, Dec. 2016. DOI: 10.5303/JKAS.2016.49.6.289.

[42] M. Steindorfer, G. Kirchner, F. Koidl, and P. Wang, "Recent space debris related activities at the slr station graz", in *1st NEO and Debris Detection Conference*, 2019.

[43] W. Wiesel, *Modern Orbit Determination*. Beavercreek, OH: Aphelion Press, 2003, ISBN: 9780974827209.

[44] J. R. Alarcón, H. Klinkrad, J. Cuesta, and F. M. Martinez, "Independent orbit determination for collision avoidance", in *4th European Conference on Space Debris*, D. Danesy, Ed., ser. ESA Special Publication, vol. 587, Aug. 2005, p. 331.

[45] B. Wilson, "Robust orbit determination via convex optimization", Project Report, EE364B, Stanford University, Tech. Rep., 2014.

[46] R. Ziegler, "Levenberg-marquardt filter for orbit estimation", M.S. thesis, The Faculty of the Department of Aerospace Engineering San José State University, 2019.

[47] L. Porcelli, A. Cano, P. Gago, L. C. Quadri, and D. Escobar, "Methods for improved robustness in batch orbit estimation and propagation", in *6th International Workshop on Key Topics in Orbit Propagation Applied to SSA (KePASSA)*, Arrás, Frances, Jun. 2024.

[48] S. Kazemi, N. L. Azad, K. A. Scott, H. B. Oqab, and G. B. Dietrich, "Orbit determination for space situational awareness: A survey", *Acta Astronautica*, vol. 222, pp. 272–295, 2024, ISSN: 0094-5765. DOI: https://doi.org/10.1016/j.actaastro.2024.06.015.

[49] M. Duncan and A. Long, "Realistic covariance prediction for the earth science constellation", in *AIAA/AAS Astrodynamics Specialist Conference and Exhibit*, American Institute of Aeronautics and Astronautics, Aug. 2006. DOI: 10.2514/6.2006-6293.

[50] M. Schubert, C. Kebschull, and S. Horstmann, "Analysis of different process noise models in typical orbit determination scenarios", in *8th European Conference on Space Debris*, vol. 8, Darmstadt, Germany: ESA Space Debris Office, 2021.

[51] B. D. Tapley, "Orbit determination in the presence of unmodeled accelerations", Air Force Office of Scientific Research, Tech. Rep., 1975.

[52] R. Zanetti and C. D'Souza, "Recursive implementations of the schmidt-kalman 'consider' filter", *The Journal of the Astronautical Sciences*, vol. 60, pp. 672–685, 2013, ISSN: 2195-0571. DOI: 10.1007/s40295-015-0068-7.

[53] A. Jazwinski, *Stochastic processes and filtering theory* (Mathematics in science and engineering). New York: Academic Press, Jan. 1970, vol. 64, ISBN: 9780080960906.

[54] J. Emmert, H. Warren, A. Segerman, J. Byers, and J. Picone, "Propagation of atmospheric density errors to satellite orbits", *Advances in Space Research*, vol. 59, no. 1, pp. 147–165, Jan. 2017. DOI: 10.1016/j.asr.2016.07.036.

[55] F. Schiemenz, J. Utzmann, and H. Kayal, "Least squares orbit estimation including atmospheric density uncertainty consideration", *Advances in Space Research*, vol. 63, no. 12, pp. 3916–3935, Jun. 2019. DOI: 10.1016/j.asr.2019.02.039.

[56] D. A. Vallado, *Fundamentals of Astrodynamics and Applications* (Space Technology Library), Forth. Hawthorne, CA: Springer and Microcosm Press, 1997, p. 1055, ISBN: 978-0-387-71831-6.

[57] L. Sagnieres and I. Sharf, "Uncertainty characterization of atmospheric density models for orbit prediction of space debris", in *Proceedings of the 7th European Conference on Space Debris*, Darmstadt, Germany: ESA Space Debris Ofice, 2017.

[58] P. J. Brockwell and R. A. Davis, *Introduction to Time Series and Forecasting*. Springer, 2016.

[59] M. Wilkins and K. Alfriend, "Characterizing orbit uncertainty due to atmospheric uncertainty", in *Astrodynamics Specialist Conference*, American Institute of Aeronautics and Astronautics, Aug. 2000. DOI: 10.2514/6.2000-3931.

[60] J. H. Frisbee, "An empirical state error covariance matrix for weighted least squares estimation method", NASA Johnson Space Center Houston, TX, United States, Tech. Rep. JSC-CN-24133, Jan. 2011. [Online]. Available: https://ntrs.nasa.gov/api/citations/20110014000/downloads/20110014000.pdf.

[61] W. Cerven, "Improved empirical covariance estimation", *Advances in the Astronautical Sciences*, vol. 150, pp. 879–895, Jan. 2014.

[62] P. M. Djuric *et al.*, "Particle filtering", *IEEE signal processing magazine*, vol. 20, no. 5, pp. 19–38, 2003.

[63] O. Cappé, S. J. Godsill, and E. Moulines, "An overview of existing methods and recent advances in sequential monte carlo", *Proceedings of the IEEE*, vol. 95, no. 5, pp. 899–924, 2007.

[64] B. Ristic, S. Arulampalam, and N. Gordon, *Beyond the Kalman Filter: Particle Filters for Tracking Applications*. Artech House, 2004, ISBN: 1-58053-631-x.

[65] J. S. McCabe and K. J. DeMars., "Particle filter methods for space object tracking", in *AIAA/AAS Astrodynamics Specialist Conference*, San Diego, CA: American Institute of Aeronautics and Astronautics (AIAA), 2014.

[66] Z. Folcik, A. Lue, and J. Vatsky, "Reconciling covariances with reliable orbital uncertainty", in *Advanced Maui Optical and Space Surveillance Technologies Conference*, Sep. 2011, E34, E34.

[67] S. Laurens, P. Seimandi, J. Couetdic, and J. Dolado, "Covariance matrix uncertainty analysis and correction", in *68th International Astronautical Congress*, id: IAC-17,A6,7,2,x37415, 2017.

[68] J. L. Junkins, M. R. Akella, and K. T. Alfriend, "Non-gaussian error propagation in orbital mechanics", *Journal of The Astronautical Sciences*, vol. 44, pp. 541–563, 1996.

[69] C. Sabol *et al.*, "Linearized orbit covariance generation and propagation analysis via simple monte carlo simulations", *Advances in the Astronautical Sciences*, vol. 136, p. 22, Jan. 2010.

[70] G. Baù, J. Hernando-Ayuso, and C. Bombardelli, "A generalization of the equinoctial orbital elements", *Celestial Mechanics and Dynamical Astronomy*, vol. 133, pp. 1–, Dec. 2021. DOI: 10.1007/s10569-021-10049-1.

[71] D. A. Vallado and S. Alfano, "Curvilinear coordinate transformations for relative motion", *Celestial Mechanics and Dynamical Astronomy*, vol. 118, 2014, ISSN: 1572-9478. DOI: 10.1007/s10569-014-9531-1.

[72] W. Clohessy and R. Wiltshire, "Terminal guidance system for satellite rendezvous", *Journal of the Aerospace Sciences*, vol. 27, no. 9, pp. 653–658, 1960.

[73] S. Laurens, J. Dolado, G. Cavallaro, M. Jouisse, and P. Seimandi, "Towards the maintenance of Gaussianity on state vector uncertainty propagation", in *69th International Astronautical Congress*, id: IAC-18,A6,9,3,x42351, Oct. 2018.

[74] CCSDS, *Navigation data: Definitions and conventions (green book)*, The Consultative Comittee for Space Data Systems (CCSDS), May 2010. [Online]. Available: https://public.ccsds.org/Pubs/502x0b2c1.pdf.

[75] J. T. Horwood and A. B. Poore, "Gauss von mises distribution for improved uncertainty realism in space situational awareness", *SIAM/ASA Journal on Uncertainty Quantification*, vol. 2, no. 1, pp. 276–304, Jan. 2014. DOI: 10.1137/130917296.

[76] R. B. D'Agostino and M. A. Stephens, *Goodness-of-fit techniques* (STATISTICS: Texbooks and Monographs). New York: MARCEL DEKKER, INC, 1986, vol. 68.

[77] D. A. Vallado and J. H. Seago, "Covariance realism", in *AAS/AIAA Astrodynamics Specialist Conference*, 2009.

[78] P. Mahalanobis, "On the generalised distance in statistics", in *Proceedings of the National Institute of Sciences of India*, vol. 2, 1936, pp. 49–55.

[79] K. Hill, C. Sabol, and K. T. Alfriend, "Comparison of covariance based track association approaches using simulated radar data", *The Journal of the Astronautical Sciences*, vol. 59, no. 1-2, pp. 281–300, Jun. 2012. DOI: 10.1007/s40295-013-0018-1.

[80] F. J. S. Mecinas, J. S. Sánchez, and C. Hernández, "Conan: Conjunction analysis tool for eusst ca service users", in *International Conference on Space Situational Awareness*, Madrid, Spain, 2022.

[81] E. Stevenson, S. Lemmens, and J. Siminski, "Deriving a unified space object catalogue for the purpose of space debris monitoring and modelling", in *1st NEO and Debris Detection Conference*, 2019.

[82] J. R. Michael, "The stabilized probability plot", *Biometrika*, vol. 70, no. 1, pp. 11–17, 1983. DOI: 10.1093/biomet/70.1.11.

[83] P. Royston, "Graphical detection of non-normality by using michael's statistic", *Applied Statistics*, vol. 42, no. 1, p. 153, 1993. DOI: 10.2307/2347417.

[84] K. Alfriend and M. Wilkins, "Covariance as an estimator of orbit prediction error growth in the presence of unknown sensor biases", *American Astronomical Society*, vol. 103, pp. 99–422, Jan. 2000.

[85] W. T. Cerven, "Covariance error assessment, correction, and impact on probability of collision", in *AAS/AIAA Space Flight Mechanics Meeting*, 2011.

[86] D. A. Vallado and S. Alfano, "Curvilinear coordinates for covariance and relative motion operations", in *AAS/AIAA Astrodynamics Specialist Conference*, AAS 11-464, 2011.

[87] S. Lopez-Jimenez, A. Pastor, and D. Escobar, "Improving orbital uncertainty realism through covariance determination", *Acta Astronautica*, vol. 181, pp. 679–693, 2021, ISSN: 0094-5765. DOI: https://doi.org/10.1016/j.actaastro.2020.09.026.

[88] A. Cano, A. Pastor, and D. Escobar, "Covariance determination for improving uncertainty realism", in *8th European Conference on Space Debris*, ESA Space Debris Office, 2021.

[89] A. Cano, S. Fernandez, A. Pastor, and D. Escobar, "Improving orbital uncertainty realism through covariancedetermination in GEO", in *22nd Advances Maui Optical and Space Surveillance Technologies (AMOS) Conference*, 2021.

[90] R. Storn and K. Price, "Differential evolution - a simple and efficient heuristic for global optimization over continuous spaces", *Journal of Global Optimization*, vol. 11, pp. 341–359, Jan. 1997. DOI: 10.1023/A:1008202821328.

[91] "Models of the earth's upper atmosphere", Committee on Space research (COSPAR) International Reference Atmosphere, Tech. Rep., 2012.

[92] A. Cano, A. Pastor, D. Escobar, J. Míguez, and M. Sanjurjo-Rivo, "Covariance determination for improving uncertainty realism in orbit determination and propagation", *Advances in Space Research*, 2022, ISSN: 0273-1177. DOI: https://doi.org/10.1016/j.asr.2022.08.001.

[93] A. Cano *et al.*, "Improving orbital uncertainty realism through covariance determination in geo", *The Journal of the Astronautical Sciences*, vol. 69, no. 5, 2022, ISSN: 2195-0571. DOI: 10.1007/s40295-022-00343-x.

[94] D. J. Gondelach and R. Linares, "Atmospheric density uncertainty quantification for satellite conjunction assessment", in *AIAA Scitech 2020 Forum*. DOI: 10.2514/6.2020-0232.

[95] T. Kelso, *Celestrack SATCAT*, [Online; accessed 22-January-2020], 2020. [Online]. Available: https://celestrak.com.

[96] 18th Space Control Squadron, *Space-track*, [Online; accessed 12-February-2020], 2020. [Online]. Available: https://www.space-track.org.

[97] A. Cano, M. Sanjurjo-Rivo, J. Miguez, A. Pastor, and D. Escobar, "Stochastic consider parameters for covariance realism in orbit determination", in *AAS/AIAA Astrodynamics Specialist Conference*, 2023.

[98] F. Schiemenz, J. Utzmann, and H. Kayal, "Propagation of grid-scale density model uncertainty to orbital uncertainties", *Advances in Space Research*, vol. 65, no. 1, pp. 407–418, 2020, ISSN: 0273-1177. DOI: https://doi.org/10.1016/j.asr.2019.10.013. [Online]. Available: https://www.sciencedirect.com/science/article/pii/S0273117719307471.

[99] S. Paul, P. Sheridan, P. Mehta, and S. Huzurbazar, "Satellite drag coefficient modeling and orbit uncertainty quantification using stochastic machine learning techniques", in *AAS/AIAA Astrodynamics Specialist Conference*, 2021.

[100] S. N. Paul, P. L. Sheridan, R. J. Licata, and P. M. Mehta, "Stochastic modeling of physical drag coefficient – its impact on orbit prediction and space traffic management", *Advances in Space Research*, vol. 72, no. 4, pp. 922–939, 2023, ISSN: 0273-1177. DOI: https://doi.org/10.1016/j.asr.2023.06.006. [Online]. Available: https://www.sciencedirect.com/science/article/pii/S0273117723004362.

[101] S. N. Paul, R. J. Licata, and P. M. Mehta, "Advanced ensemble modeling method for space object state prediction accounting for uncertainty in atmospheric density", *Advances in Space Research*, vol. 71, no. 6, pp. 2535–2549, 2023, ISSN: 0273-1177. DOI: https://doi.org/10.1016/j.asr.2022.12.056. [Online]. Available: https://www.sciencedirect.com/science/article/pii/S0273117722011723.

[102] A. Cano, A. Pastor, J. Míguez, M. Sanjurjo-Rivo, and D. Escobar, "Catalog-based atmosphere uncertainty quantification", *The Journal of the Astronautical Sciences*, vol. 70, no. 42, Sep. 2023, ISSN: 2195-0571. DOI: https://doi.org/10.1007/s40295-023-00403-w.

[103] ESA, *Copernicus data space*, May 2024. [Online]. Available: https://dataspace.copernicus.eu.

[104] A. Cano, A. Pastor, M. Sanjurjo-Rivo, J. Miguez, and D. Escobar, "Catalog-based atmosphere uncertainty quantification", in *23rd Advanced Maui Optical and Space Surveillance Technologies*, Maui Economic Development Board, 2022.

[105] R. C. Gómez *et al.*, "Initial operations of the breakthrough spanish space surveillance and tracking radar (s3tsr) in the european context", in *1st NEO and Debris Detection Conference*, ESA Space Safety Programme Office, Darmstadt, Germany, Jan. 2019.

[106] F. Hoots, V. Baral, A. Cano, S. Martínez, and M. Hejduk, "International sharing of satellite tracking data for improved orbital safety", in *AAS/AIAA Astrodynamics Specialist Conference*, Broomfield, United States, 2024.

[107] A. Sancho *et al.*, "The gssac mission system: A new solution for space objects cataloguing from dlr", in *25th Advanced Maui Optical and Space Surveillance Technologies (AMOS) Conference*, Maui, Hawaii, Sep. 2024.

[108] A. Cano *et al.*, "Covariance determination for uncertainty realism in collision probability estimates", in *5th international workshop on Key topics in orbit Propagation Applied to Space Situational Awareness*, 2022.

[109] A. Cano, J. Míguez, M. Sanjurjo-Rivo, A. Pastor, and D. Escobar, "Uncertain parameter estimation for improved realism in ssa products", in *2nd International Orbital Debris Conference*, Houston, Texas, Dec. 2023.

Glossary

CBTA Covariance-Based Track Association
CHAMP CHAllenging Minisatellite Payload
CNES Centre National D'Études Spatiales
CvM Cramer-von-Mises
DoF Degrees of Freedom
EOPs Earth Orientation Parameters
ESA European Space Agency
EUSST European Union Space Surveillance and Tracking
GCRF Geocentric Celestial Reference Frame
GEO Geostationary Orbit
GNSS Global Navigation Satellite System
IADC Inter-Agency Space Debris Coordination Committee
IERS International Earth Rotation Society
JSC Johnson Operations Center
KS Kolmogorov-Smirnov
LEO Low Earth Orbit
MEO Medium Earth Orbit
NEOs Near-Earth Objects
OD Orbit Determination
PDF Probability Density Function
PoC Probability of Collision
RSO Resident Space Object
S3TOC Spanish Space Surveillance and Tracking Operations Center
S3TSR Spanish Space Surveillance and Tracking Radar
SCP Stochastic Consider Parameters
SDE Stochastic Differential Equations
SRP solar radiation pressure
SSA Space Situational Awareness
SST Space Surveillance and Tracking
STM Space Traffic Management
UNCOPUOS United Nations Committee on the Peaceful Uses of Outer Space
UNOOSA United Nations Office for Outer Space Affairs
UP Uncertainty Propagation
UQ Uncertainty Quantification
UR Uncertainty Realism